MEASUREMENT OF THE NOISE POWER SPECTRUM OF A MICROWAVE OSCILLATOR

by

DAVID I. KOSOWSKY

B.E.E., City College of New York
(1951)

SUBMITTED IN PARTIAL FULFILLMENT OF THE
REQUIREMENTS FOR THE DEGREE OF
MASTER OF SCIENCE

at the

MASSACHUSETTS INSTITUTE OF TECHNOLOGY
(1952)

Signature of Author _____
Department of Electrical Engineering, August 22, 1952

Certified by _____
Thesis Supervisor

_____
Chairman, Departmental Committee on Graduate Students

MEASUREMENT OF THE NOISE POWER SPECTRUM OF A MICROWAVE OSCILLATOR

38

by

DAVID I. KOSOWSKY

Submitted to the Department of Electrical Engineering on AUGUST 22, 1952 in partial fulfillment of the requirements for the degree of MASTER OF SCIENCE

ABSTRACT

The development of long-range c-w radar has necessitated the investigation of low-frequency noise sidebands present on the output of a microwave oscillator. Amplitude modulation and frequency modulation due to noise at frequencies within the "Doppler" band may result in serious range limitations and spurious signal information.

Primarily, this research is concerned with the design and construction of an analyzer which yields the power spectra of amplitude and frequency-modulation noise sidebands on an X-Band carrier.

A c-w klystron or magnetron supplies the microwave signal, which is demodulated in a silicon crystal detector circuit to seperate the a-m noise voltages from the carrier. A resonant microwave cavity is used to convert frequency-modulation sidebands to equivalent amplitude modulation prior to detection. An audio "bucking" circuit is described which provides a means of seperating a-m from f-m spectra, and enables the noise generated within the detector circuit to be measured.

The analyzer is capable of accepting noise voltages from the detector as small as 150 decibels below one volt, and in a frequency range of 20 cycles per second to 60 kilocycles per

Vail - Dec. 15, 1952

second. A narrow-band portion of the input signal is selected, amplified and recorded on the paper tape of a Brush Recorder.

The entire range of input frequencies is covered by the narrow band width through the use of a superheterodyne circuit, which converts each signal frequency to a fixed intermediate frequency by beating the input signal against the signal of a local oscillator. At the intermediate-frequency level, the narrow-band filtering is accomplished by a quartz-crystal lattice filter, which provides band widths of 10 cps or 100 cps. A logarithmic attenuator makes it possible to record input variations as large as 40 decibels without alteration of the system gain. Linearity of the analyzer is maintained through the use of overload meters at various points in the system. By this expedient, and by mechanically driving the local oscillator over a sufficient range of frequencies to cover the entire input spectrum, the data is obtained automatically and accurately.

In addition to the narrow-band power spectrum, the r-m-s value of the input noise in several wide band widths may be obtained with a thermal voltmeter built into the analyzer.

Finally, the noise spectra obtained from the outputs of a c-w magnetron and a microwave klystron under various operating conditions are presented and discussed.

Thesis Supervisor: Professor Henry J. Zimmermann

Title: Associate Professor of Electrical Engineering

Acknowledgement

The author would like to express his gratitude to the directors of the Research Laboratory of Electronics for making available the facilities of the laboratory for this research. He is especially indebted to Professor Henry J. Zimmermann for his supervision and constant guidance, to Mr. Carl Barus and Mr. Joseph M. Dunn for their many helpful suggestions, and to Mr. G.O. Johnson, Mr. Jack Sears and Mr. L. Chetkauskas for their skilled help in constucting the noise analyzer and associated experimental equipment.

TABLE OF CONTENTS

LIST OF ILLUSTRATIONS

CHAPTER I

THE VACUUM TUBE NOISE PROBLEM

A. Development of the Problem

The problem of determining the low frequency noise output of microwave oscillators enters into the design of all c-w microwave communication and measurement equipment. This noise problem is probably most critical in its relation to c-w radar. The simple c-w radar obtains its information through the measurement of a shift of the carrier frequency, commonly called the "Doppler" shift.[1] The frequency range of the carrier shift or Doppler may extend from very low audio to frequencies of 50 or 60 kilocycles, depending on the carrier frequency and the relative velocity of target and radar.

In the more common pulsed radar, low frequency noise sidebands present on the transmitter can have no effect on receiver sensitivity, for the transmitter is gated off when the receiver is required to perform its measurements. Furthermore, the range of signal frequencies of interest in pulsed radar falls far above the sonic or Doppler, so that the danger of obtaining spurious information due to low frequency noise is eliminated.

In direct contrast to this, the transmitter in the c-w radar is continuously on and generally located in close proximity to the receiver. Since complete decoupling between transmitter and receiver is impossible, some transmitter signal or "feed-through" will appear at the input terminals of the receiver. Note that although the feed-through differs slightly in frequency from the returning signal, and is thereby distinguishable from that signal,

the noise sidebands present on the transmitter will raise the receiver noise level.

In practice, attenuation between transmitting and receiving antennas seldom exceeds 40 db. Furthermore, the effective range of a radar varies inversely with the fourth root of the ratio of received to transmitted power. Since this ratio can be no smaller than that permitted by overall receiver sensitivity, transmitter noise will limit the maximum range of a c-w radar because of its adverse effect on receiver noise level.

It should also be observed that any large components of noise (such as hum or microphonics) present on the envelope of transmitter feed-through might be misconstrued as Doppler signal and thereby yield false information.

In addition to amplitude-modulation noise sidebands, frequency-modulation noise (deviation of carrier frequency due to noise modulation) is also of great interest in c-w radar design. F-M noise sidebands present on either the transmitter or local oscillator outputs of a c-w radar may lead to spurious Doppler information.

The microwave carrier frequency investigated in the research lies at X-Band or 10,000 megacycles. At this wavelength (3 cm.), the power output required for a long-range radar transmitter (10-100 watts) is generally supplied by a magnetron. Within the receiver, the local oscillator signal, usually about 100 milliwatts of power, is supplied by a klystron, generally of the reflex, single-cavity type.

Although most books and papers on c-w radar will point out the noise problem mentioned here[1,2], little work has been done on the development of accurate and rapid techniques for obtaining

the noise vs. frequency spectra of microwave oscillators, a step which must be completed before low-noise equipment design can procede very far.

Before outlining the general requirements of a noise measuring system or discussing equipment and techniques already developed for that purpose, it will be helpful to mention briefly the types and character of noise encountered in vacuum tube circuits.

B. Sources of Noise in Vacuum Tubes

1. Classification of Noise. Noise, as it is related to radar and communication practice may be defined as spurious voltage or current which appears at the output of a circuit. Whether or not this spurious output is significant depends of course on its character and relation to the desired signal. It is possible by careful choice of operating conditions to completely eliminate many forms of noise, while other forms are fundamental in nature and may never be completely removed.

Noise generated within an electronic system is attributable to several causes. It is made up of impulse noise, having random repetition period and continuous frequency spectrum, and non-random noise, having a definite repetition period and a discrete line frequency spectrum.

2. Random Noise.

(a) Thermal noise. In all electronic equipment, thermal noise is an ultimate irreducible quantity. It is generated in all impedances by the minute currents set up by the thermal motion of electrons.[3] The open circuit thermal noise voltage generated in an impedance has the mean-square value

$$E_n^2 = 4KT\Delta f R \qquad (1)$$

where

E_n^2 = mean-square value of thermal noise voltage

K = Boltzmann's constant: $1.37 \cdot 10^{-23}$ ergs/degree

T = absolute temperature in degrees Kelvin

R = resistive component of the impedance

Δf = bandwidth over which E_n^2 is measured, (cps)

The frequency spectrum of thermal noise is uniform up to frequencies higher than a thousand megacycles, because the thermal motion producing the noise currents retains its impulsive character even at these frequencies.

(b) Shot noise. The emission from a hot vacuum tube cathode is made up of finite electrons which leave the cathode surface in a random fashion. As a result of this corpuscular behavior, minute fluctuations will appear in the plate current of the tube. This phenomenon was named Shot Effect by W. Schottky[3] in 1918.

As is the case with thermal noise, shot noise is important out to very high frequencies. In fact, thermal and shot noise are the principal sources of internal noise in radio equipment. For this reason, it is very convenient to express them in comparable units. An equivalent grid resistor has been defined for this purpose. This equivalent input resistance generates a thermal noise of sufficient magnitude to reproduce the effect of plate current shot fluctuations.

For the space-charge limited triode, for example, a close approximation for the equivalent grid resistor is

$$R_{eq} = \frac{2.5}{g_m} \qquad (2)$$

where g_m is the tranconductance of the triode.

It is interesting to note that the signal-to-noise ratio of the triode amplifier improves directly as $\sqrt{g_m}$.

(c) Flicker noise. Another form of random noise that at low frequencies becomes large enough to exceed the shot effect by several orders of magnitude is flicker noise. Random changes in the condition of the cathode surface due to dif-

fusion, evaporation, gas-ion bombardment and other such causes are responsible for this phenomenon.[4]

(d) Partition noise. In general, it is found that triodes tend to be quieter than tetrodes and pentodes. The excess noise in multicollector tubes, called partition noise, has been found to be due to the division of tube current between the collector electrodes, whereby the noise-reduction effects due to space charge are reduced.[3]

It should finally be pointed out that use of a vacuum tube as a mixer will greatly increase its apparant shot noise level. Multigrid mixers are, as expected, the noisiest of the mixer group.

(e) Magnetron noise. The magnetron is a diode which, with the aid of a magnetic field, produces short electromagnetic waves. In the usual design of a microwave magnetron, the resonant circuit is a number of closely coupled cavities within the evacuated portion of the tube.

The carrier output of a magnetron contains noise modulation sidebands which are attributable to two causes.[5] One source of noise is the ever-present shot effect. The second noise source is believed to be modulation due to ions in the interaction space of the magnetron. There positive ions neutralize space charge in a random fashion and thereby cause variations in the electron current. The resultant current fluctuations appear on the output envelope as noise modulation.

(f) Klystron noise. The klystron is a microwave oscillator which makes use of the comparatively long transit times pre-

sent at very high frequencies to produce oscillations in a resonant cavity.[6] The reflex kylstron, most commonly used at X-Bant, makes use of a single resonator and a retarding field (produced by a reflector electrode maintained at a potential negative with respect to the cathode) to create the electronic configuration necessary to produce oscillation.

As is to be expected, shot and partition noise will contribute to the low frequency modulation of the reflex kylstron. There are, in addition, random interaction effects between the electron streams within the resonator which result in considerable enhancement of the noise.

As is true for the magnetron, there is little data available on klystron noise in the frequency range of interest to this research.

(g) Crystal noise. One final type of random noise, which although not related to the vacuum tube, is nevertheless of great importance here. This noise is the low frequency noise output current of a silicon crystal rectifier. The silicon point-contact crystal detector, whose properties will be more fully discussed in Chapter II, was used as the diode detector in the spectrum analyzer built in this investigation.

Little is known about the origin of noise in crystal rectifiers. Especially difficult is the problem of analyzing crystal noise with r-f excitation.[7]

Within the crystal rectifier are generated both thermal and shot noise. However, in the audio range, the noise varies inversely with the frequency, and is orders of magnitude greater at these frequencies than at higher frequencies. However, since thermal and shot noise are independent of frequency,

some other mechanism must be responsible for the excess noise at low frequencies, which is sometimes called "converted noise"[8]. No adequate hypothesis for such a mechanism has as yet been suggested.

3. Non-Random Noise.

(a) Hum. Spurious output fluctuations of an electronic circuit at the power line frequency or its harmonics is commonly known as hum. High-gain amplifiers often exhibit large output hum levels caused by the introduction of hum components into low-level stages through the plate circuits, by coupling of a-c heater voltages into cathode circuits and by such phenomena as magnetic and electrostatic pick-up.

(b) Microphonics. Noises produced by the effects of mechanical vibration are classed as microphonics. Electrode motion in the low-level stages of an amplifier produces interelectrode capacitance variations and fluctuations of transconductance which appear as current variations at the resonant frequencies of the tube structure. Some tubes have been specially designed structurally for low-microphonic operation.

Microphonics and hum may appear on the output of microwave oscillators unless precautions such as shock mounting, well-filtered power supplies and d-c filament excitation are taken.

C. General Requirements of Measurement System

An outline will now be given of the general requirements for a system which would accomplish a noise analysis on a microwave oscillator.

For simplicity, the system will be divided into three sections:

1. Preselector and Detector. In this section, the spectrum to be measured is seperated from the microwave carrier by demodulation. Since both a-m and f-m spectra are desired, this section must contain the auxiliary equipment necessary to convert the f-m noise to an equivalent a.m.

2. Measurement Section. The heart of the system is contained here. The measurement section must accept frequencies ranging from low audio (20-40 cps) to the ultrasonic (50-60 kc.). Voltages encountered at the input to this stage may be as low as 140 db. below one volt, so that the input circuits must be carefully designed and constructed to obtain the necessary sensitivity. The system must select a narrow-band portion of the noise input spectrum and amplify the signal in that band width to a level which can easily be measured. The narrow-band filtering is necessary to provide sufficient resolution for separating fixed frequency noise components such as hum and microphonics from similar components at neighboring frequencies, and to provide an indication of the character of the noise as a function of frequency.

3. Recording Section. The output of the measurment section is fed into these last stages, wherein are contained the recording mechanism and associated equipment to yield the final spectrum as a plot of voltage vs. frequency.

D. Commercial and Other Analyzers

Several commercial spectrum analyzers are available at present, but they all fall short of the desired characteristics either in frequency range, sensitivity of resolution. For example, the General Radio Wave Analyzer, which has an excellent narrow-band filter, requires a pre-amplifier to obtain sensitivity, has a maximum frequency of only 20 kc, and requires a tedious point-by-point analysis to obtain the complete spectrum. The Sonic and Ultrasonic Analyzers built by Panoramic Radio Products, Inc., provide an oscilloscopic representation of the input spectrum. However, a pre-amplifier is necessary, two seperate analyzers are required to cover the entire frequency range, and resolution falls short of that desired for noise analysis.

A spectrum analyzer built specifically for the purpose of obtaining noise spectra was designed by R. L. Kelleher.[9] The system covers the range of frequencies from 40 cps to 20 kc. It uses a "Q-Multiplier" narrow-band circuit, and the output is read on a long-time-constant thermal milliameter. The analyzer was designed to yield the the a-m spectrum of a u-h-f transmitter by a point-by-point analysis.

All the equipment mentioned here has been used in preliminary work relative to this thesis, and this investigation has made clear the need for a good narrow-band filter with sharp "skirts" (the Q-Multiplier, for instance, provides a narrow band width, but retains the gradually sloping-off characteristic of a simple tuned circuit). Also it is highly desirable to avoid slow point-by-point analysis methods. The system described in the following chapter has attempted to incorporate these characteristics, in addition to extending the range of noise frequencies which can be measured, and providing a method of obtaining the f-m spectrum.

CHAPTER II

DESIGN AND CONSTRUCTION OF A NOISE SPECTRUM ANALYZER

A. Discussion of Proposed System

The block diagram shown in Fig. 1 shows the system which was proposed to accomplish the requirements stated in Chapter I, section C. A brief discussion of the entire system will be followed by a more detailed analysis of the design and construction of each section.

1. Preselector and Detector. For a-m measurements the microwave carrier is demodulated by a silicon crystal detector and the noise sidebands are fed to the measurement section. For f-m spectral data, the f-m is converted to an equivalent a.m. through the use of a resonant cavity and the resultant carrier is again demodulated. The preselector stage contains a special circuit for measuring crystal as well as removing amplitude-modulation noise from the frequency-modulation spectrum. Also in this section is contained a calibration circuit and an input attenuator to prevent overload of the measurement section.

2. Measurement Section. The noise voltage is first amplified in the pre-amplifier, after which it is fed to the r-m-s indicator for wide-band thermal measurement and to the balanced mixer as the first step in narrow-band spectral analysis. The spectrum analyzer makes use of the well-known superheterodyne principle. The noise input, whose magnitude is desired in a narrow band centered about frequency f_i (let f_i be 1 kc), is mixed with a strong local oscillator signal of frequency $f_1 = f_i + f_o$, where f_o is a fixed intermediate frequency (in this case 80 kc). The output of the mixer

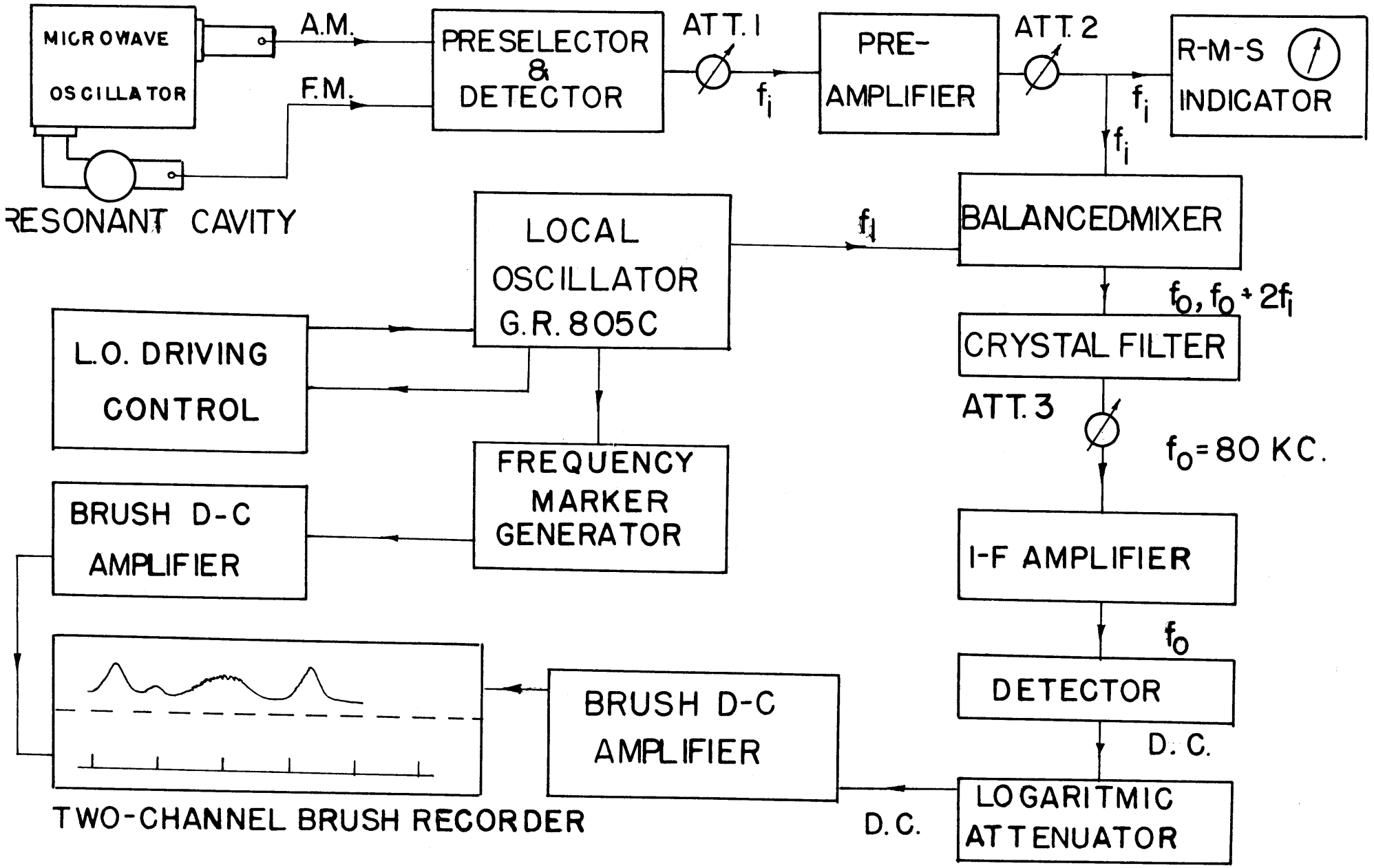

FIG. 1 BLOCK DIAGRAM OF ANALYZER SYSTEM

contains many frequencies, but those which fall within the pass band of the i-f amplifier are f_o (80 kc), f_1 (81 kc) and f_o+2f_i (82 kc). The components of frequencies 80 kc and 82 kc are of equal voltage magnitudes (proportional to input signal voltage), and are small compared to the local oscillator voltage at 81 kc. It is necessary that such a voltage relationship be maintained if linear mixing is desired.[10] Only the component at the i-f center frequency f_o (80 kc) must be allowed to enter the i-f amplifier. The other two frequencies are eliminated by using a narrow-band crystal filter (which does not pass 82 kc), and by employing a balanced mixer, which does not contain the local oscillator signal in its output.

The full range of input noise frequencies are covered by mechanically driving the local oscillator from 80 kc to 140 kc, thereby providing for coverage of input frequencies up to 60 kc.

The input noise signal, converted in the mixer to 80 kc, is amplified, detected and processed by a logarithmic attenuator. The latter device extends the range of input voltages which can be measured without a change in circuit gain. Finally, the signal, now d.c., is fed to the recording section.

3. Recording Section. Because the local oscillator is continuously driven, the recording section must be capable of presenting the system output in a continuous fashion as it comes from the measurement section. This is accomplished by using a Brush Recorder which presents the data on a strip of ruled paper tape driven by a synchronous motor. The Recorder has two channels, one of which is used to record the spectral data, and the other to record frequency markers which indicate the input noise frequency being measured. The latter channel is fed by the frequency marker generator, which is in turn triggered by the local oscillator.

The entire system is operated over the linear regions of the various sections, with overload meters placed at key points to insure that linearity is maintained during a noise analysis. In this way, the analyzer is made direct reading after an initial calibration.

Finally, once several initial controls are set, the analyzer is designed to run automatically and shut itself off after an entire run has been completed.

A detailed analysis of each stage of the spectrum analyzer will now be undertaken. The discussion will begin with the measurement section, of which the pre-amplifier is the input stage.

B. The Pre-Amplifier

The pre-amplifier must have two basic characteristics. First of all, the noise generated within the amplifier must be sufficiently low to allow for the detection of the smallest input signal. The second requirement is that the band width of the stage to the 3 db points be approximately 20 cps to 60 kc.

As was pointed out in Chapter I, the ultimate irreducible noise source in an amplifier is the thermal noise generated in its input resistor. For this system the value of that resistor is 200 ohms, the crystal detector load resistance. Further, the minimum measurement band width provided by the crystal filter will be shown to be 10 cps. Using Johnson's formula for thermal noise (equation 1), the minimum noise at the input to the pre-amplifier is calculated to be 165 db below one volt or .00562 microvolts.

In addition to the thermal noise generated in the input resistance, the shot noise, flicker noise, hum and microphonics generated in the input tube will limit the sensitivity of the pre-amplifier. In order to make the amplifier sensitivity as large as possible, a transformer is introduced between the detector load resistance and the first tube. This input transformer may be seen in the schematic diagram of the pre-amplifier, Fig. 2.

The problem of designing an audio transformer with a 200 ohm input impedance, a reasonable response from 10 cps to 60 kc, and a voltage gain of 10, was solved by the Freed Transformer Co. of New York, who supplied the unit used here. Figure 3 shows the frequency response characteristic of the input transformer. The sudden rise of the response curve near 40 kc is due to the self-resonance of the transformer leakage inductance with distributed and stray capacity. This rise is equalized in the pen-

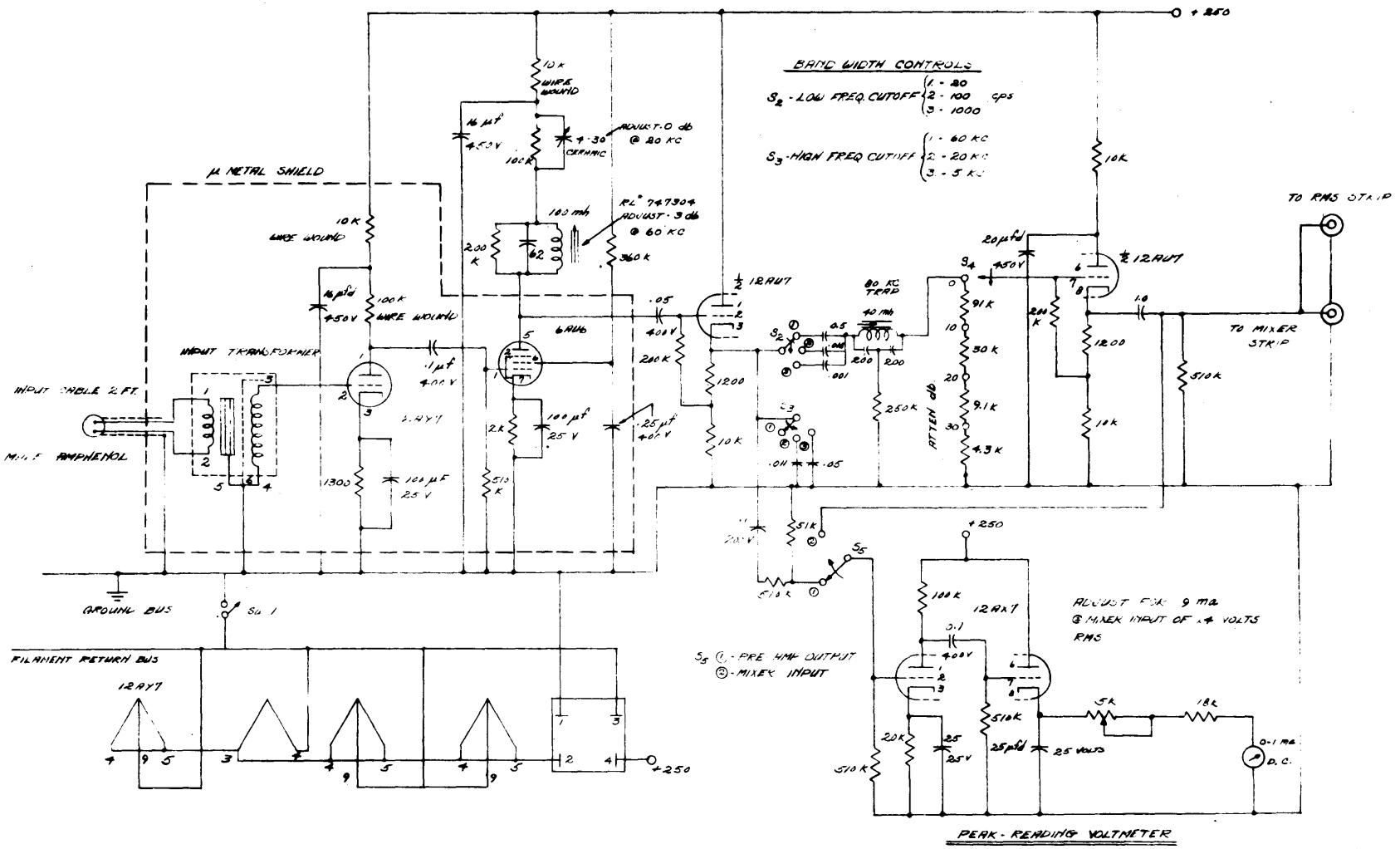

FIG. 2 PRE-AMPLIFIER SCHEMATIC

FIG. 3 FREQUENCY RESPONSE CURVE OF FREED TRANSFORMER NO. 23679

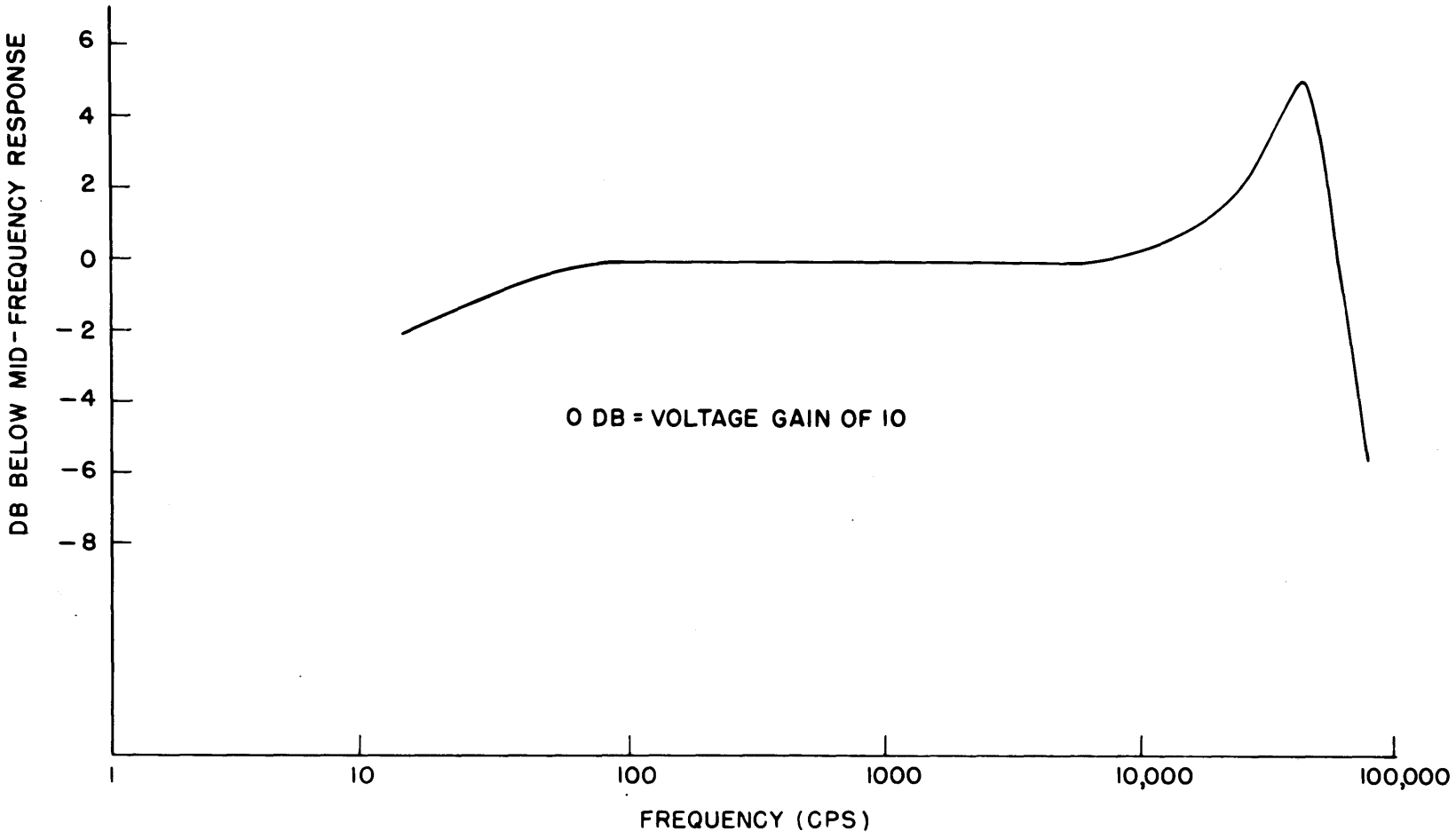

tode stage of the pre-amplifier by the variable capacitor across the load resistance, which flattens the response above 20 kc. The tuned plate circuit then raises the response near 60 kc.

The first vacuum-tube stage is a 12AY7, a General Electric miniature triode with special low-microphonic construction. The equivalent shot noise resistor (Chapter I, section B-2) given by equation (2) is 1,930 ohms. Because of the transformer present between this resistance and the 200 ohm input resistance, the shot noise resistance must be referred to the input by dividing by the square of the transformer turns ratio or 100. The total effective input resistance is then 200 + 19.3 = 219.3 ohms, while without the input transformer it would have been 200 + 1,930 = 2,130 ohms!

The three stages of gain, transformer, triode and pentode supply a total gain of 90 db, about the maximum which could be obtained together with the desired band width. These stages are shock mounted and enclosed in a mu-metal shield to avoid stray hum pickup. Wire-wound plate resistors are used as suggested by Terman[11*] to reduce resistor noise.

A buffer stage, in the form of a cathode follower, is placed between the pentode stage and the band width controls, output attenuator, and the peak-reading voltmeter. The second cathode follower provides a low impedance output from the pre-amplifier.

Figure 4 shows the overall frequency response characteristic of the pre-amplifier, as well as the effect of inserting the various band width control filters.

To insure that linearity of the system is not destroyed by overload, a peak-reading voltmeter was added to the amplifier. This unit consists of a triode amplifier and an infinite input impedance detector.[11**] The 1 ma. d-c meter is adjusted to give a

* p. 366

** p. 563

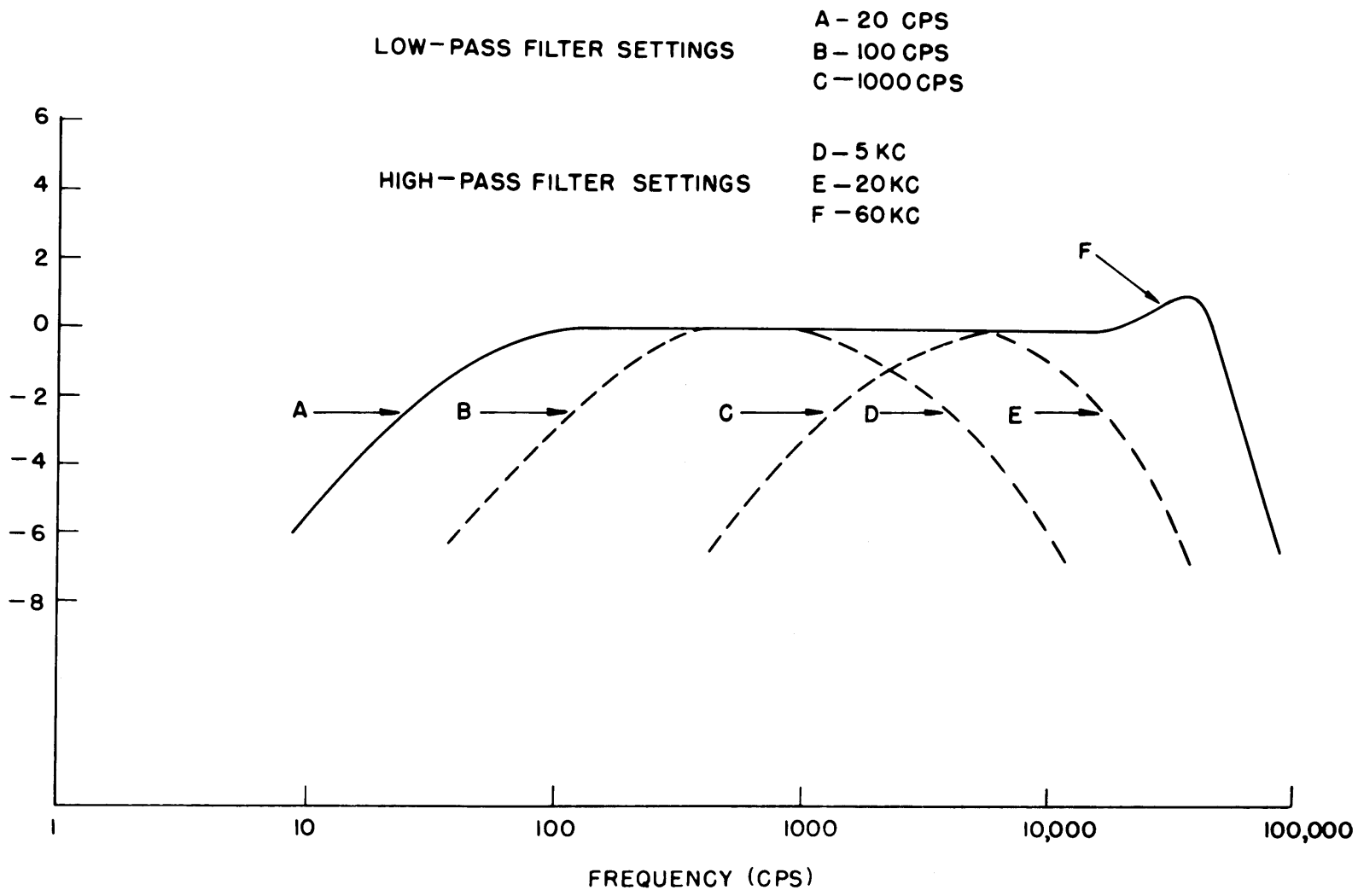

FIG. 4 FREQUENCY RESPONSE CURVE OF PRE-AMPLIFIER

pre-set reading of 0.9 ma. when the pre-amplifier is overloaded (see Fig. 5). Switch 5 (Fig. 2) selects the input to the peak-reading voltmeter, which may be either the pre-amplifier output or the mixer input. These two voltages are seperated by an attenuator and the band width controls. Such an arrangement is necessary because the mixer overloads at a voltage which is 20 db below the maximum pre-amplifier output of 20 volts peak. The meter circuit is so designed that the meter reading which indicates overload is the same for either position of switch 5.

The 80 kc trap inserted between the cathode followers insures that no signal at the intermediate frequency passes through the pre-amplifier.[12] The trap is a bridged-T filter.

Plate voltage is supplied by a well filtered and regulated power supply. Any tendency to oscillate is removed by the use of several decoupling filters in the amplifier plate circuits. Tube filaments may be operated from an a-c or d-c source, but runs are taken with the filaments on d.c.

FIG.5 VOLTAGE LINEARITY CURVE OF PRE-AMPLIFIER

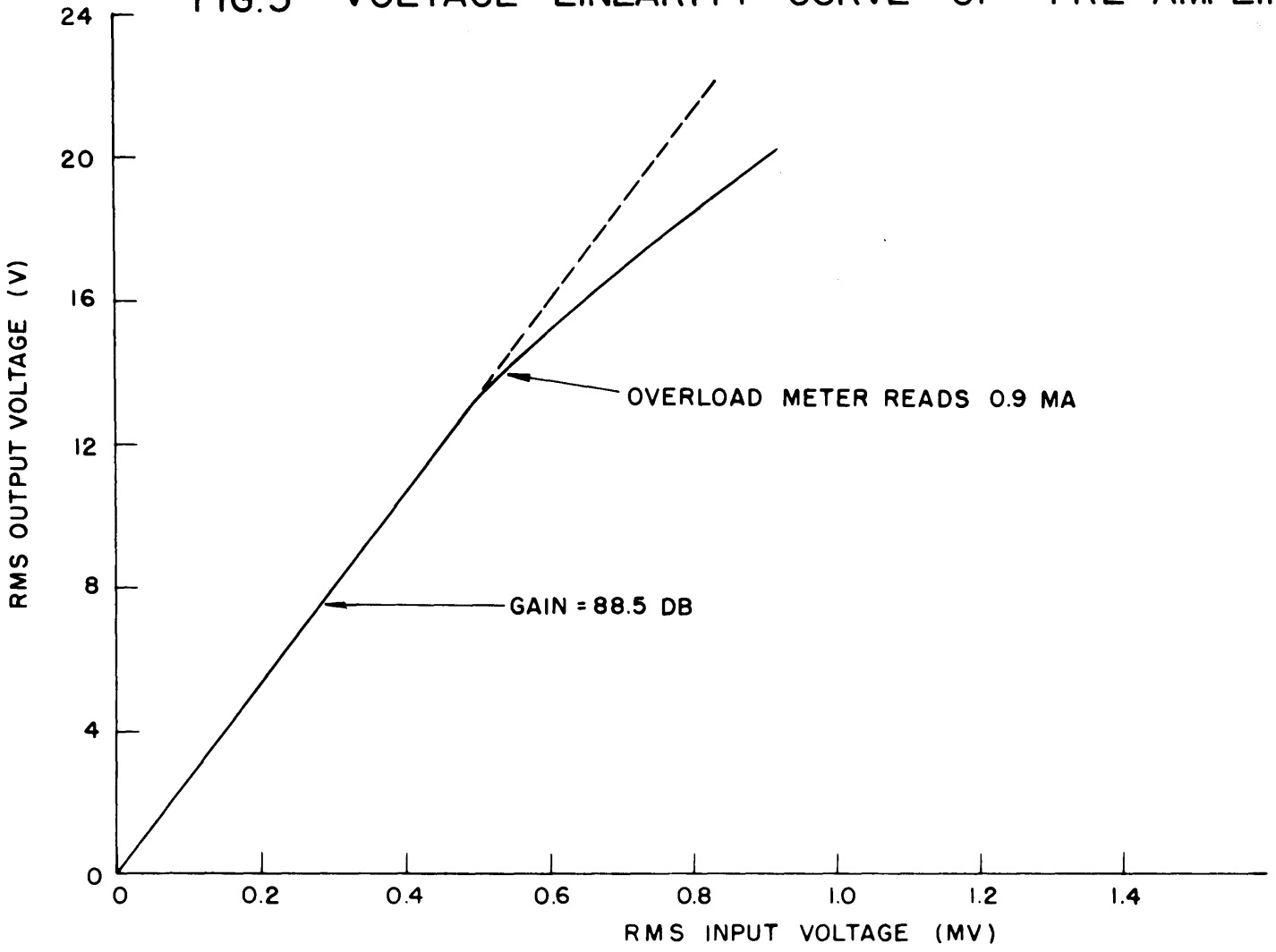

C. The Balanced Mixer

As was pointed out in section A. of this chapter, the mixer stage of the analyzer was made of the balanced type in order to remove the strong local oscillator signal from the mixer output. At low signal frequencies, the corresponding local oscillator frequency will be within the band pass of the crystal filter, and unless balanced out, the local oscillator signal will appear in the system output.

The balanced mixer is shown schematically in Fig. 6. The first tube (6C4) is a phase inverter. Although this cathode-follower type of phase inverter provides little in the way of gain, it is extremely reliable and simple to adjust. The 5 Kilohm potentiometer in the cathode resistor balances the inverter output and prevents the generation of harmonics of the input frequencies in the mixer.

The mixer itself is made up of two 6SJ7 pentodes designed to operate on the non-linear portion of their characteristics.[13] The signal voltages are applied in phase opposition to the first grids, while a strong local oscillator signal of approximately 10 volts is injected between cathodes and ground.

The local oscillator signal, which is in the same phase in both tubes, is balanced out in the common plate circuit. Balance control is supplied by a Gain and Fine Balance, both of which vary the screen supply voltage, and a Phase Balance, which varies the impedance of the plate circuit presented to each mixer tube.

The voltage linearity curve of the mixer is shown in shown in Fig. 7. Linearity is maintained up to an inout voltage of two volts peak, at which point the peak-reading meter on the pre-amplifier strip indicates overload.

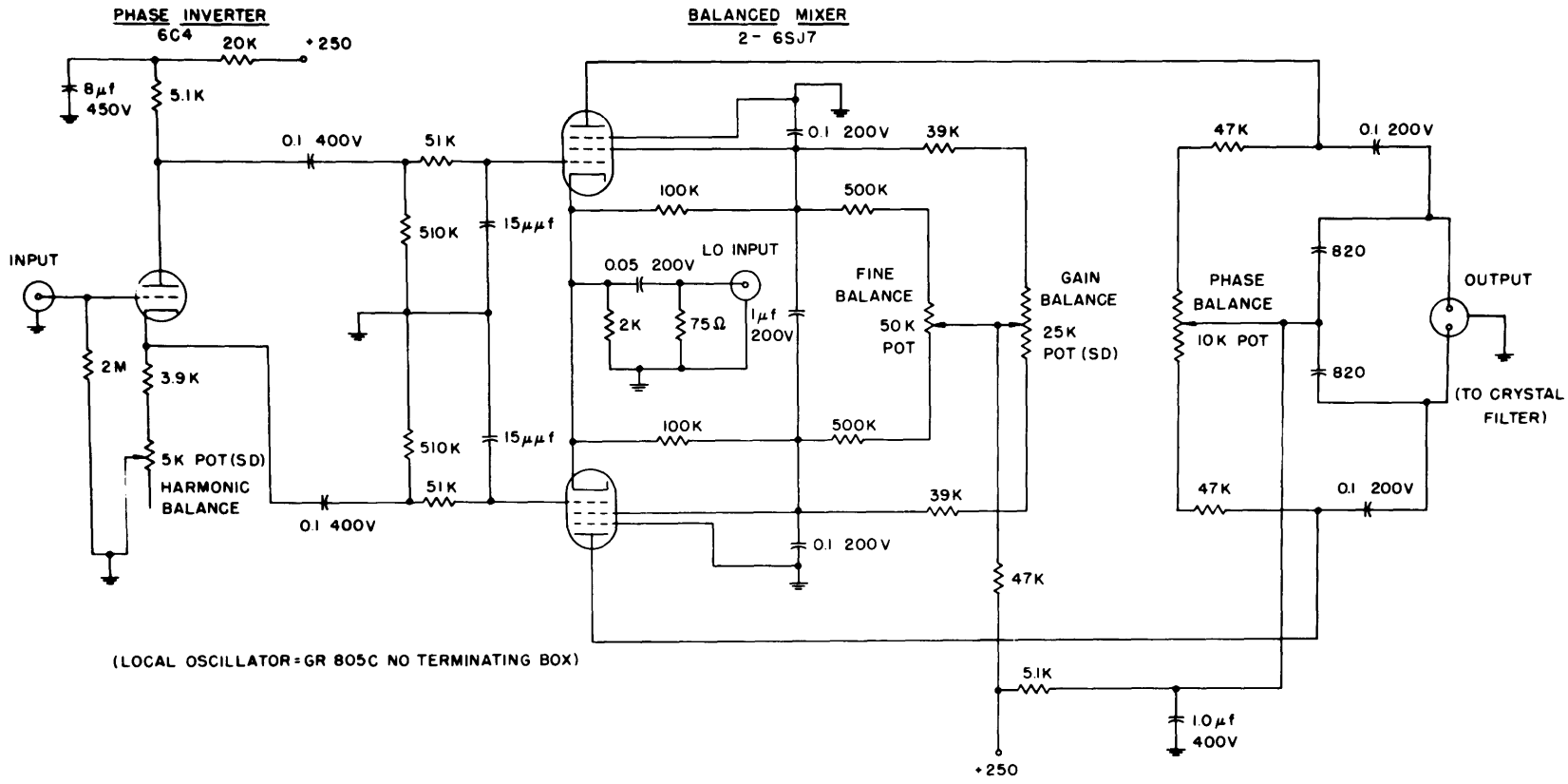

FIG. 6 BALANCED MIXER STRIP SCHEMATIC

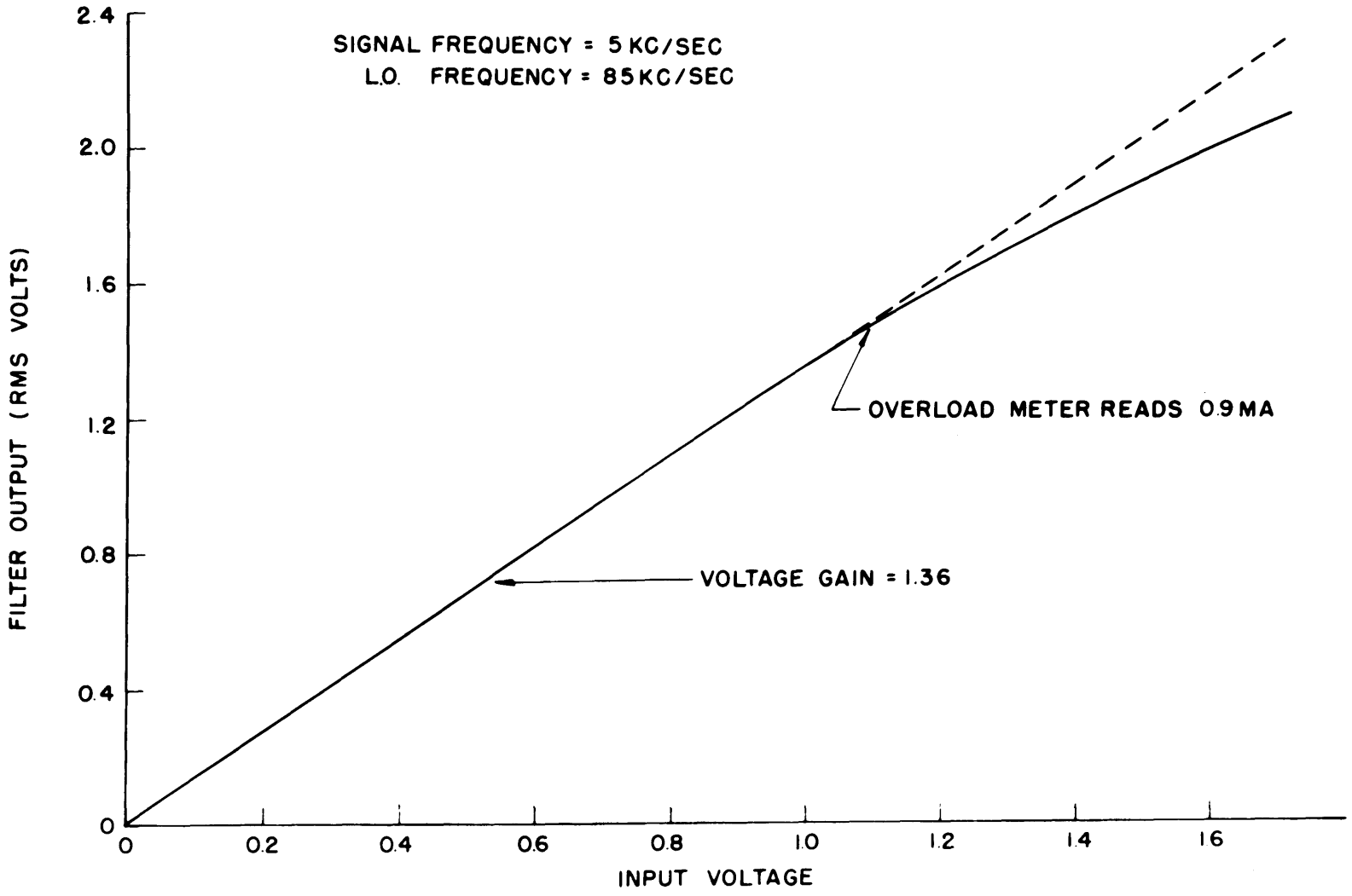

FIG. 7 VOLTAGE LINEARITY CURVE OF MIXER

D. The Crystal Filter

1. Requirements of the Filter Stage. The characteristics of the filter stage of the spectrum analyzer are determined by the following considerations:

(a) The band width of the filter must be sufficiently narrow to provide for seperation of closely spaced line spectra.

(b) In order to make measurements down to low audio frequencies, the attenuation characteristic must rise very sharply beyond the filter pass band. For example, in making a measurement at 20 cps, the output of the balanced mixer will contain equal signal components at 80 kc (filter center frequency), and 80 kc plus 40 cps. The filter must therefore have sufficient rejection 40 cycles off center to eliminate the unwanted signal.

(c) The time in which a measurement can be made depends inversely on the measurement band width. Because of the wide range of frequencies which are to be measured, too narrow a filter band width would necessitate very slow driving speeds and result in a prohibitively long strip of Recorder tape.

In order to satisfy these requirements, it was necessary to provide a filter with two different band widths. For frequencies up to 2 kc, where hum is predominant and sharp rejection is important, a 10 cps band width is desirable. Above 2 kc, such fine resolution is not necessary, and a 100 cps band width allows for a reasonable driving speed.

Preliminary investigation indicated that a filter having the characteristics mentioned above could be constructed using quartz crystals as elements.[14, 16, 17] Furthermore, the symmetrical lattice filter,[15] because it lends itself so easily to analysis, was chosen as the

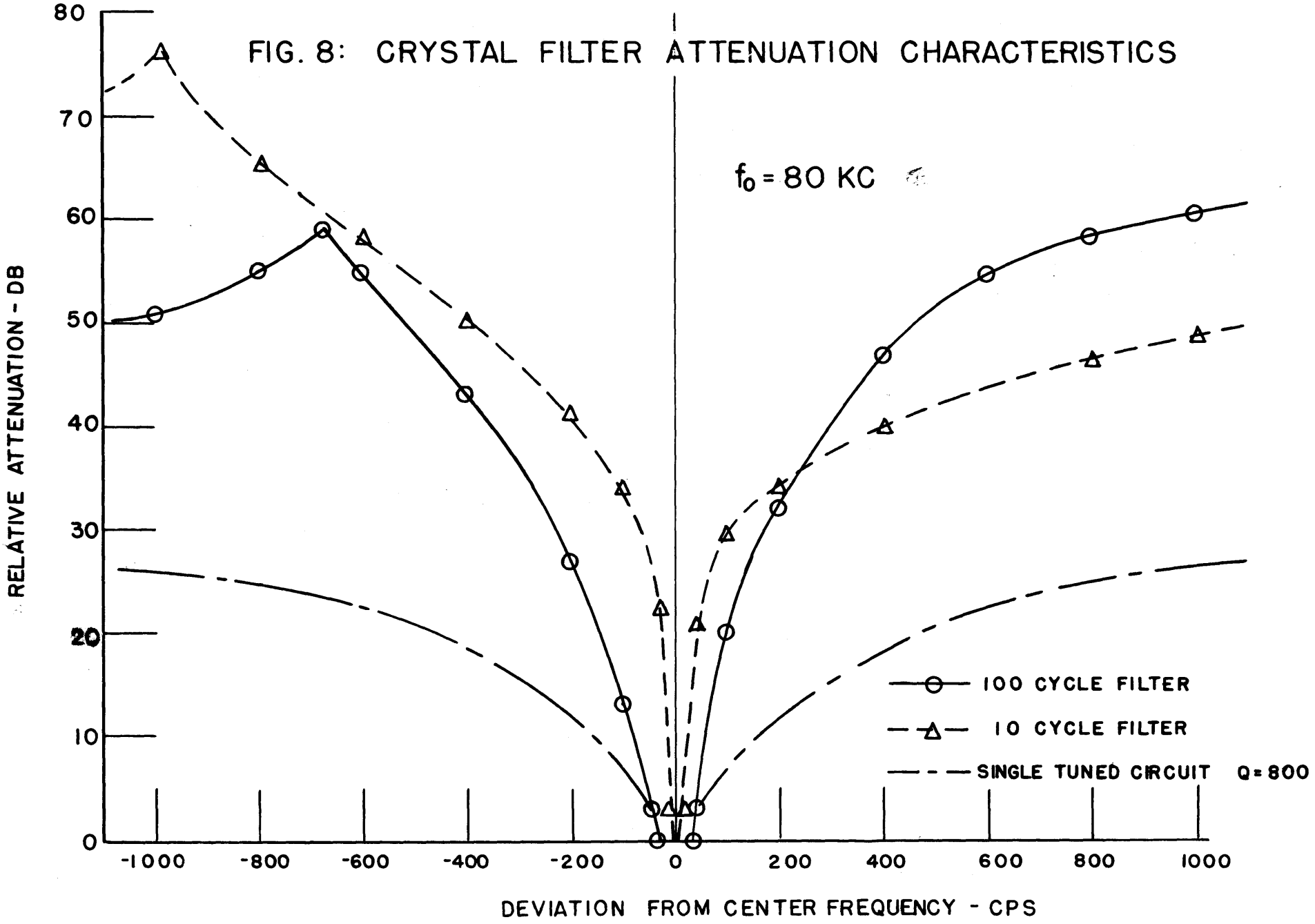
FIG. 8: CRYSTAL FILTER ATTENUATION CHARACTERISTICS
f_0 = 80 KC
RELATIVE ATTENUATION - DB
80
70
60
50
40
30
20
10
0
-1000
-800
-600
-400
-200
0
200
400
600
800
1000
DEVIATION FROM CENTER FREQUENCY - CPS
100 CYCLE FILTER
10 CYCLE FILTER
SINGLE TUNED CIRCUIT Q = 800

basic design structure.

2. Characteristics of the Crystal Lattice Filter. Investigation into the literature available on the design and construction of the crystal lattice filter indicated a definite need for a simple and practical method of designing such a filter. The author has attempted the derivation of such a design technique as part of this research. A complete discussion of the analytical development of the design procedure and the experimental techniques necessary to carry it out, as well as a description of the construction of the filter used in the spectrum analyzer, have been relegated to Appendix I of this thesis.

The characteristics of the 10 and 100 cycle crystal filters, both of which employ the same four quartz crystals, are shown in Fig. 8, along with the response curve of a simple tuned circuit. Note the two distinct differences between the 100 cycle filter and the tuned circuit, both of which have the same band width to 3 db points. First, the filter has very sharply rising skirts compared to the gradual rise of the tuned circuit. Secondly, the response of the filter is "flat" over most of the pass band, whereas the characteristic of the tuned circuit follows the normal resonance curve and is never flat. Although the pass band is not well shown in Fig. 8, it was observed (on the oscilloscopic display device described in Appendix I) to be flat, except for minor ripples never exceeding 0.5 db, over about 60 cycles of the pass band.

The crystal filter is shown pictorially in Fig. 9. A single selector switch accomplishes the changeover from the 10 cycle to the 100 cycle band width. The "compensator" is used to provide equal voltage outputs at both band widths for a fixed sinusoidal input.

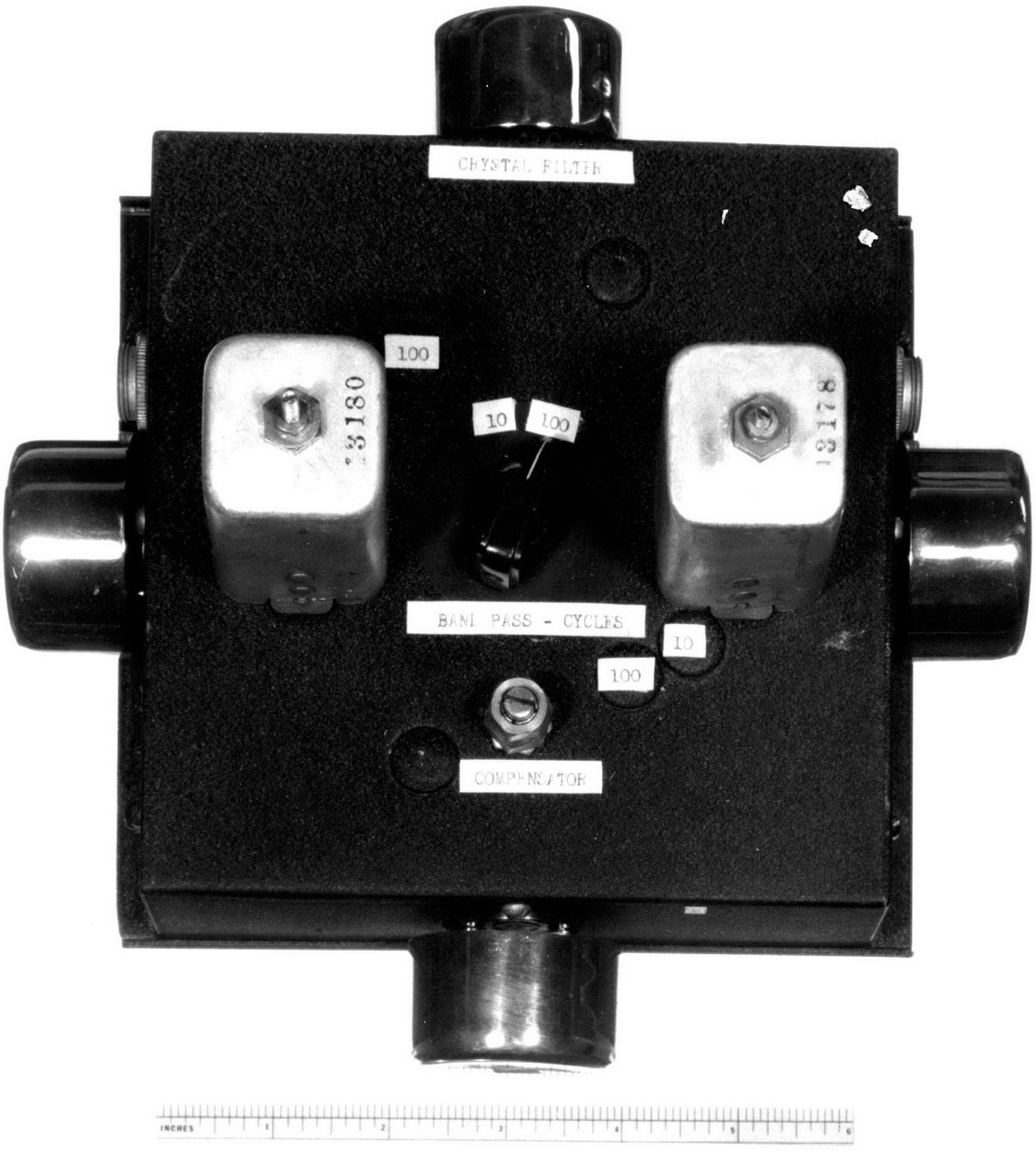

FIG. 9 PHOTOGRAPH OF CRYSTAL FILTER

E. The Intermediate-Frequency Amplifier Strip

The crystal filter, which may be seen schematically in Fig. 34 of Appendix I, is terminated in two double-tuned 80 kilocycle transformers. The input transformer primary is also the output coil of the balanced mixer, while the output transformer secondary presents the filtered signal to the i-f strip.

1. I-F Amplifier. The purpose of the i-f amplifier is to amplify the signal output of the filter stage to a level which can be detected and recorded. The intermediate frequency of 80 kilocycles was chosen on the basis of the following considerations:

(a) The i.f. should be far enough above the highest input signal frequency (60 kc) to prevent spurious feed-through at the intermediate frequency.

(b) A crystal filter must be built at the i.f. (The filter stage was, of course, designed after the choice of i.f.).

(c) The entire range of local oscillator frequencies should be obtained without the necessity of switching bands of the local oscillator (G.R. 805C Signal Generator) during a run.

The entire i-f strip is shown schematically in Fig. 10. The input cathode follower (6C4) acts as a buffer between the crystal filter and the filter compensator and i-f input attenuator. The gain control in the grid circuit of the 6AH6 is used to calibrate the analyzer with a fixed signal input.

The overall gain of the two tuned 80 kc pentode amplifiers is about 70 db. This is the gain required to amplify the minimum input signal to the minimum signal level of the Logaten (section E-3). The i-f band width is about 1500 cycles.

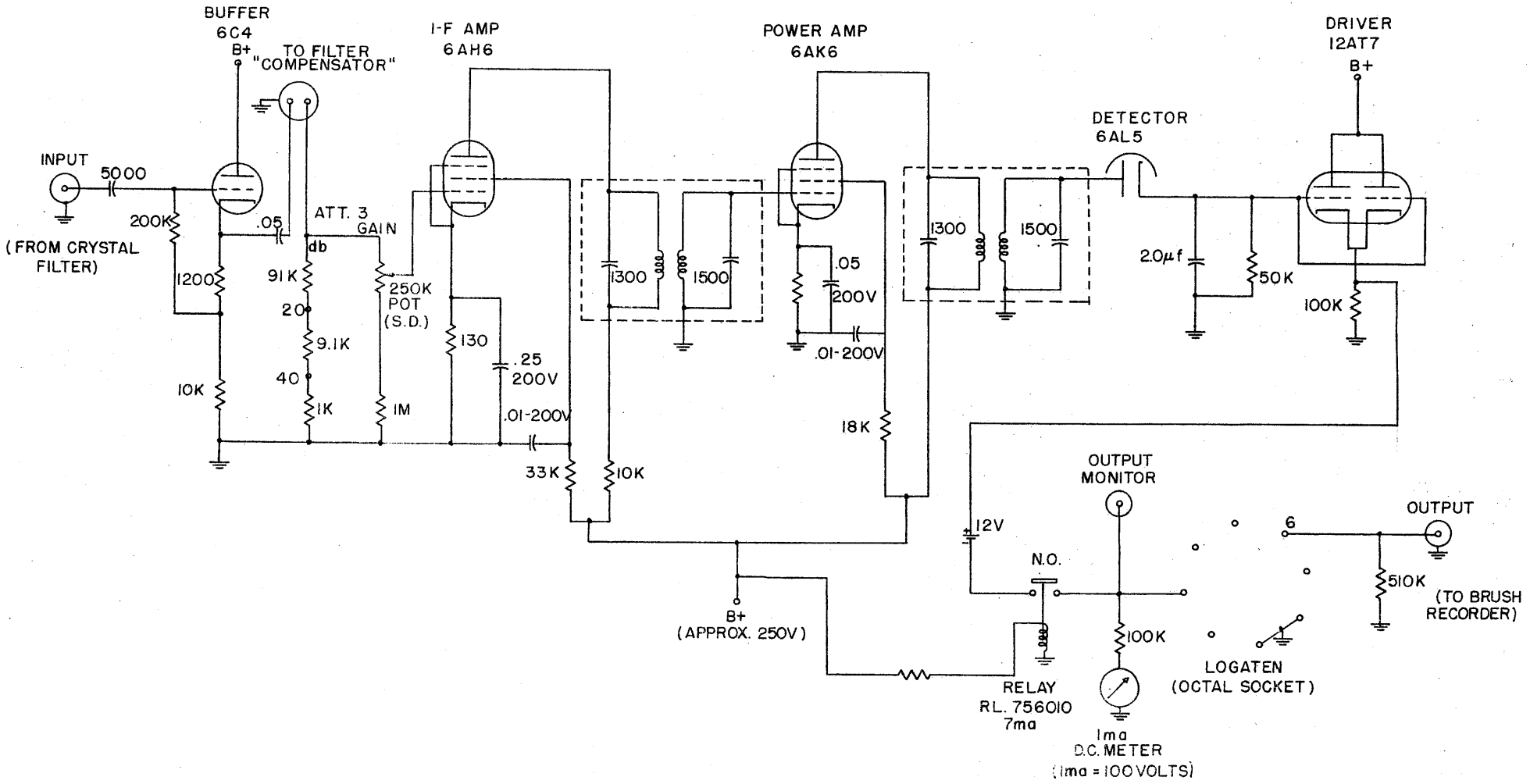

FIG. 10 I-F STRIP SCHEMATIC

2. Detector. The 80 kc i-f signal is converted to an equivalent d-c voltage in a conventional 6AL5 peak-reading diode detector. The detector handles voltages ranging from under 1 volt to a peak of 100 volts. The value of the detector load capacitor (2 microfarads) was selected experimentally after the entire analyzer was completed. The following considerations place the upper and lower limits on the value of the capacitor:

(a) Much of the noise to be measured is of a random nature. A small value of detector capacitance will allow the large random variations of the input signal to be recorded, while a large capacitor will tend to smooth out the recorded data and make it more readable.

(b) Too large a value of capacitance may cause some line-frequency spectral data to be "missed", as a large detector time constant will prevent the detector from following the input signal variations.

The value of 2 μf was selected by inserting a fixed-frequency input signal and increasing the detector capacitance until the shape of the recorded output began to distort.

At the output of the detector is a monitoring d-c voltmeter which is helpful in calibrating the analyzer, and provides a convenient indication of the signal level being recorded.

3. Logarithmic Attenuator.* The Kay-Lab Logaten is a network of non-linear circuit elements adjusted to give an output voltage whose amplitude is proportional to the logarithm of the amplitude of the input signal. This relationship is linear within one db, according to specifications, for input voltages form 0.3 to 100 volts, a 50 db dynamic range. Because the diode detector is not

* Kalbfell Laboratories Inc., San Diego, California

linear below one volt of output voltage, the range of Logaten input voltages used is one volt to 100 volts, a 40 db variation. The corresponding Logaten outputs, however, have a ratio of only 4:1, a variation which can quite easily be recorded. With the logarithmic attenuator then, the analyzer may be made to yield an output which reads directly and linearly in decibels. Furthermore, variations of input signal voltages as large as 100:1 or 40 db may be recorded with no change in signal gain.

The Logaten has an input impedance of 20,000 ohms and must be fed by a low impedance source of 500 ohms output impedance or less. It was therfore necessary to place a cathode follower between the detector and the Logaten. The cathode follower however, has a d-c output even with no input signal. In order to balance out this zero-signal bias, a 12 volt battery is placed in series with the cathode follower output. A relay opens the battery circuit when the analyzer plate voltage is off, and thereby prevents unnecessary drain on the small battery. The zero-signal cathode follower bias is generally 12 volts, but any small variations from this value may be compensated by changing the plate supply voltage slightly. This adjustment is part of the initial calibration procedure for the analyzer.

F. The Brush Recorder

The d-c output of the logarithmic attenuator, which voltage is proportional to the logarithm of the spectrum analyzer input voltage, at a frequency selected by the local oscillator and in a band width selected by the crystal filter, is finally fed to the recording section.

The spectral data is amplified by a Brush (BL 932) D-C Amplifier and thence delivered to one channel of a two-channel Brush Recorder (BL 202) Oscillograph. The data is recorded here by a magnetically driven pen.

The Brush Recorder and its associated D-C Amplifier have a maximum response frequency of 100 cycles per second. The low frequency cut-off of the Recorder, combined with the long time-constant of the diode detector, helps to smooth out the spectra of the random input voltages, and removes high-frequency transient effects from the output.

The second channel of the Brush Recorder is used to present the frequency markers which are produced by the frequency marker generator (section H). These markers indicate the input frequency of the spectral data being recorded.

Figure 11 shows the frequency response curve of the entire spectrum analyzer system. The response is 3 db down at 25 cps and at 50 kc, and may be used beyond these points with proper corrections.

FIG. 11 FREQUENCY RESPONSE CURVE OF SPECTRUM ANALYZER

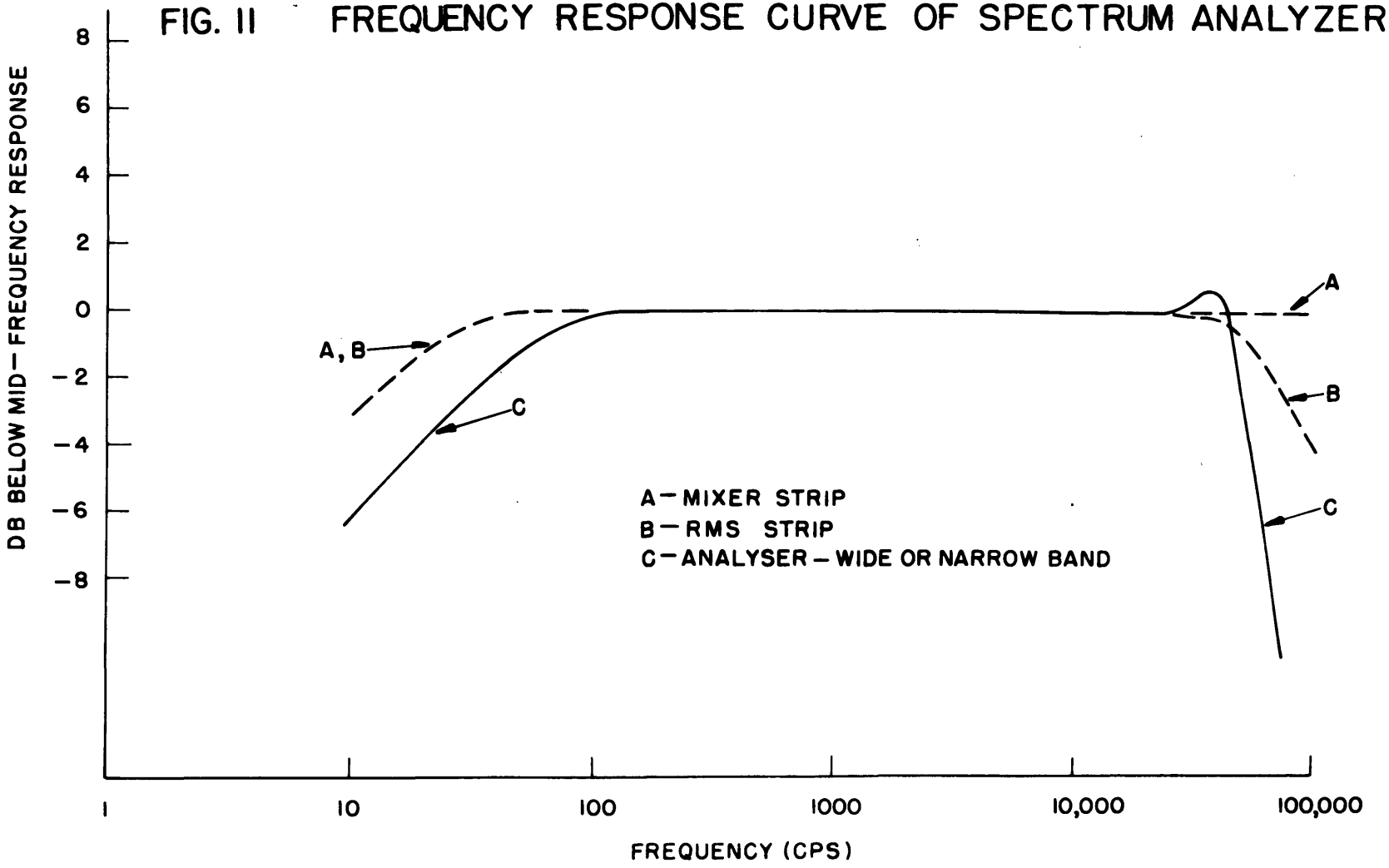

G. The Local Oscillator

A General Radio 805C Standard Signal Generator was chosen as the local oscillator. It may be seen, along with its associated driving equipment in Fig. 22. The oscillator is driven by a leather belt which runs over its vernier dial. The motor driving control unit, shown in Fig. 12, operates as follows:

1. Up to 2 kc of input frequency, the local oscillator must be driven slowly enough to allow for build-up of a signal in a 10 cps band width. The driving motor is a 10 rpm, 110 volt capacitor motor. The slow speed (approx. 1.5 rpm) is controlled by a Variac, which is in the motor circuit so long as S7 is in the "slow" position.

2. At 2 kc, the motor drive and the Brush Oscillograph are turned off by a bronze rider on the vernier dial which throws microswitch 2. At this point, the filter band pass is changed to 100 cps, and the system attenuation may be altered if necessary.

3. Throwing S7 to the "fast" position starts the analysis once more by shorting S2. The motor is now directly across the line and runs at 10 rpm for the remainder of the run.

4. At 60 kc, the end of a run, a bronze rider on the main dial of the G.R. 805C opens microswitch 1, and the drive stops.

5. The oscillator dials may now now be returned to their starting positions by throwing S4 to the "reverse" position and holding down the "press to start" switch (S3) until S1 remains closed. Microswitch 1 will again stop the motor at the end of the rewind cycle. The Brush Oscillograph may be turned off during the rewind cycle by switch 6.

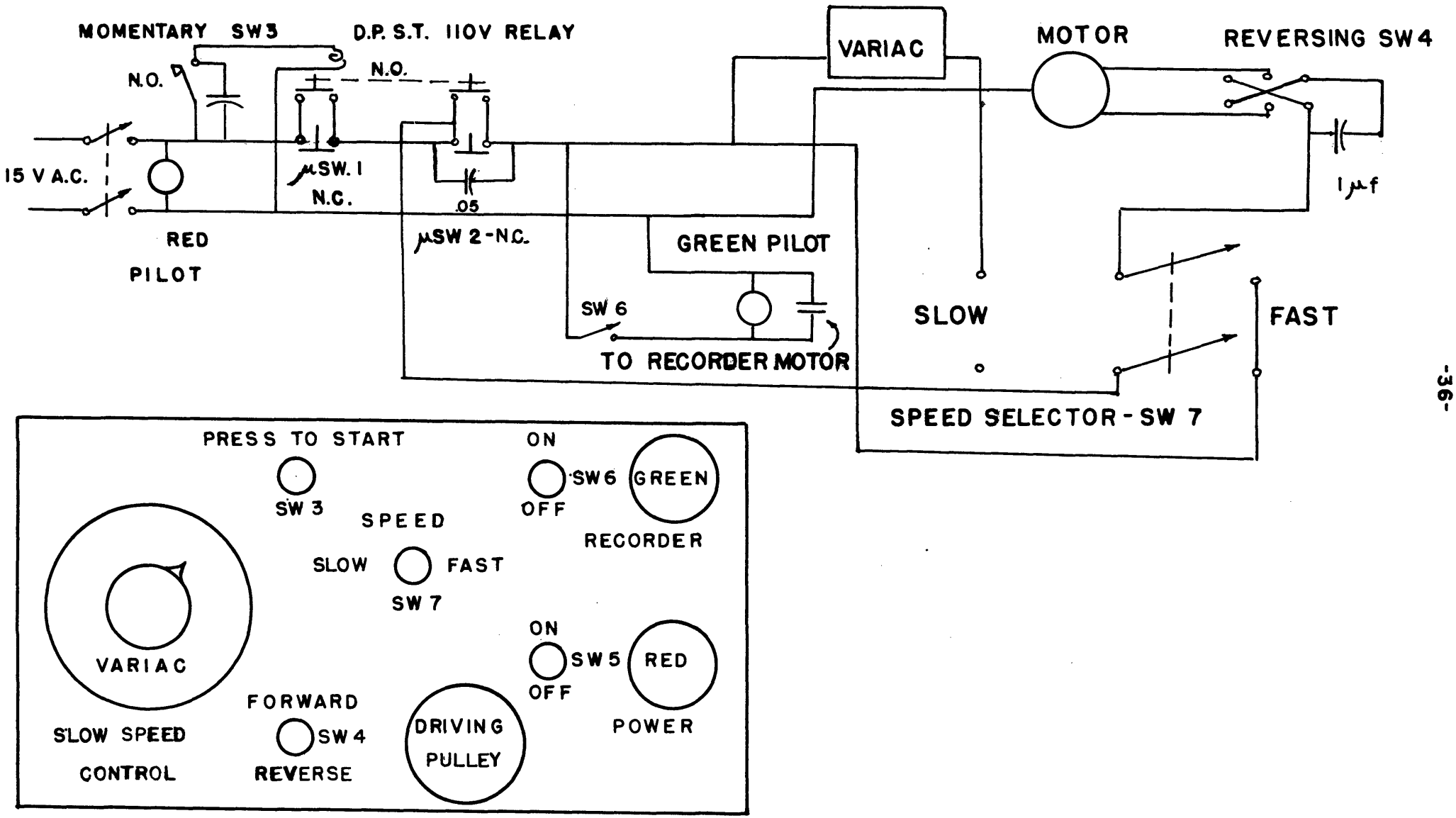

FIG. 12 MOTOR DRIVING CONTROL & POWER PANEL

H. The Frequency Marker Generator

In order that the frequency of the input signal being measured be recorded with its corresponding signal, frequency markers are provided on the lower channel of the Brush Recorder tape. The markers may be seen in the data shown in Figs. 24, 25, and 26.

The mechanism which produces these markers in synchronism with the local oscillator drive is shown in Fig. 13. A large plastic disk is ganged to the large dial of the G.R. 805C Generator. This disk is visible in Fig. 22. Small brass inserts are placed in the disk at positions corresponding to every 1000 cycles of local oscillator frequency from 80 to 100 kc. Above 100 kc (hence above 20 kc of signal frequency), the inserts are placed 2000 cycles apart.

The brass inserts trigger the relay of the marker generator (Fig. 13) whenever they contact the silvered springs which are secured to the oscillator casing and which ride on the plastic dial. The closing of the generator relay produces a narrow pulse of voltage. The pulse is amplified by a Brush (BL 932) D-C Amplifier after which it is fed to the Brush Oscillograph channel to be recorded.

The plastic dial is adjustable about its center, so that the first frequency marker, which specifies zero signal frequency, may be cause to coincide with a local oscillator frequency of 80 kilocycles per second.

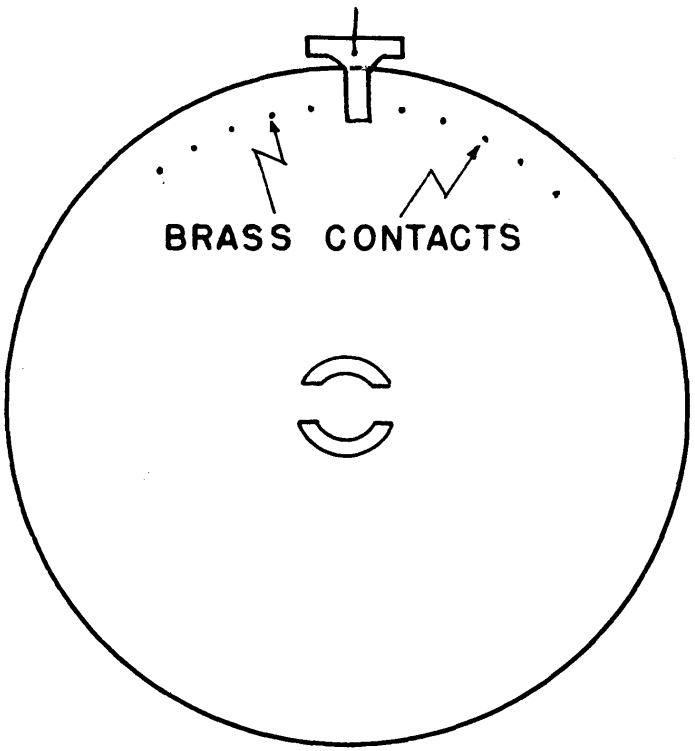

PLASTIC DISK GANGED TO
G.R. 805C DIAL

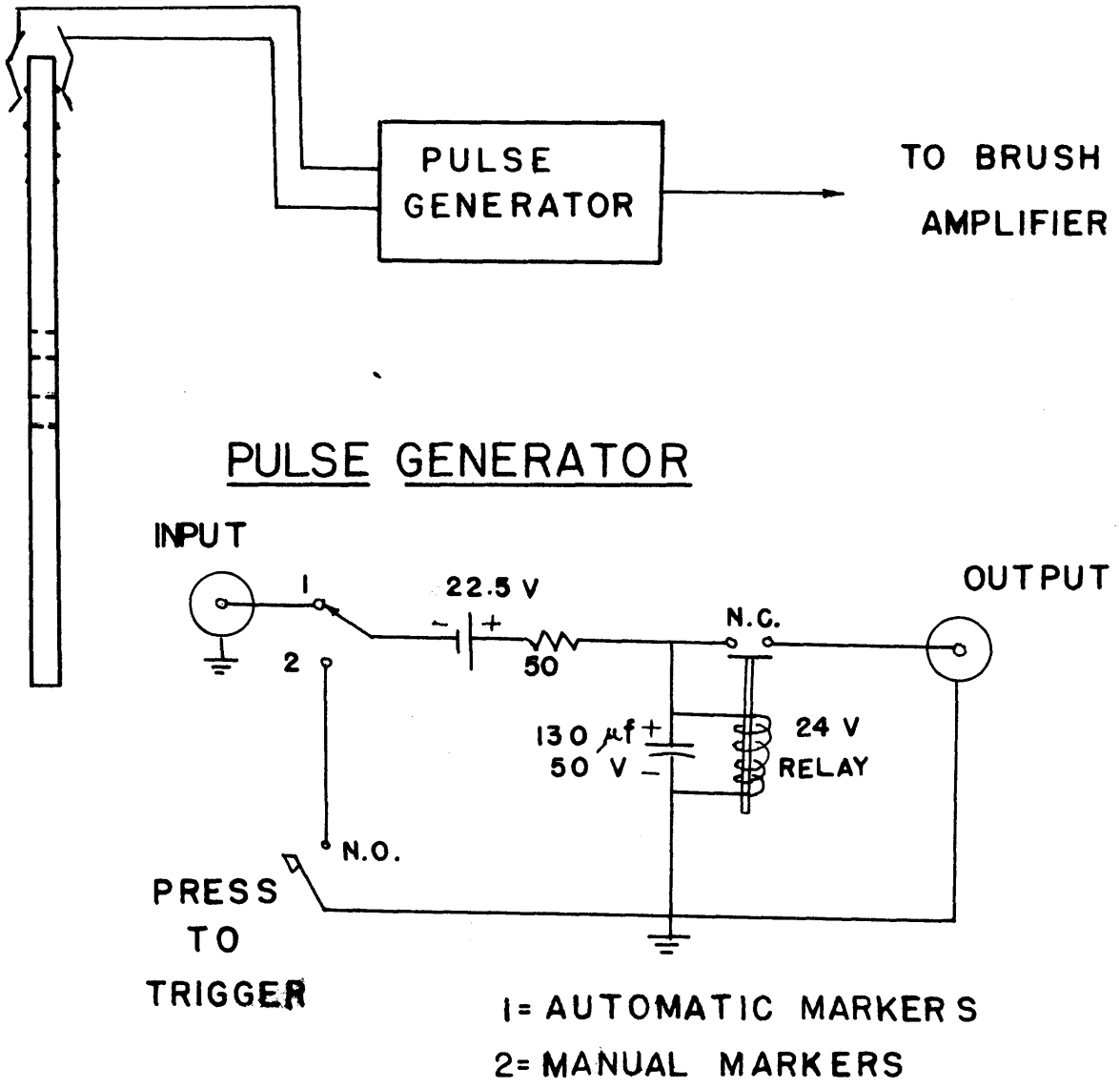

FIG. 13 FREQUENCY MARKER GENERATOR

I. The R-M-S Indicator

Because of the random nature of much of the noise to be measured, the true r-m-s value of the input signal voltage can only be obtained by a thermal measurement.

The r-m-s indicator, shown schematically in Fig. 14, is a wide-band amplifier terminated in a long-time-constant thermal milliameter.

Triode amplifiers are used to obtain the necessary band width, and a cathode follower provides a low impedance output to the 0-2 iilliampere thermal milliameter. Because a thermal meter can be damaged by small overloads, the milliameter is switched out of the circuit and replaced by a dummy load when the r-m-s indicator is not in actual use. A pilot light has been wired into the circuit to indicate that the meter is in operation.

The r-m-s indicator is connected directly to the pre-amplifier output, and the measurement band width is selected by the pre-amplifier band width controls.

The overall gain of the r-m-s indicator is approximately 60 db, which is sufficient to allow the measurement of the minimum wide-band pre-amplifier output (thermal noise in a 200 ohm resistor and in a 4 kc band width).

An adjustment is provided in the r-m-s indicator meter circuit for calibration of the indicator.

The frequency response curve of the r-m-s indicator is shown in Fig. 11. The wide band r-m-s system, including the pre-amplifier at its maximum band width setting, is 3 db down at 25 cps and 50 kilocycles per second.

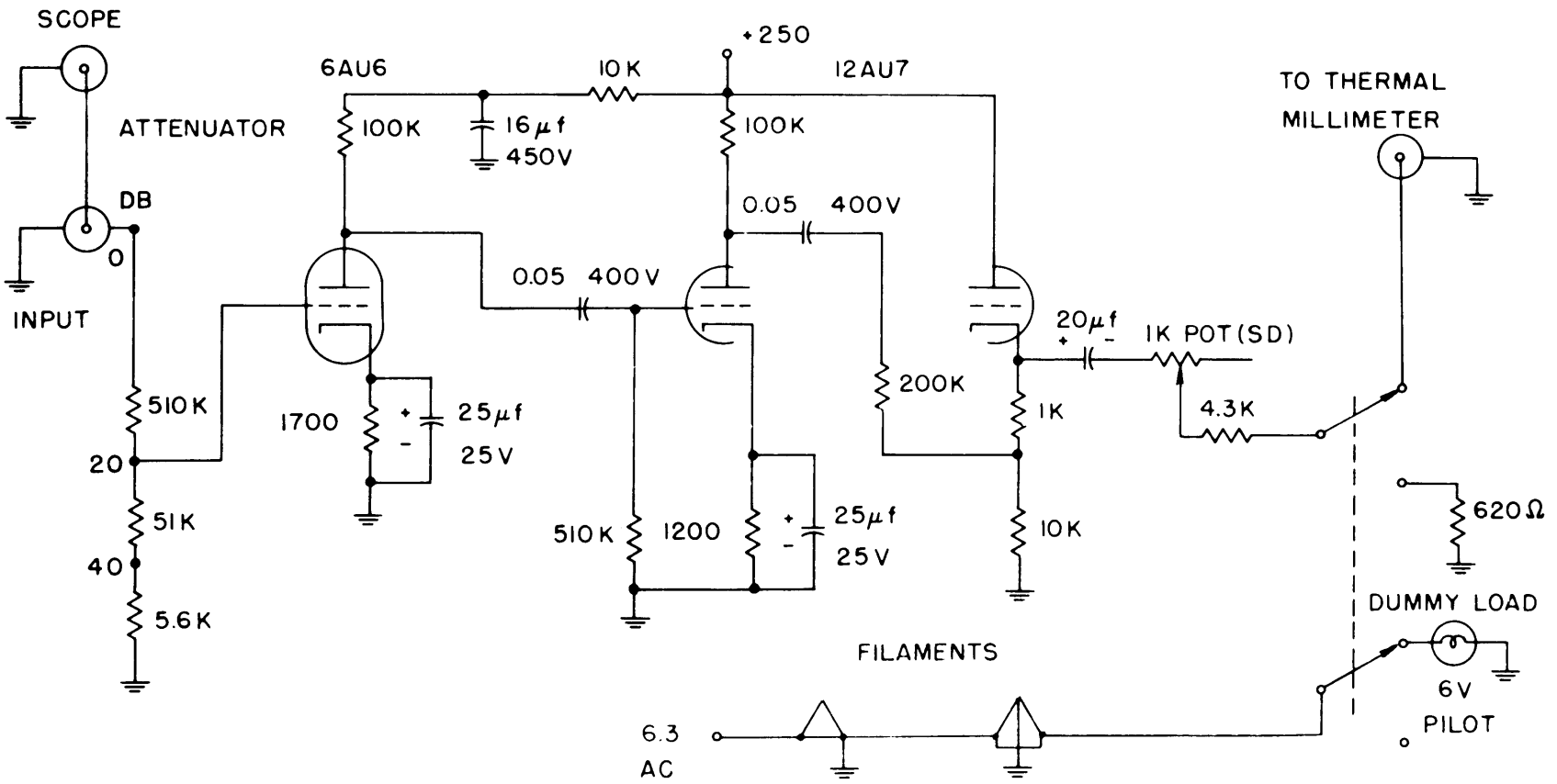

FIG 14 R-M-S INDICATOR SCHEMATIC

J. The Input Detector and Preselector Circuits

1. The Silicon Crystal Detector. The purpose of the detector section of the spectrum analyzer is to remove the X-Band carrier and present the noise modulation envelope to the analyzer. Because of the transit-time effects present in the 3 cm. band, the conventional diode detector circuits cannot be used. Rectification can still be accomplished, however, by making use of the non-linear relationship that exists between the voltage and current at a point contact with certain crystal surfaces. More specifically, a suitable rectifying element at X-Band consists of a fine tungsten wire which makes a small-area contact to a piece of silicon crystal. The resultant crystal unit has the voltage-current curve shown in Fig. 15A.

The 1N23B silicon crystal rectifier is a small cartridge which fits into a special waveguide holder (Fig. 15B). The electric field in the waveguide provides the crystal excitation, and the rectified output is removed through a coaxial connection. This arrangement is equivalent to an X-band generator with zero internal impedance to audio frequencies, a rectifying element and the crystal load. The detector load capacitance is provided by stray capacitance and the distributed capacitance of the coaxial line. This capacitance, while of the order of only a few micro-microfarads, is sufficiently large to by-pass the carrier frequency.

It is important that the crystal detector provide as little disturbance to the circuit being measured as possible. For oscillators with large power outputs, this can always be accomplished by placing padding, in the form of attenuators or directional couplers, between the oscillator and detector. However, when the power available is small, as in the case of some klystrons, the

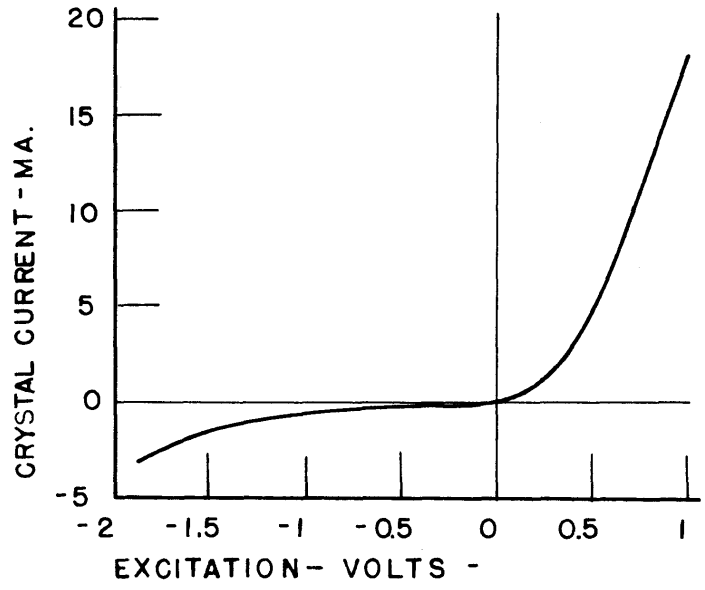

A. SILICON CRYSTAL CHARACTERISTIC

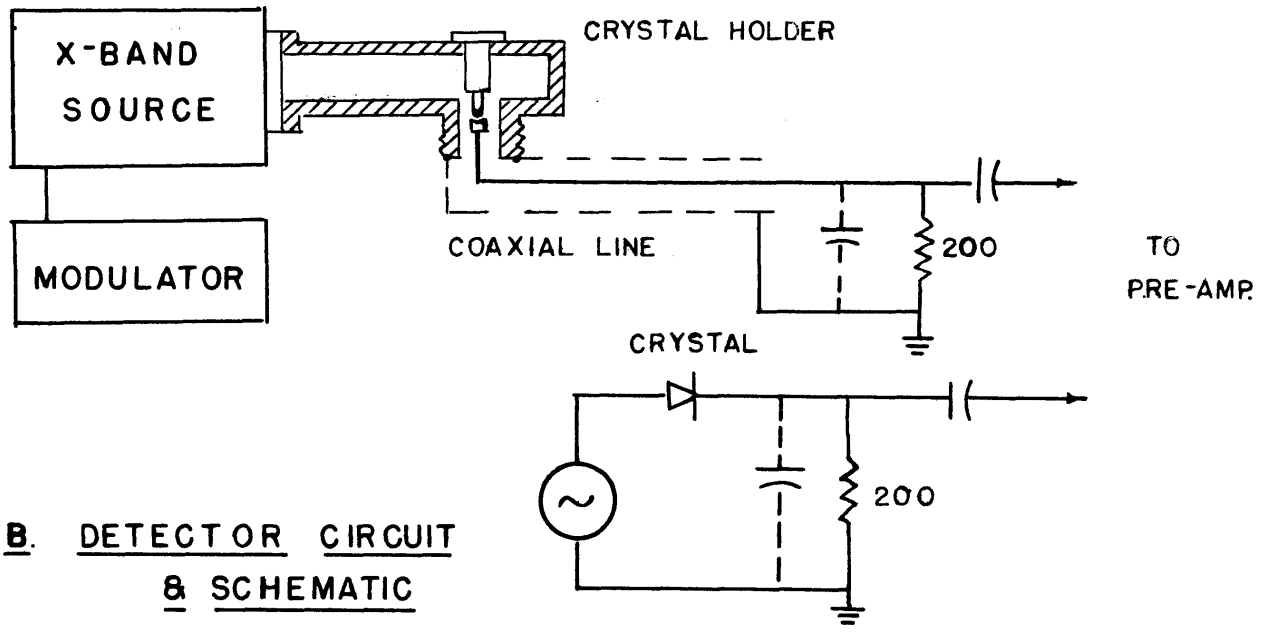

B. DETECTOR CIRCUIT & SCHEMATIC

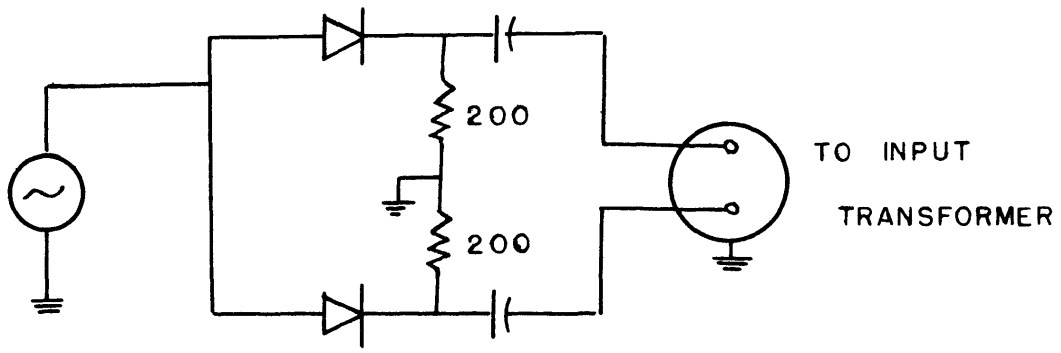

C. BUCKING CIRCUIT

FIG. 15 THE SILICON CRYSTAL DETECTOR

detector should provide as close a match as possible to the wave-quide characteristic impedance of 400 ohms. It was found experimentally that a 200 ohm detector load resistance resulted in a fairly good match, and this value is used in the analyzer.

It is worthy of note here that while the reduction of transit time effects permits the crystal rectifier to be used at very high frequencies, the efficiency of rectification (ratio of rectified d-c voltage to peak carrier voltage) is much smaller than the value which would be calculated from a consideration of the rectifier characteristic alone. This loss in efficiency is due to a small "barrier" capacitance across the point-contact area which tends to shunt the rectifying action of the crystal. However, for purposes of determining the noise modulation index, the detection efficiency is not of direct importance.

2. Determination of Modulation Index. Because the voltage-current characteristic of the crystal (Fig. 15A) is not linear for small excitation voltages, and further, since the efficiency of rectification is difficult to predict, it was necessary to determine by experimental means the relation between the measured voltages and the actual modulation index of the carrier noise.

The one fact that made such measurements feasible is that at very small voltages, the silicon crystal characteristic is almost ideally square law.[7]

It is shown in Appendix II that so long as the peak carrier input voltage to a detector falls on the square-law region of the rectifying element, then the ratio of measured r-m-s audio voltage to rectified d-c voltage (which shall be called the apparent modulation index), is 3 db above the actual modulation index (defined here as the ratio of r-m-s modulation voltage to r-m-s carrier

voltage). Note that the derivation has been carried out assuming only sinusoidal modulation, so that further analytic investigation is necessary to determine the relationship between the apparent and actual modulation indices for random phenomena in a square-law detector. So long as the above is borne in mind, the data obtained with the analyzer is useful for comparison of the noise outputs of various oscillators.

The data plotted in Fig. 16 was obtained by measuring the apparent modulation index of sinusoidal modulation on a klystron, as a function of rectified d-c voltage developed across the detector load resistance. The klystron was sinusoidally modulated at a frequency of 2,500 cps to a level far above the envelope noise, by an audio oscillator in the repeller circuit of the klystron. The audio measurement was made with the spectrum analyzer which, except for the detector section, was completed.

For rectified d-c voltages up to .02 volts, the apparent modulation index was constant, indicating that operation was on the square-law region. As the excitation was increased, the apparent index decreased until, at large voltages, the index approached the value expected for a linear detector, which is 3 db below the actual modulation index as defined herein.

This curve was taken for many good 1N23B crystals, and variations of not more than $\frac{1}{2}$ db were noted.

3. Crystal Detector Noise and Signal-to-Noise Ratio. It was mentioned in Chapter I, section B-2, that very little data is available on the character and magnitude of noise currents at low frequencies generater within a silicon crystal rectifier. It is apparent that the noise produced within the crystal will determine the system sensitivity, since no oscillator noise which is below the level of the detector noise can be measured.

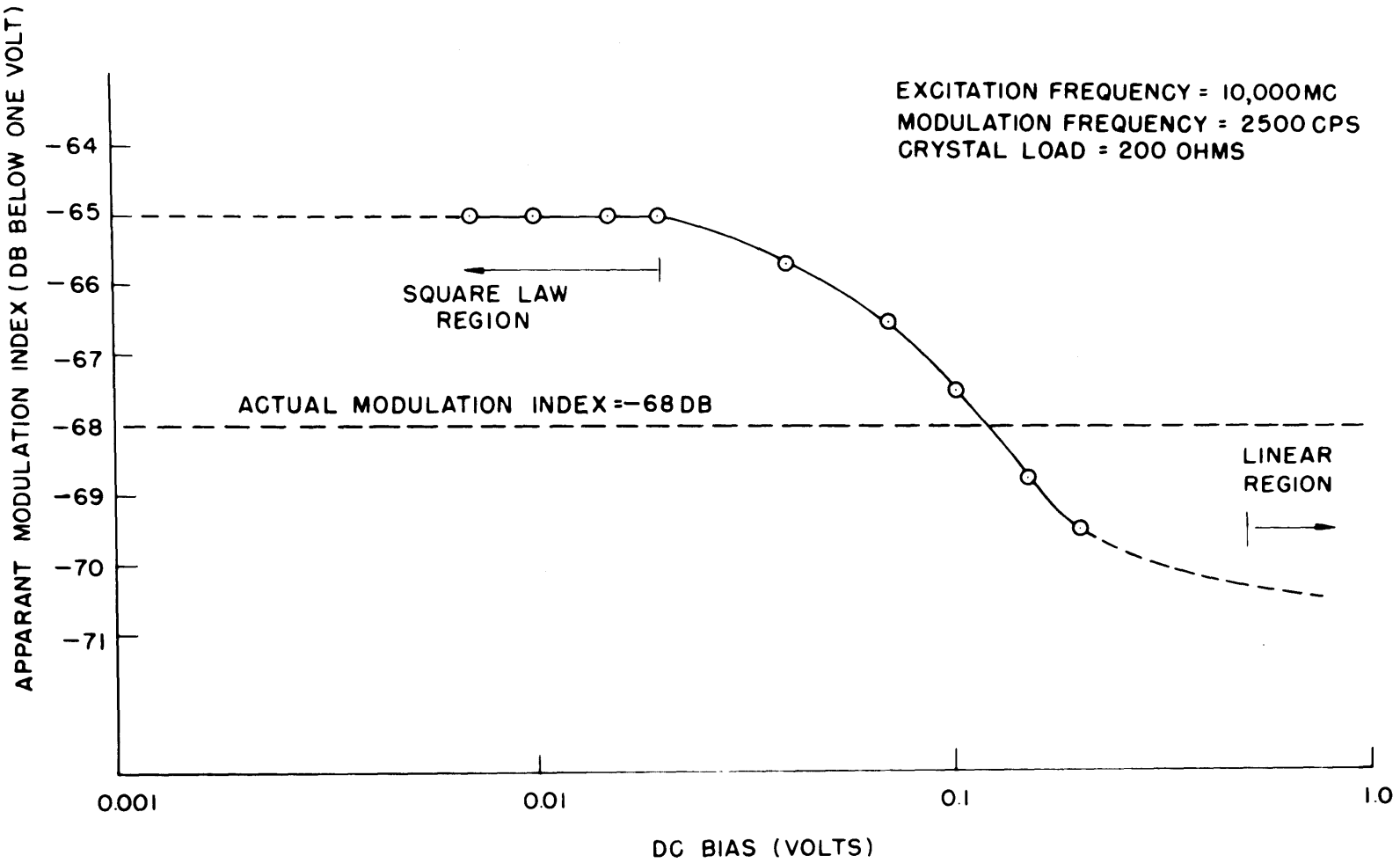

FIG. 16 APPARENT MODULATION INDEX VS. D-C BIAS IN23B CRYSTAL DETECTOR

In order to investigate the noise characteristics of silicon crystals under r-f excitation, it was necessary to find some way of eliminating from the detector noise spectrum those noise components which are due to envelope noise on the r-f carrier. The simple circuit which was devised to accomplish this is shown schematically in Fig. 15C. The audio "bucking" circuit, as it will be called here, consists of two crystal detectors which are excited by the same oscillator signal, to the same d-c level. The equal envelope modulation outputs of the two rectifiers are then cancelled out in the primary winding of the pre-amplifier input transformer. The noise generated by the crystals themselves however, while of the same random character, will never have the same time functions, and will therefore add statistically[3*] in the input transformer. The net input noise measured by the pre-amplifier will be

$$E_T = \sqrt{E_{C1}^2 + E_{C2}^2}$$

where

E_T = total r-m-s noise input to pre-amplifier

E_{C1}= r-m-s noise voltage generated by crystal detector 1

E_{C2}= r-m-s noise voltage generated by crystal detector 2

If the noise generated by each crystal has the same r-m-s voltage (E_C) then

$$E_T = \sqrt{2}\ E_C$$

The bucking circuit was first used to select low-noise crystals for future use with the analyzer. Among individual 1N23B crystals, differences in noise level of as much as 10 db were noted.

In order to find an optimum operating point for the detector, the bucking circuit was used to obtain measurements of wide-band noise generated within the detector, as a function of rectified d-c voltage level. The resultant data is shown in Fig. 17. Note

FIG. 17 R-M-S WIDE-BAND NOISE GENERATED BY A IN23B CRYSTAL

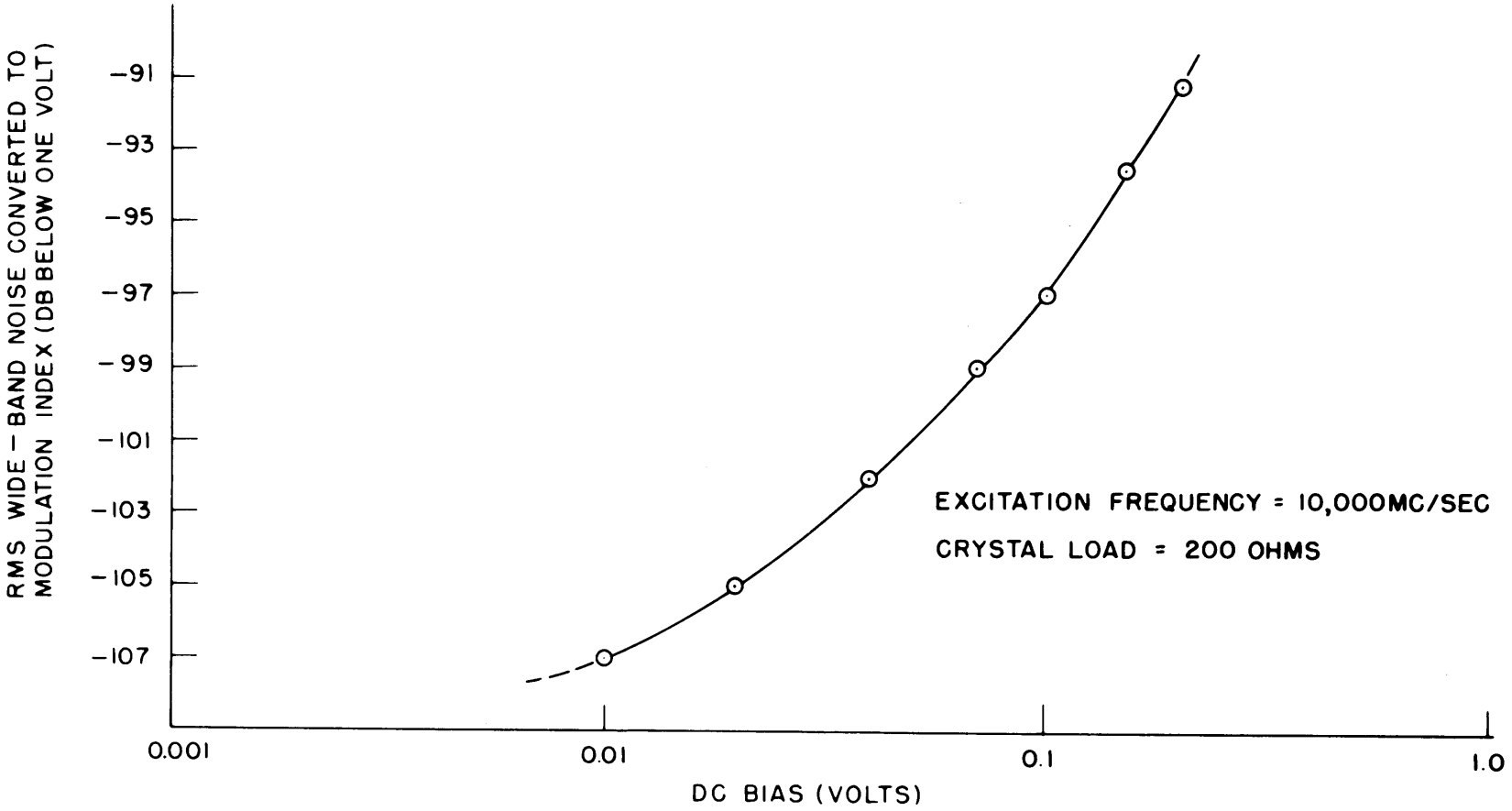

that the slope of the curve increases with increasing abscissa, and further that at about 0.15 volts the noise is increasing linearly with d-c voltage. This suggests that somewhere in the range of voltages plotted, there is a point where the ratio of input signal to crystal noise voltage is a maximum.

The curves shown in Fig. 18 bear out the validity of the last statement. The graph first shows the linear increase of signal voltage with rectified d-c voltage which would result if the crystal were entirely a square-law device. Use is then made of the data of Fig. 16 to plot the actual signal increase, taking into account the loss in signal due to operation beyond the square-law region. Finally, the signal-to-noise ratio is obtained by subtracting from each ordinate the loss due to increase of noise with d-c voltage, using the data of Fig. 17. An optimum operating point is thus obtained, lying at about 0.1 volt rectified d-c voltage, or equivalently, 0.5 ma rectified d-c current. This is the point of operation used in all data runs on the analyzer.

To calculate the actual modulation index then, it is necessary to increase all measured noise values by 18.5 db. (20 db are necessary to refer the signal to a one volt d-c level, while the actual index is 1.5 db above the apparent index from Fig. 16.)

4. Measurements on Silicon Cartridge Crystals. Because of the fine contact between wire and crystal in the silicon rectifier, the units are very susceptible to burn-out and deterioration of efficiency with age. Partial burn-out due to excessive applied voltages usually manifests itself in a distinct reduction of the inverse resistance of the crystal, with a corresponding loss in rectifying action.

In order to provide a rapid and accurate method of checking

FIG. 18 SIGNAL-TO-NOISE RATIO VS. D-C BIAS
IN23B CRYSTAL DETECTOR

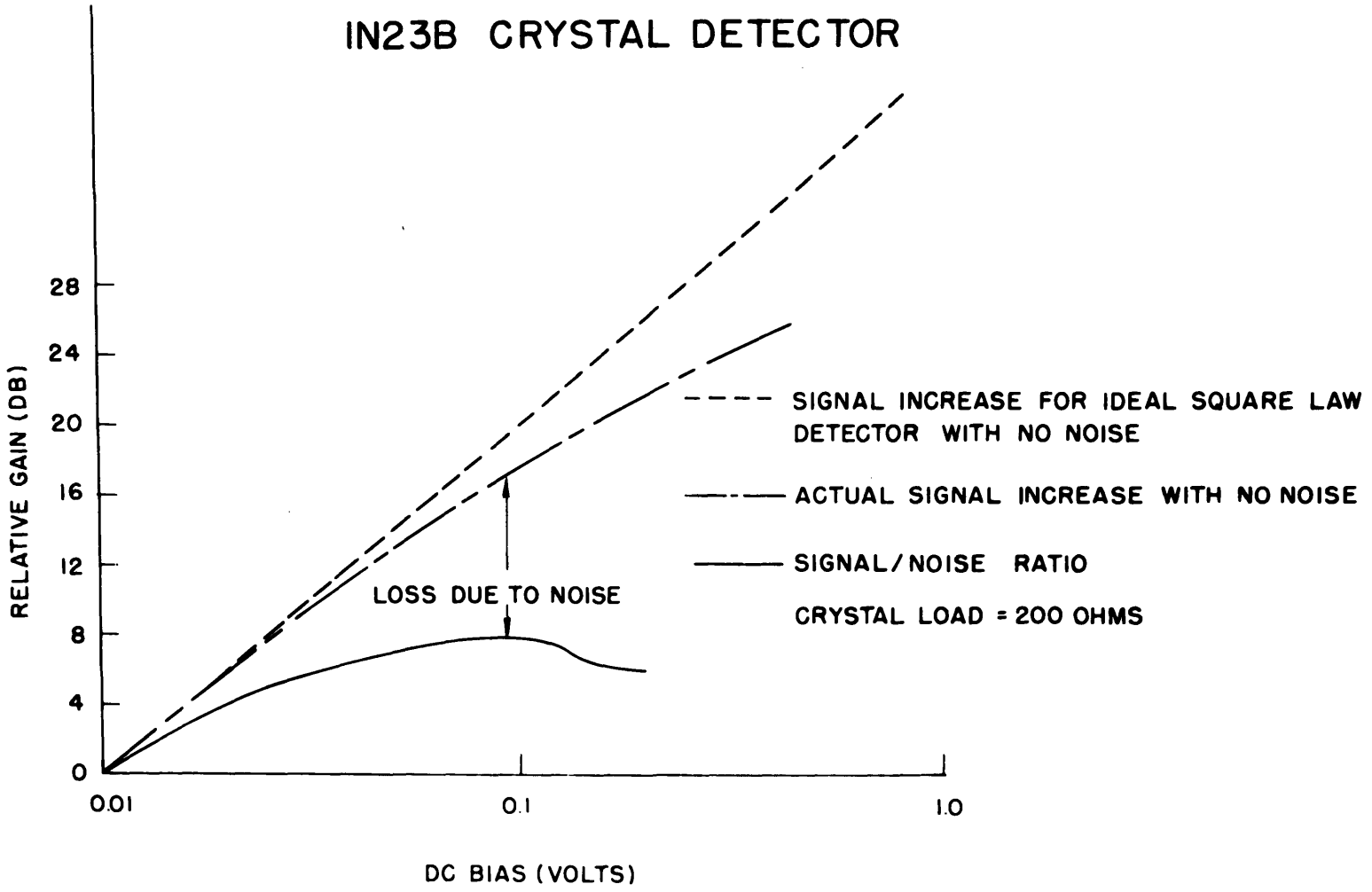

the condition of the crystals used in the analyzer, the crystal characteristic display circuit shown in Fig. 19A was built. The device yields an oscilloscope display of the voltage-current characteristic of the crystal, and thereby permits a check on the forward resistance, the inverse resistance and the shape of the square-law region.

The equipment shown in Fig. 19B measures the audio output impedance of the crystal detector circuit. It will be recalled that the pre-amplifier input transformer, which must see an impedance of 200 ohms for proper operation, is directly across the detector load resistance. The output impedance of the detector circuit however, is the 200 ohm load resistance in parallel with the dynamic audio impedance of the excited crystal. This latter impedance is a complex function of the crystal characteristic, the detector operating point and the efficiency of rectification. Experimental determination of the audio output impedance of the detector circuit is quite simple. The measurement circuit is essentially a 60 cycle constant-current generator terminated in a Ballantine (Model 300) VTVM which measures the voltage across the impedance to be determined. Before the crystal rectifier is connected, the VTVM is across an impedance of 200 ohms, and the reading of the voltmeter is adjusted to 20 millivolts by the 10 kilohm potentiometer. The circuit is now direct reading, the value of the impedance measured being ten times the number of millivolts. When the coaxial line from the crystal holder is connected to the measuring device, the 200 ohm calibrating resistor becomes the crystal load and the detector output impedance may be determined at any d-c operating point.

Using this equipment, the value of the detector output

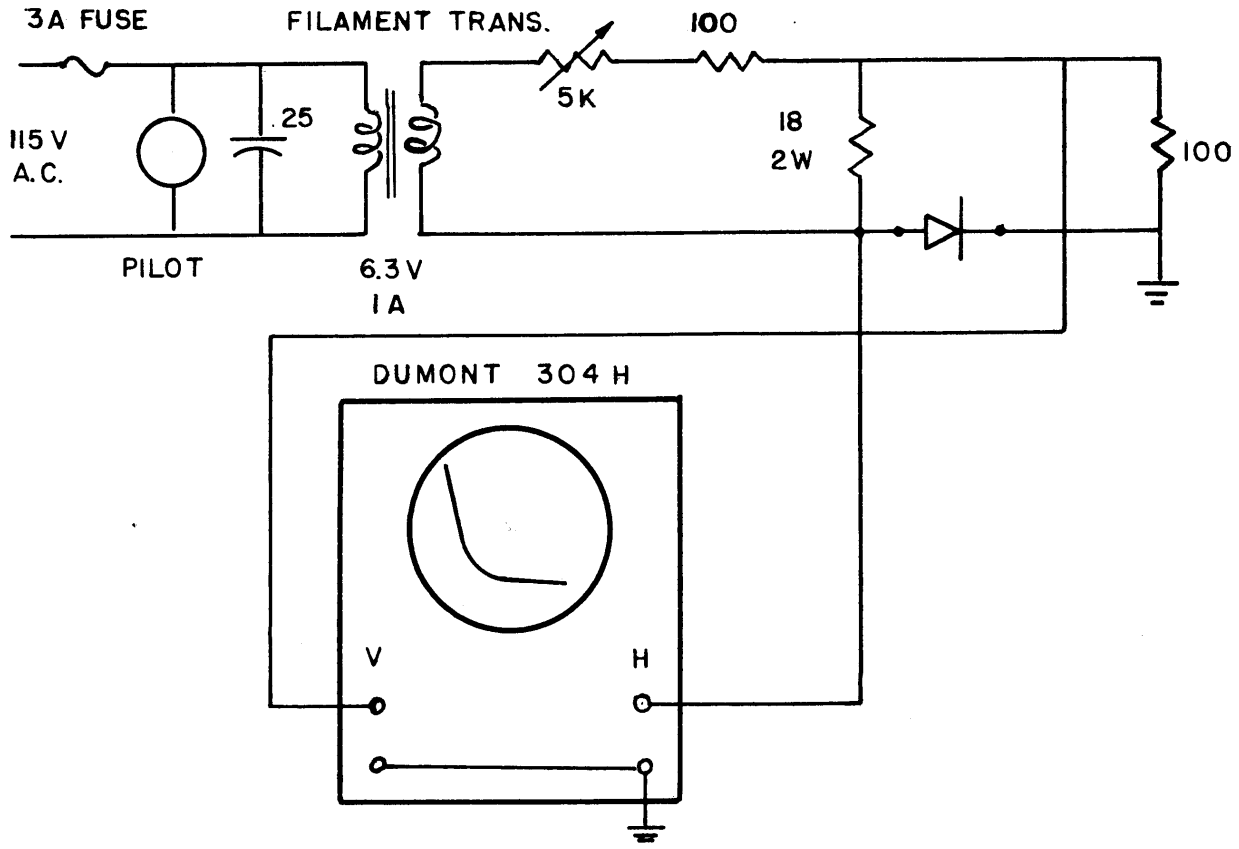

A. CRYSTAL CHARACTERISTIC DISPLAY

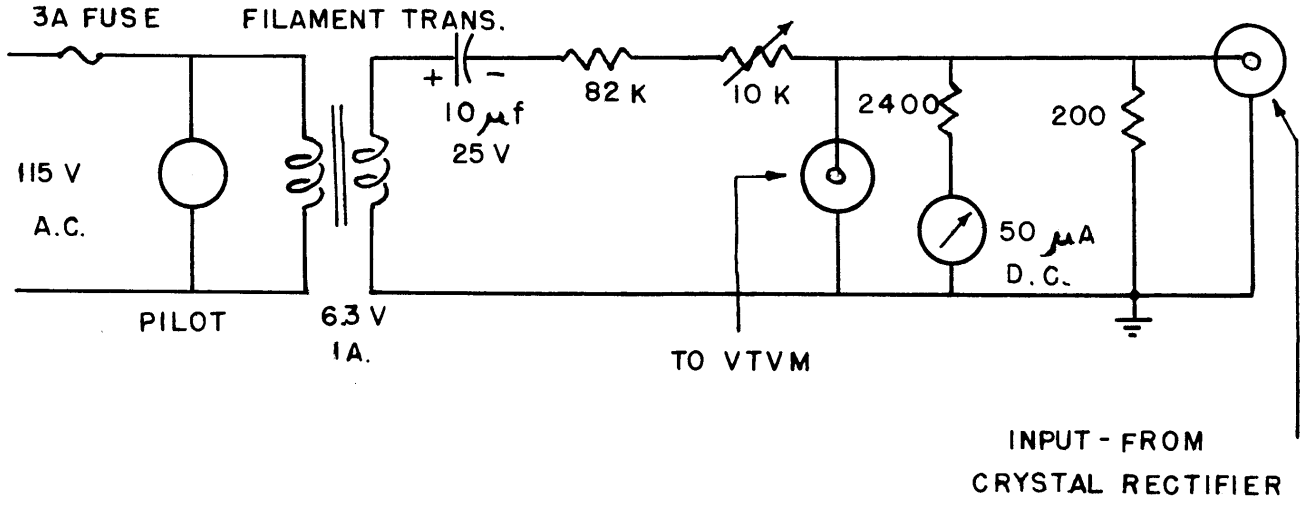

B. DETECTOR OUTPUT IMPEDANCE MEASUREMENT

FIG. 19 SILICON CRYSTAL MEASUREMENT EQUIPMENT

impedance was found to be 150 ohms at a rectified d-c voltage level of 0.1 volts. For proper operation of the pre-amplifier, it is therefore necessary that 50 ohms be added in the primary circuit.

5. The Preselector. The input stage of the spectrum analyzer is shown schematically in Fig. 20. The circuit incorporates both a preselector and an audio bucking circuit. The outputs of two crystal rectifiers may be connected to the preselector, which contains the detector load resistors. A d-c voltmeter which reads 0.1 volts at half scale, is placed across each load resistor to facilitate adjustment of the microwave power level to the desired operating point. The voltmeter is switched out of the circuit during a run to avoid the recording of its microphonics.

The preselector permits the selection of either detector output voltage, or permits the two output voltages to appear simultaneously in the bucking circuit. The use of the audio bucking circuit to measure crystal noise has already been described. It will also find use in making certain f-m spectral measurements. The latter application will be described in Chapter III.

An input attenuator in the preselector prevents overload of the preamplifier. One position of the attenuator switch permits a calibration signal to be fed to the analyzer. The resistors which are placed in series with the pre-amplifier input at each attenuator position are necessary to provide a 200 ohm impedance level to the input transformer. These resistors produce no signal attenuation because the input impedance of the transformer itself is approximately 10,000 ohms.

The entire preselector is housed in a mu-metal shield to guard against stray hum pickup. The cover of the shield is removed during the initial attenuator and d-c level adjustments.

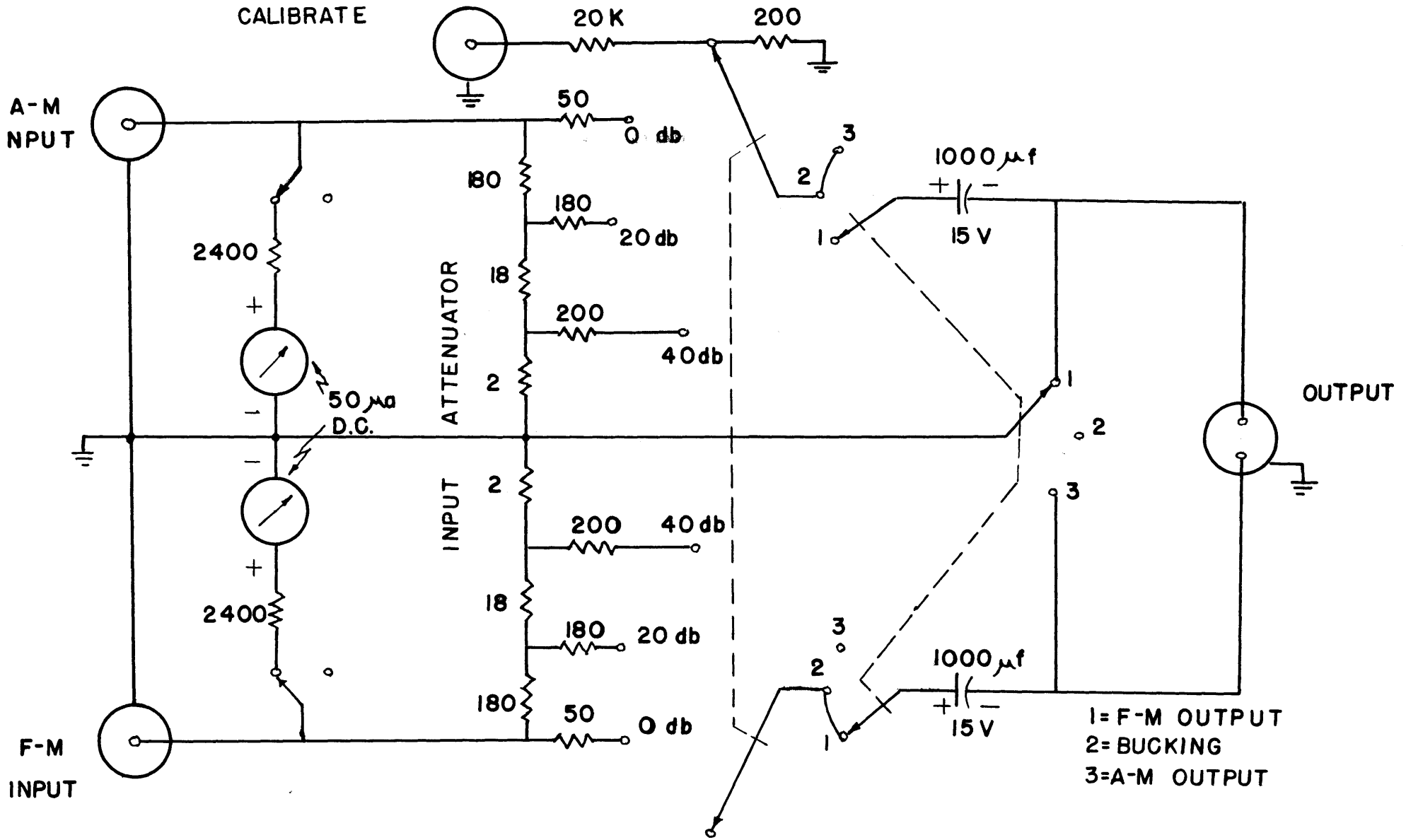

FIG. 20 PRESELECTOR SCHEMATIC

K. The Completed Analyzer

The entire spectrum analysis equipment is shown pictorially in Figs. 21 and 22. The analyzer alone is shown in Fig. 21. The circuitry has been constructed on three horizontal rack-mounted strips. The top strip contains the pre-amplifier. On the center strip are the balanced mixer, i-f amplifier, detector and Logaten circuits. The crystal filter, which in the analyzer chain lies between the mixer and i-f amplifier, is mounted on the bottom strip and connected by cables to its proper circuit position. On the left of the filter is a power control panel, which facilitates the control of filament and plate supply voltages. The meter on the control panel reads the voltage of the storage battery used to supply d-c filament power to the pre-amplifier. To the right of the crystal filter is the r-m-s indicator, connected by cable to the pre-amplifier output and to the thermal milliameter which is bracket-mounted at the top right of the analyzer chassis.

Fig. 22 again shows the analyzer, but this time with its associated equipment. On the table holding the analyzer will be found the Brush Recorder and Amplifiers, the system power supply and an oscilloscope and Ballantine VTVM (both connected to the pre-amplifier wide-band output). On the table to the left is the local oscillator and its driving control, the frequency marker generator, a Hewlett Packard Audio Oscillator and General Radio Microvolter (for calibration), and finally, the preselector.

Chapter III will contain detailed instructions for calibrating and running the analysis equipment as well a discussion of the system performance. Finally, data taken from two X-Band microwave oscillators will be presented.

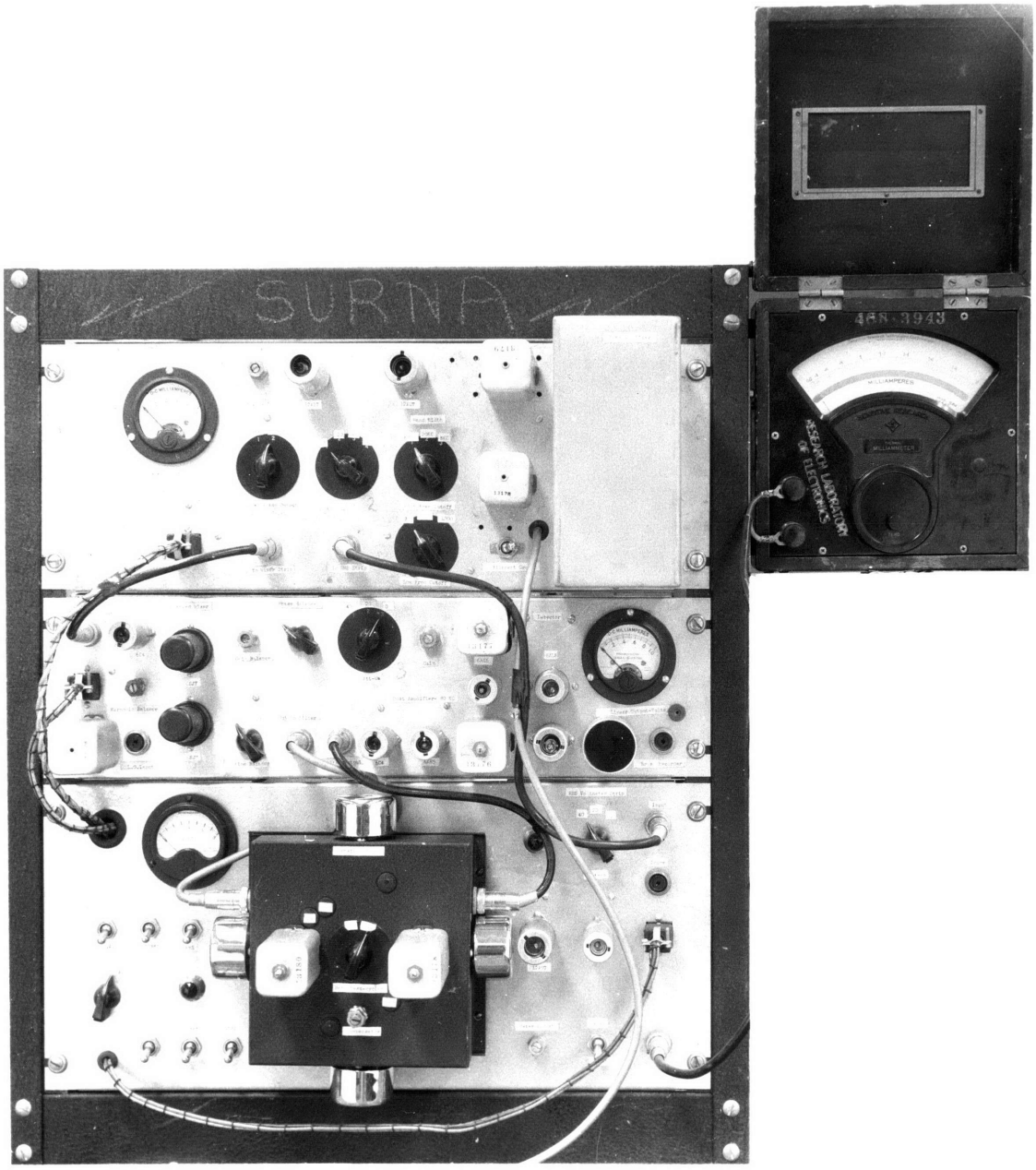

FIG. 21 PHOTOGRAPH OF SPECTRUM ANALYZER

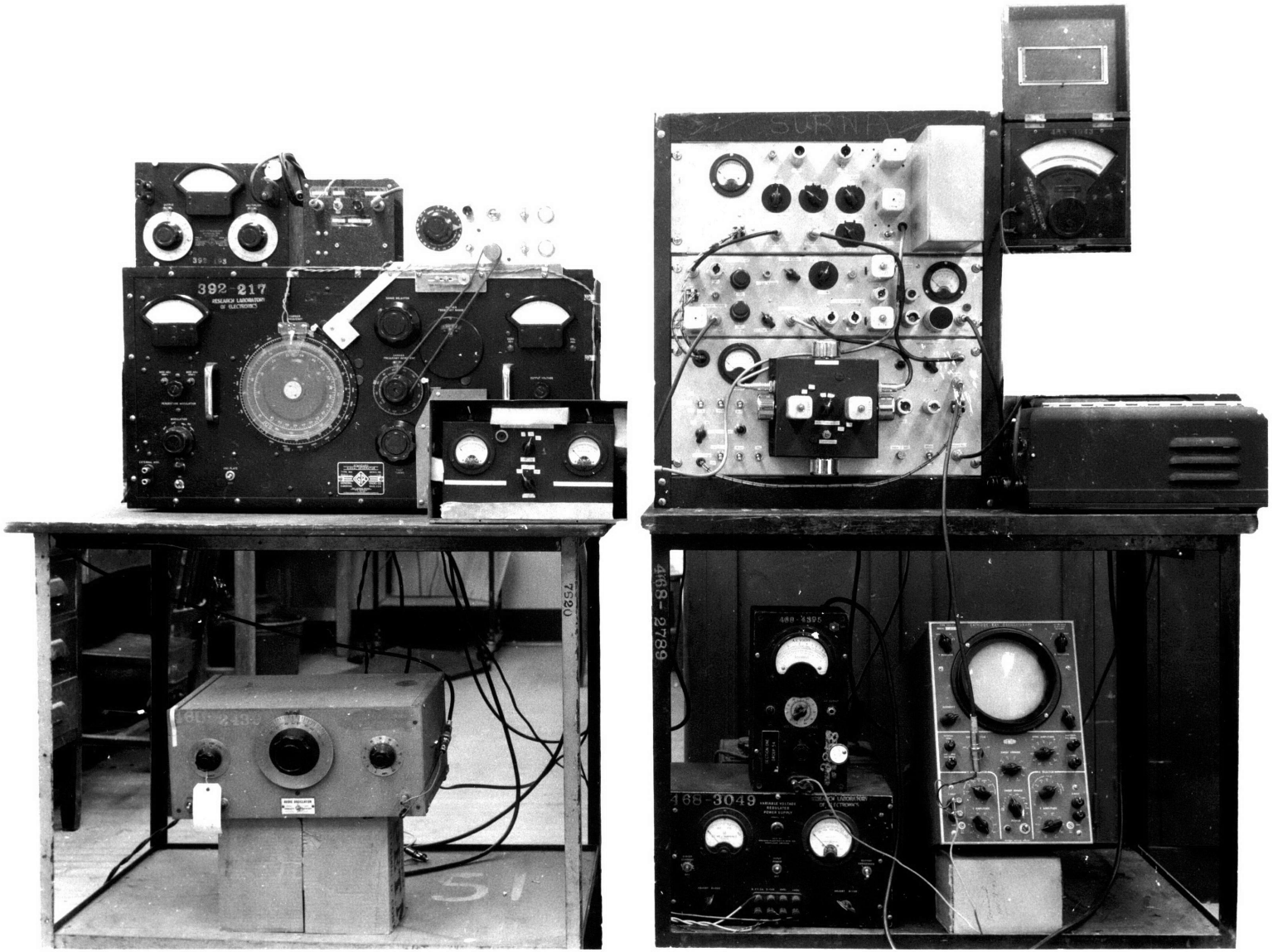

FIG. 22: PHOTOGRAPH OF ANALYZER AND ASSOCIATED EQUIPMENT

CHAPTER III

OPERATION OF THE SPECTRUM ANALYZER

A. Calibration and Preliminary Adjustment

Because of the linear relationship which is maintained between the voltages in the various sections of the spectrum analyzer, it is necessary to calibrate the analyzer at only one point before taking a series of runs. In addition to the calibration procedure, other initial adjustments such as mixer balancing and driving control adjustment will be described in this section. In the discussion to follow, the four system attenuators will be designated as follows:

Att. 1 - Input attenuator of preselector

Att. 2 - Input attenuator of mixer (located on pre-amplifier strip)

Att. 3 - Input attenuator of i-f amplifier

Att. 4 - Input attenuator of r-m-s indicator.

An asterisk (*) will be used to mark those steps of the procedure which need only be performed if the equipment has not been in use for a long period of time.

1. For voltage calibration, begin by inserting voltage of 562 microvolts (-85 db, referred to one volt) at a frequency of 2 kc at the "calibration input" socket of the preselector, using an audio oscillator and a G.R. Microvolter.

2. Set Att. 1 in "calibrate" position and all other attenuators to "20 db". Switch crystal filter to 10 cps bandwidth.

3. Tune local oscillator until signal is indicated by the monitor voltmeter located on the i-f strip. Adjust the i-f gain control

to yield a reading of 10 volts on the monitor voltmeter.

4*. Switch filter to 100 cps band width and adjust "compensator" until monitor voltmeter again reads 10 volts.

5. Center the Brush Oscillograph pen on the Recorder tape, then increase the calibration signal by 20 db. The gain of the Brush D-C Amplifier should now be adjusted so that the recording pen lies at the top line of the tape scale. Decreasing the input signal by 40 db at this point should cause the pen to drop 40 divisions to the lowest line of the tape scale. If the pen does not rest exactly on the bottom line, adjust the analyzer plate supply voltage until it does. Repeat step 3 if the plate voltage is altered.

The analyzer data is now direct reading at one db per scale division. The lowest scale line represents an input voltage of 165 db below one volt, if all attenuators are at "0 db".

6* Increase the calibration signal until the Ballantine Voltmeter at the pre-amplifier output reads 1 volt. With Att. 4 at "40 db", adjust "meter adjust" potentiometer to yield 1 ma. reading of the thermal milliameter in the r-m-s indicator circuit.

7. The mixer should now be balanced by tuning the local oscillator to the i-f frequency (80 kc), and adjusting the "fine balance" and "phase balance" (and if necessary the "gain balance") for a null on the monitor voltmeter. The filter band is at 10 cps for step 7.

8* The remaining preliminary adjustments are synchronization of the first frequency marker with the i-f frequency (as explained in Chap. II, section H), and positioning of the bronze riders on the local oscillator dials so that the motor driving control performs the functions explained in Chapter II, section G. The slow driving speed is adjusted to yield a scale of about 10 cycles per division.

B. Procedure for Obtaining Noise Spectra

The general arrangement of the microwave equipment necessary for making a noise analysis on an X-Band magnetron or klystron is shown in Fig. 23. The directional couplers provide a convenient means of taking power from the oscillator while causing a minimum amount of disturbance in the main waveguide line. Power is measured with a Thermistor Power Bridge.

Between each crystal rectifier and its corresponding directional coupler is an insulating section composed of a strip of mica dielectric between two small waveguide sections. The insulating section provides sufficient capacity to block power-frequency ground currents which would otherwise circulate between the microwave equipment and the analyzer and appear in the recorded output.

After the microwave oscillator has been put into operation, a spectral analysis is accomplished as follows:

1. A-M Spectrum. The output of the a-m crystal rectifier is connected to the "A-M Input" socket of the preselector, and the preselector switch is turned to "A-M". The level of the rectified d-c detector output voltage is adjusted to 0.1 volts using the waveguide attenuator in the a-m line.

Attenuator 1 and Att. 2 are adjusted so that the overload meter (on the pre-amplifier strip) reads below 0.9 ma. with the meter selector switch in the "pre-amp. output" and "mixer input" position, respectively. The above attenuator settings and the reading of the r-m-s indicator should now be recorded.

A noise spectrum may now be taken using only Att. 3 to adjust the level of the recorded output. As has been previously explained, the analyzer is run up to 2 kc with the crystal filter set at a 10 cps band width. At 2 kc the drive automatically stops

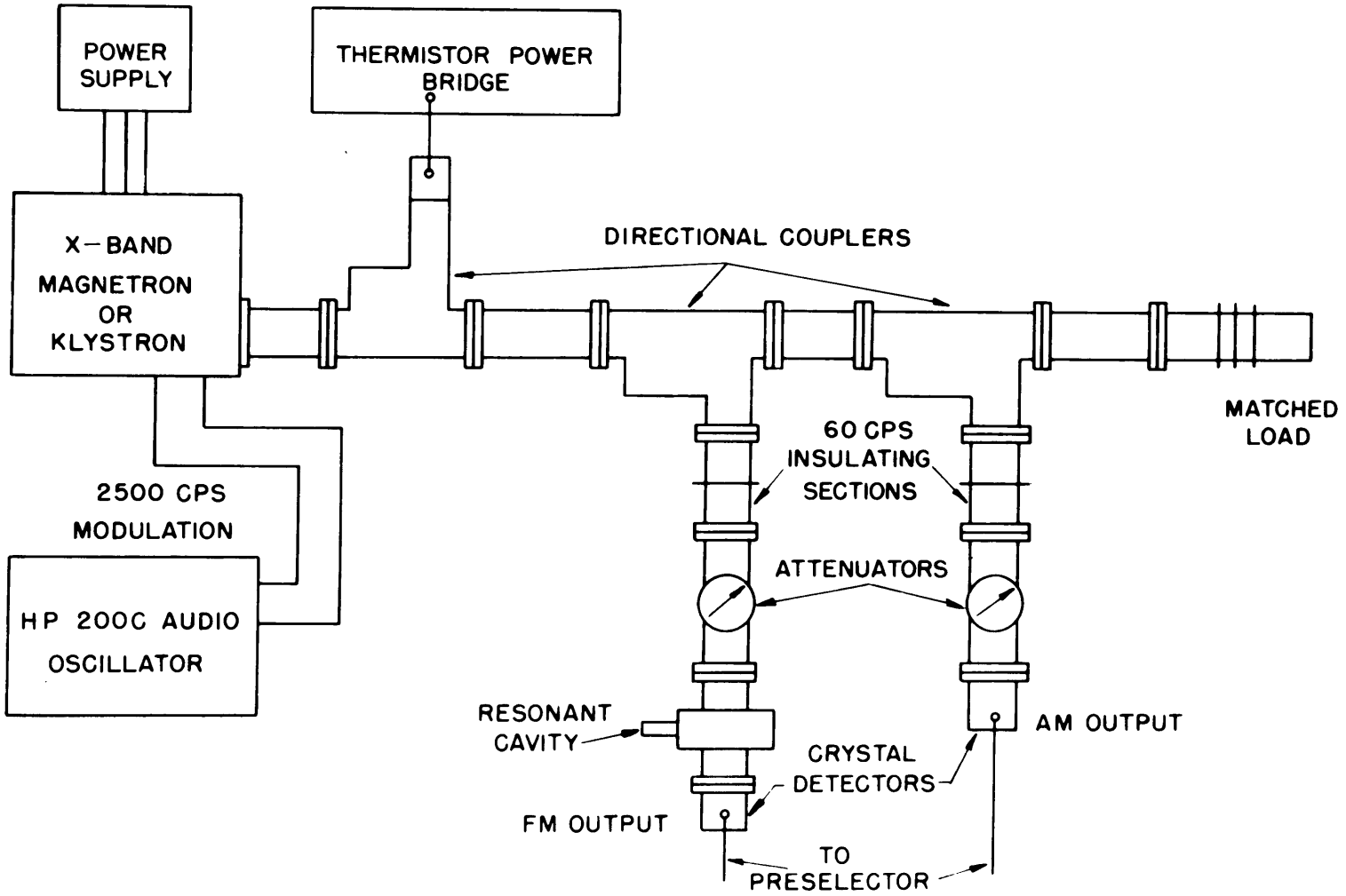

FIG. 23 MICROWAVE OSCILLATOR AND ASSOCIATED EQUIPMENT

to allow the band width to be changed to 100 cps and the setting of Att. 3 to be altered, if necessary. The remainder of the run is taken at a faster speed. The reader is referred to Chapter II, section G for a description of the operation of the motor driving controls during the course of a noise run.

2. F-M Spectrum. In order to convert the carrier frequency deviation due to noise modulation into an equivalent amplitude modulation, a resonant cavity is employed. The cavity is tuned until a peak indication is obtained on the preselector d-c voltmeter. With the cavity in this position, the f-m waveguide attenuator is adjusted to yield a voltmeter reading of 0.14 volts. The cavity is now detuned to the half-power point of its characteristic at which time the voltmeter will read 0.1 volts.

All remaining operations procede as though an a-m spectrum were being taken.

The f-m spectral data obtained should now be compared to the a-m spectrum. If the voltage levels of the two spectra are within 20 db of each other at any point, then the analysis should be repeated with both the a-m and f-m channels feeding the preselector simutaneously, and the preselector switch set to "bucking". The significance of this procedure will be discussed in section C-3.

3. Crystal Noise. To determine the character of the noise generated by the crystal rectifiers, a second a-m channel is produced by removing the cavity from the f-m waveguide channel. The outputs of both crystal detectors are then connected simultaneously to the preselector, adjusted to 0.1 d-c levels, and placed in the "bucking" arrangement. The spectrum obtained will be that of crystal noise, as explained in Chapter II, section J-3.

C. Interpretation of Noise Data

1. A-M Data. The spectrum analyzer has been calibrated to yield a minimum reading of 165 db below one volt r-m-s when all attenuators are in the "0 db" position. The bottom line on the Brush Recorder scale for any run will therefore represent an input voltage in db below one volt of 165 minus the combined readings of attenuators 1,2 and 3. All other scale readings are obtained by adding one db per division to this figure.

The r-m-s wide band input voltage is obtained by converting the r-m-s indicator reading to db below one volt and subtracting from that figure the quantity 88.5 minus the combined readings of attenuators 1 and 2. (The full gain of the pre-amplifier is 88.5 db).

It was shown in Chapter II, section J-3 that the actual modulation index is 18.5 db above the measured value of the input signal. To obtain the r-m-s modulation index in db below one volt it is therefore necessary to subtract 18.5 from the values of input noise as calculated above.

The a-m spectrum should be compared to the crystal noise spectrum to determine whether the data recorded is oscillator or detector noise. The noise in a single crystal will be 3 db below the value for two crystals in a bucking arrangement, if the crystals are equally noisy.

2. F-M Data. It is shown in Appendix III that when a deviation in carrier frequency is converted to an equivalent amplitude modulation through the use of a resonant cavity tuned to the half-power point of its response characteristic, then an r-m-s modulation index of 105 db below a volt represents a deviation of 10 cps from the carrier frequency, for sinusoidal modulation.

The f-m data is therefore treated in the same manner as the

a-m data for the purpose of computing the actual modulation index for narrow-band and wide-band data. The frequency deviation is computed from the modulation index using the relationship mentioned above.

3. Bucking Circuit Data. Because the resonant cavity has no effect on the original amplitude modulation present on the carrier envelope, the f-m spectrum will contain a-m data. In general if the f-m spectral data obtained for an oscillator is at all frequencies at least 20 db above the corresponding spectral data obtained in an a-m run on the oscillator, then the effect of the original amplitude modulation on the f-m spectrum may be neglected.

However, where the recordings seem to be of the same order of magnitude, a-m noise voltages may be removed from the f-m spectrum by using the audio bucking circuit as indicated in section B-2. The d-c levels of the two crystal detectors, one of which carries f-m data, are adjusted to the same value so that the a-m output of each detector is the same and is balanced out. The resultant spectrum will have a smaller voltage magnitude than an f-m spectrum taken without the bucking circuit wherever amplitude modulation was originally responsible for the recorded data. It should be pointed out however, that if the original data in both a-m and f-m spectra represented crystal noise, then the bucking circuit spectrum will have larger voltage magnitudes, since the noise generated by two crystals rather than one will now appear at the input.

D. System Sensitivity and Noise Figure

The minimum input noise voltage which can be measured by the spectrum analyzer is limited by the noise generated in the measurement equipment itself. The noise generated by the system under different attenuator settings is shown in Fig. 24. This data was obtained by removing the preselector from the input circuit and terminating the pre-amplifier input transformer in 200 ohms.

Consider first the spectral data in the region up to 2 kc, which is traversed at a slow speed and with a 10 cps band width. The data of runs 1 and 2 in this region is the large local-oscillator signal which cannot be completely balanced out and is sufficiently strong to pass through the crystal filter and be recorded. This "spillover" reduces the minimum measureable input signal to about 145 db below one volt at some points below 2 kc. However, crystal noise and oscillator noise in this region is always great enough to require that attenuator 3 be in the "20 db" or "40 db" positions, and the data of run 3 shows that spillover has negligible effect when Att. 3 is so adjusted.

The spectral data above 2 kc is obtained with a faster driving speed and a 100 cps band width. Here the recorded data is apparently only thermal noise in a 200 ohm resistor. The r-m-s value of thermal noise voltage generated by a 200 ohm resistor is 155 db* below one volt for a measurement band width of 100 cps. The recorded noise voltage varies from point to point as it must since the noise is a random phenomenon and measurement at a given frequency is performed in a short time interval. The average level of the data however, may be seen (run 2 shows it best) to be 155 db below one volt over most of the frequency range above 2 kc ex-

* Calculated by equation (1), Chapter I.

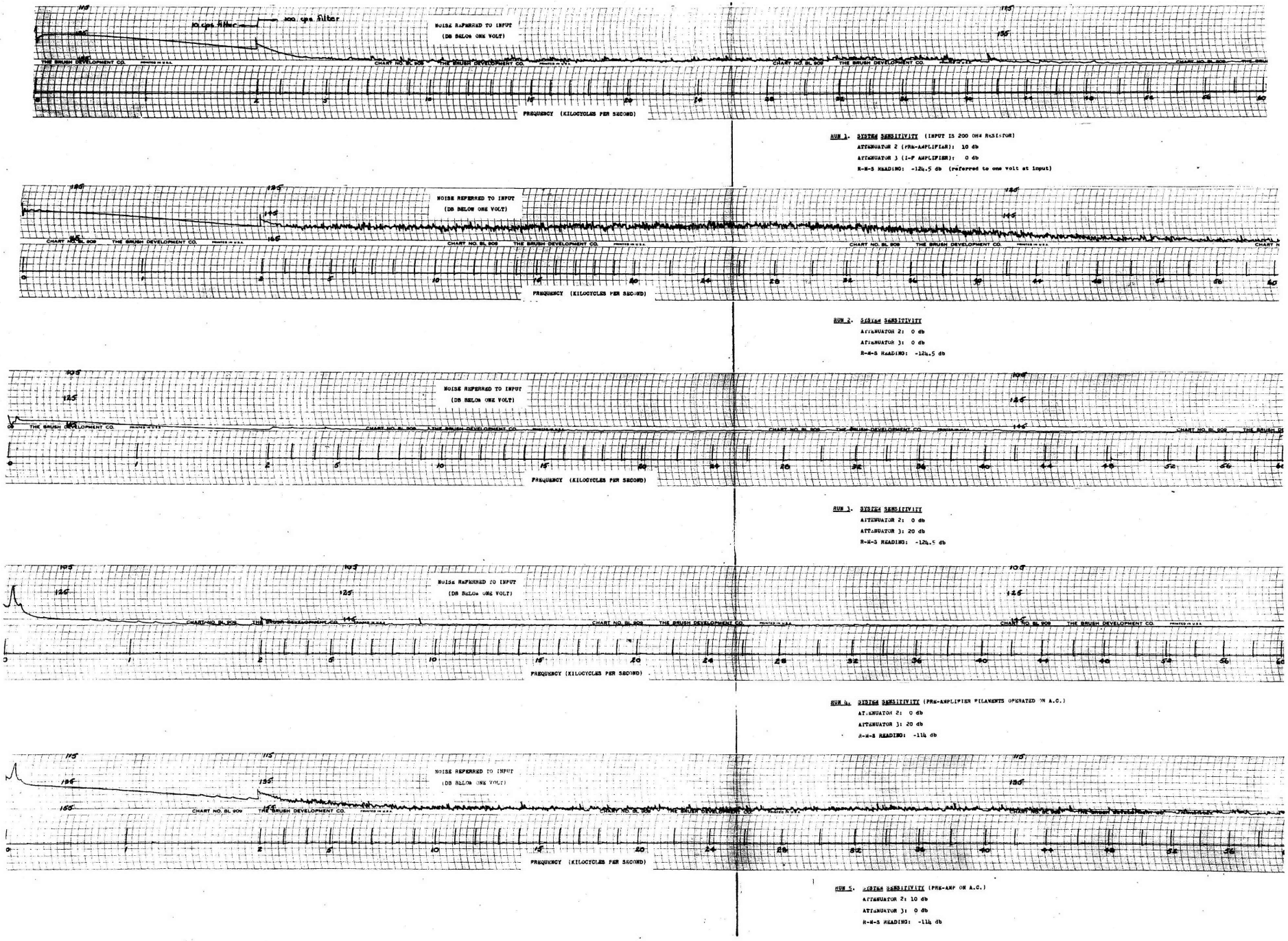

FIG. 24: RECORDED DATA ON SYSTEM SENSITIVITY

cept at the higher frequencies where the level follows the frequency response curve of the analyzer (Fig. 11). The minimum amplitude modulation index which can be measured above 2 kc is therefore about 150-18.5 = 131.5 db below one volt. In all data runs taken to date, this sensitivity was found to be sufficient.

Runs 4 and 5 of Fig. 24 have been included to show the effect of operating the pre-amplifier filaments from an a-c source. Note the large power-frequency voltages which result.

It is of interest to compare the r-m-s wide-band internal noise generated in the pre-amplifier (referred to the input), with the theoretical wide-band thermal noise voltage generated in the 200 ohm input resistor. The ratio of these two quantities is defined as the noise figure of the amplifier. The minimum value of this ratio is unity, and the noise figure will increase as the internal noise of the amplifier increases.

The value of thermal noise generated by a 200 ohm resistor and measured in a 60 kc band is, by equation (1), Chapter I, 127 db below one volt. (The actual band width of the wide-band analyzer is 50 kc to 3 db points, but the effective band width,[9*, 18**] which takes into account the contribution of frequencies beyond the 3 db points, is about 60 kc.) The measured r-m-s noise is 124.5 db below one volt. The noise figure is therfore 2.5 db, or a voltage ratio of 1.35. The use of an input transformer in the pre-amplifier as well as careful shielding and construction of the amplifier are responsible for the low noise figure of the wide-band analyzer.

* Appendix I

** p. 104

E. Noise Spectra of Microwave Oscillators

Ten noise runs on two microwave oscillators are included here (Figs. 25 and 26) to illustrate the types of spectra which are obtained using the spectrum analyzer. (Due to an error in calculation, the values of modulation index indicated in the a-m runs are 3.5 db below the correct values.)

1. X-Band Klyston. Fig. 25 contains five noise runs taken on a Varian X-13 Klystron. Complete information regarding operating conditions and type of noise measurement made are included for convenience below each spectrum.

Run 6 shows the noise produced in a crystal rectifier under X-Band excitation. The audio bucking circuit was used, so that the spectrum shown is for two crystals. The magnitude of the noise has the inverse-frequency dependence which was expected in light of the discussion of Chapter I, section B-2.

Run 7 is an a-m spectrum taken with the klystron operated on a-c filament power. Note the large hum components. The low Q oscillation present near 13 kc was an internal oscillation in the anode power supply. Switching to d-c excited filament and readjusting the anode supply slightly to remove the oscillation produced the spectrum shown in run 9. At low frequencies, out to about 5 kc, the noise seems to be largely hum and crystal noise, while above 5 kc the spectrum takes on the uniform frequency distribution characteristic of shot noise or other electronic fluctuation.

Runs 8 and 10 are f-m spectra taken under different operating conditions. Note that the f-m voltages are at all times much greater than the corresponding a-m voltages, so that there is no need to employ the bucking circuit here.

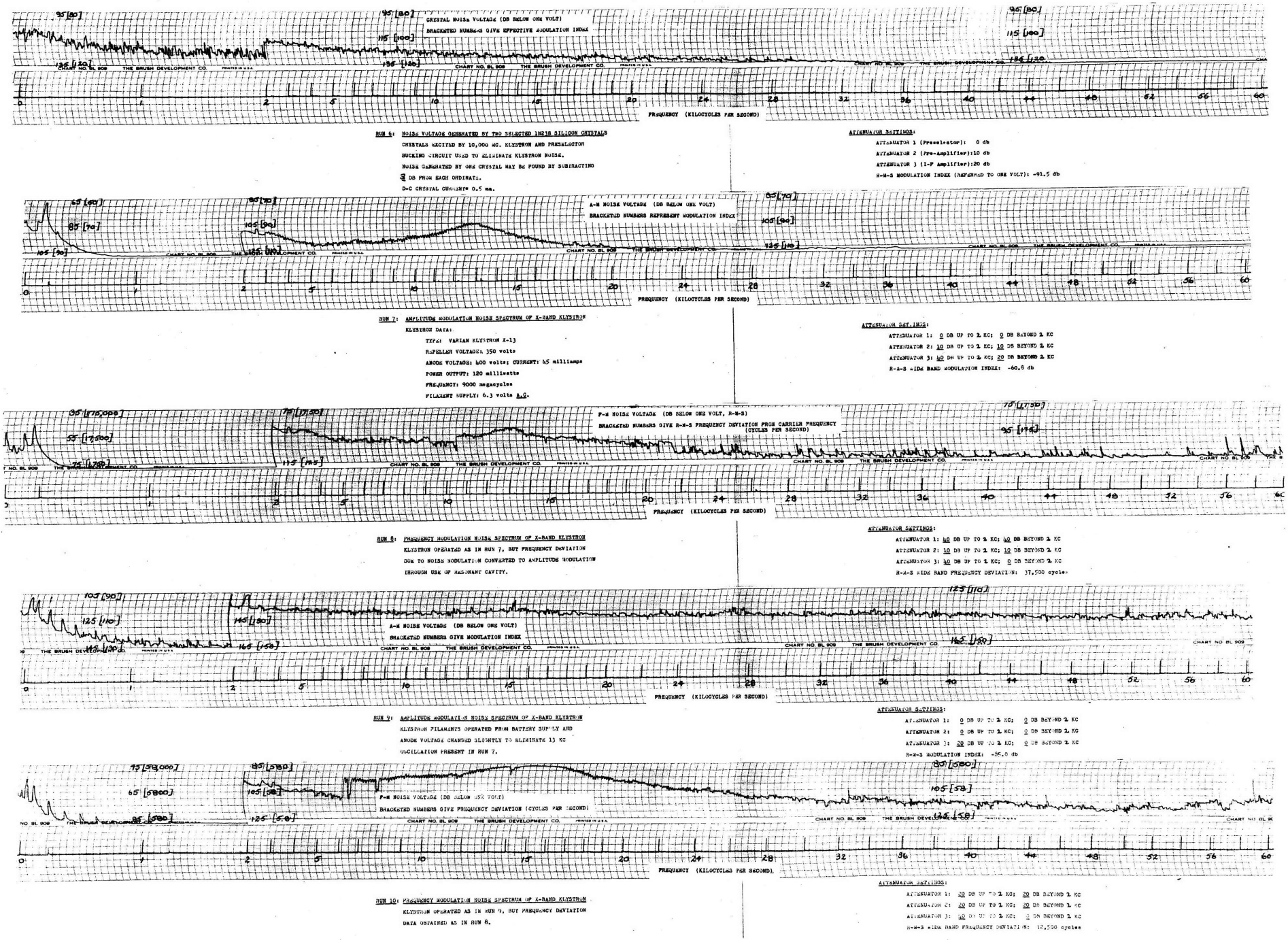

FIG. 25: NOISE SPECTRA OF X-BAND KLYSTRON

2. X-Band Magnetron. Figure 26 contains five noise runs taken on a Raytheon Magnetron.

Run 11 was included merely to show the effect of operating the magnetron with a-c filament excitation.

Run 12 is an a-m noise spectrum. It is interesting to compare this spectrum with run 9. Up to about 5 kc, the two spectra have the same character and level, but above this region although the spectra both indicate electronic or ionic disturbances, the magnetron noise level is generally lower than that of the klystron. This is perhaps due to the partition noise effects present in the klystron.

Run 15, which appears to be almost the duplicate of run 12, is an a-m noise spectrum taken with the power output of the magnetron doubled. The noise modulation has apparently remained independent of the power output, except at very low frequencies where some of the power supply hum components have been reduced by the alteration of the point of operation.

Run 13 is an f-m spectrum. Below 2 kc, the f-m spectrum has the same character as the a-m spectrum of run 12, suggesting that these noise components, which are largely hum frequency phenomena, are produced in the power supply external to the magnetron. The large frequency deviation at 5 kc, on the other hand, is apparently due to some internal effect which does not effect the carrier voltage but does produce f.m. Beyond 5 kc, the f-m noise voltages begin to approach the level of the a-m voltages (run 12). To seperate the spectra, the bucking circuit was employed in run 14. Although it is not very clear in the data, it may be observed that above 15 kc, where the voltages of runs 12 and 13 both had values of -145 db, the voltage of run 14 is somewhat less. Note finally that the f-m noise in the magnetron is far less than in the klystron.

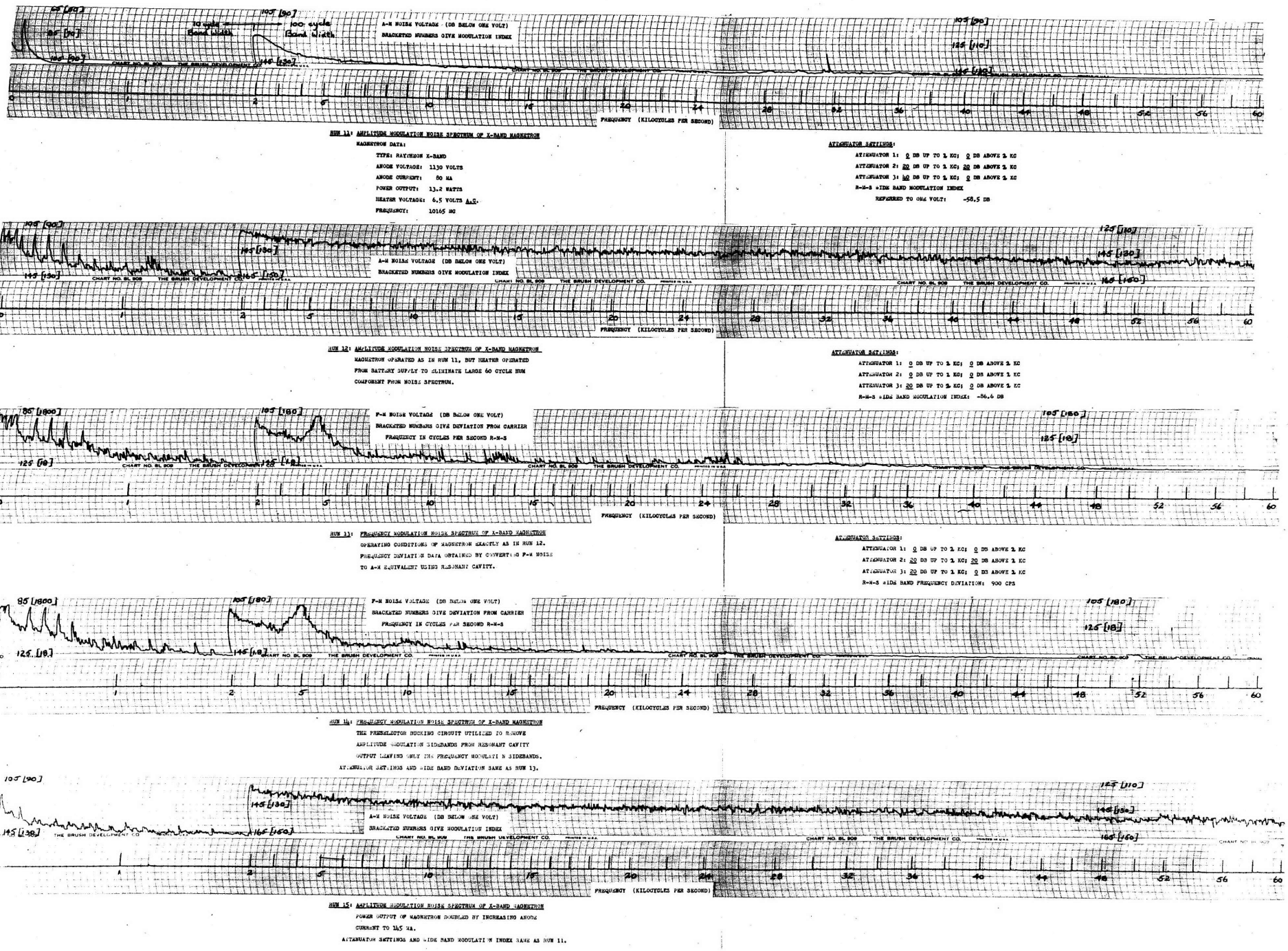

FIG. 26: NOISE SPECTRA OF X-BAND MAGNETRON

F. Conclusion

The spectrum analyzer described in this thesis has been designed and built primarily for the purpose of obtaining the a-m and f-m noise spectra of microwave oscillators. Accuracies of about 2 db are obtained in the recorded spectra, and higher accuracy may be obtained by direct calibration at any point. Perhaps the most desirable feature of the analyzer is the ease with which a spectrum may be obtained.

The analyzer itself, with a suitable detector, can be used to measure the noise sidebands present on a carrier of any frequency. The equipment can be used wherever a high sensitivity, narrow-band wave analyzer is desired. The measurement of crystal rectifier noise has already been described, and the measurement of noise in vacuum tubes and transistors are other possible applications. Voltages as low as 145-150 db below one volt can easily be measured at any frequency from 20 cps to 60 kc.

It has been pointed out that some analytical and perhaps experimental work is necessary to determine the exact significance in terms of modulation index of the data obtained on random noise. An analytical investigation would also be desirable on the magnitude of error which can be expected in measuring a random phenomenon in a narrow band width over a short time interval.

The author is hopeful that the data obtained with the spectrum analyzer in subsequent experiments will be useful in the design of low-noise microwave oscillators, and will perhaps provide a better understanding of the sources and character of noise generation in crystal rectifiers.

APPENDIX I

DESIGN OF A QUARTZ CRYSTAL LATTICE FILTER

A. The Quartz Crystal

The quartz crystal, shown in Fig. 27A, is an electromechanical transducer[14] which has the property of producing a voltage across the faces perpendicular to the electrical axis, whenever the crystal is mechanically set into vibration. This process is reversible, so that electrical excitation will produce mechanical vibrations and mechanical resonances.

The behavior of the quartz crystal, in terms of electrical phenomena, may be entirely represented by an electrical equivalent circuit. Figure 27B shows the electrical analogues of the quartz crystal. The two forms shown are equivalent. The form containing L_1, C_1, and C_0 is called the Foster admittance form[15], while the other circuit is known as the Foster impedance form.

Many crystal cuts are possible from the raw block of quartz, each cut having specific characteristics which make it most suitable for some crystal application. The cut shown in Fig. 27A is called the -18.5° X-cut because of its geometrical relationship to the three axes of a quartz block. The axes are orthogonal imaginary lines which run in specific directions within the uncut prismatic quartz block. The -18.5° X-cut is generally chosen for filter applications in the high audio and ultrasonic frequency range because of the high-Q resonances exhibited by this cut.

The relationship between the parameters of the electrical equivalent circuit and the physical dimensions of the crystal as shown in Fig. 27A is given by the following formulae:

$$L_1 = 118 \frac{WT}{L} \text{ henries} \qquad (1)$$

$$C_1 = .0029 \frac{WL}{T} \text{ micromicrofarads} \qquad (2)$$

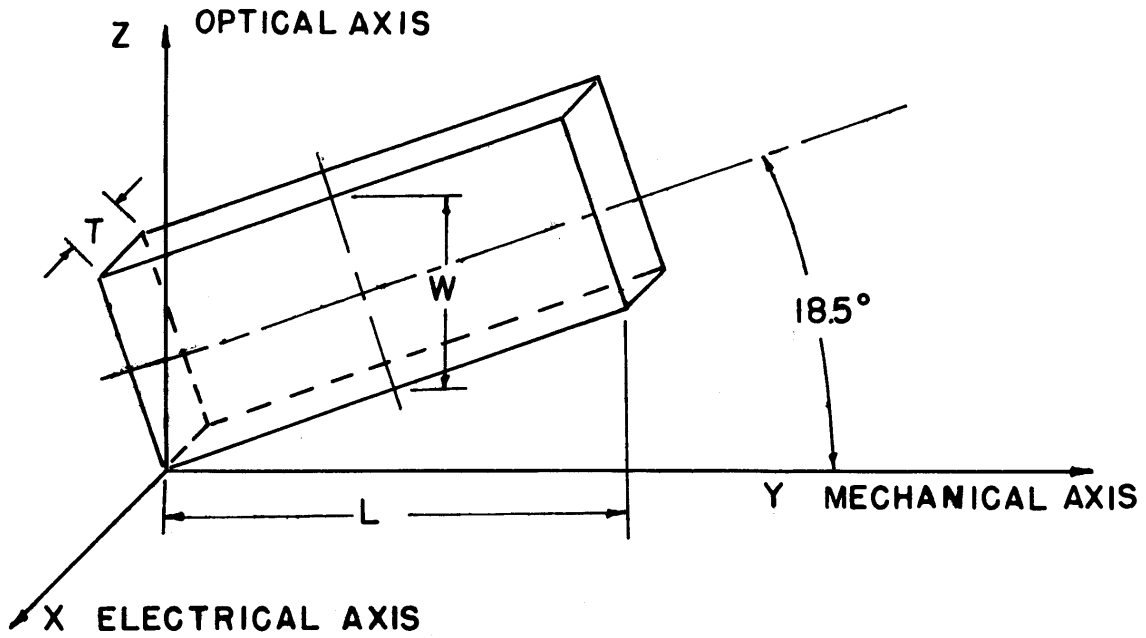

A. -18.5° X-CUT QUARTZ CRYSTAL

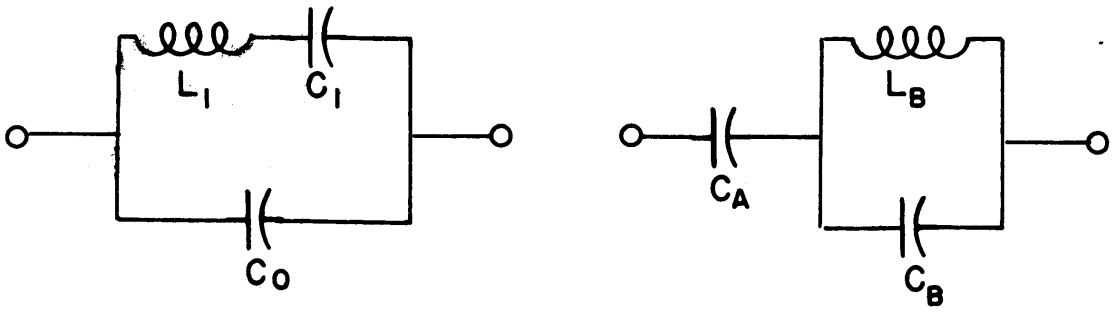

B. EQUIVALENT CIRCUITS

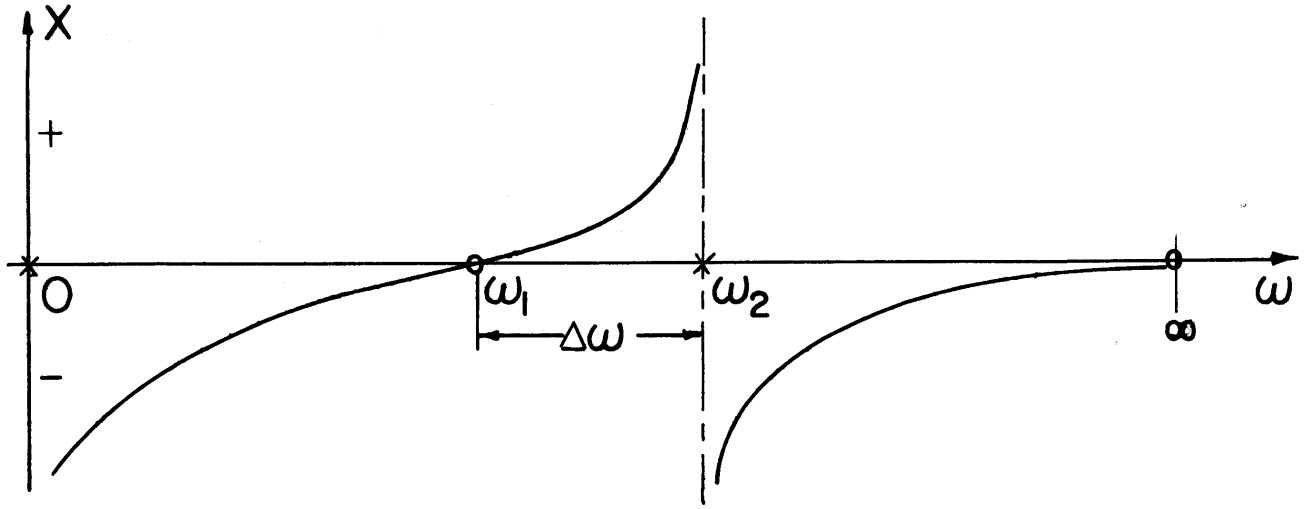

C. REACTANCE-FREQUENCY CURVE

FIG. 27 THE QUARTZ CRYSTAL

$$C_0 = .40 \frac{WL}{T} \text{ micromicrofarads} \qquad (3)$$

Referring to the equivalent circuits of Fig. 27B, the parameters of the two forms may be shown to be related as follows:

$$L_1 = L_B(C_A + C_B) \qquad (4) \qquad L_B = L_1\left(\frac{C_1}{C_1 + C_0}\right)^2 \qquad (7)$$

$$C_1 = \frac{C_A^2}{C_A + C_B} \qquad (5) \qquad C_A = C_1 + C_0 \qquad (8)$$

$$C_0 = \frac{C_A C_B}{C_A + C_B} \qquad (6) \qquad C_B = \frac{C_0}{C_1}(C_1 + C_0) \qquad (9)$$

For purposes of analysis it will be convenient to define a ratio r, such that

$$r \equiv \frac{C_0}{C_1} = \frac{C_B}{C_A} \qquad (10)$$

For the unmounted crystal, the ratio r has a definite constant value of 138 (divide eq. 3 by eq. 2). Placing any capacitance across the terminals of the crystal (such as the capacitance of the crystal mount and socket), will raise the value of C_0 and increase r. Furthermore, placing capacitance in series with the crystal will lower C_A and once again raise r. The minimum value of r is therefore fixed by the crystal cut.

A more exact equivalent circuit of the quartz crystal than that of Fig. 27B would contain a resistance in series with the effective inductance. However, because of the high Q values which are commonly obtained from crystal elements, only the reactive elements need be considered for most analytical purposes. As a matter of fact, it is the high values of Q obtainable from crystals, and their high stability which makes these elements desirable for filter applications.

Writing the driving-point impedance of the equivalent circuit in terms of real radian frequency w, yields the formula

$$Z = -j \frac{w}{C_0} \frac{(w^2 - w_1^2)}{w^2(w^2 - w_2^2)} \tag{11}$$

where

Z = impedance between circuit terminals

C_0= total effective parallel capacitance (includes the effect of any added circuit capacitance)

$$w_1 = \frac{1}{\sqrt{L_1 C_1}} = \text{resonant frequency of circuit} \tag{12}$$

$$w_2 = \frac{1}{\sqrt{L_B C_B}} = \text{antiresonant frequency of circuit} \tag{13}$$

Deleting the j from formula (11) gives the reactance of the crystal network and any added capacitance as a function of radian frequency. The reactance equation is sketched in Fig. 27C. In order to provide clarity to the curve, considerable liberty has been taken in drawing the frequency scale. Numerical values may help to provide perspective to the reactance-frequency curve. For the crystals used in this research, f_1, the resonant frequency or zero of reactance might occur at 80,000 cps, while the antiresonant frequency f_2, might occur at 80,100 cps, only 100 cycles removed from f_1. The letter f will be used throughout to mean $\frac{w}{2\pi}$, and denotes real frequency.

Before proceeding with a discussion of the filter itself, one final derivation is necessary. The separation between w_1 and w_2 is defined as Δw. That is,

$$\Delta w \equiv w_2 - w_1 . \tag{14}$$

Consider the following;

$$\left(\frac{w_2}{w_1}\right)^2 = \left(\frac{w_1 + \Delta w}{w_1}\right)^2 = \left(1 + \frac{\Delta w}{w_1}\right)^2 \tag{15}$$

Since Δw is very small compared to w_1, eq.(15) becomes

$$\left(\frac{w_2}{w_1}\right)^2 = 1 + \frac{2\Delta w}{w_1} \tag{16}$$

But from equations (12) and (13)

$$\left(\frac{w_2}{w_1}\right)^2 = \frac{L_1C_1\cdot(C_1 + C_0)}{L_1C_1C_0} = 1 + \frac{C_1}{C_0} \tag{17}$$

Combining eqs.(16) and (17), and using eq.(10),

$$\frac{2\Delta w}{w_1} = \frac{C_1}{C_0} = \frac{1}{r}$$

Rewriting the above equation in terms of f, and solving for f, yields finally the relationship

$$\boxed{\Delta f = \frac{f_1}{2r}} \tag{18}$$

This important relationship between Δf and the ratio r indicates that the spacing between resonant and antiresonant frequencies of the crystal network has a maximum value fixed by the crystal cut, and that this spacing may be decreased by adding series or parallel capacitance to the network, which as previously explained, increases r.

There is a significant distinction between the use of a series and a parallel capacitor in reducing Δf. A cpacitor placed <u>across</u> the crystal terminals will <u>lower f_2</u>, while a <u>series</u> capacitor cannot affect the antiresonant frequency, but will <u>raise f_1</u>. The two critical frequencies can thus be theoretically moved arbitrarily close together, both being mobile, but with direction of motion restricted as explained here.

B. The Lattice Filter

The symmetrical lattice structure, which was chosen because it lends itself so readily to analysis, is shown at the top of Fig. 28. The impedance Z_a, which lies in the top series arm of the lattice, has an identical twin in the bottom series arm. This is likewise true for the shunt arms which contain the impedances Z_b.

Because the lattice is a balanced or bridge-type structure, there can be no common ground between input and output circuits as this would result in the shorting of a lattice arm.

The properties of any symmetrical two terminal-pair network may be completely characterized by two quantities known as the image parameters.[15]

1. The image impedance Z_o of a symmetrical network is the input impedance presented by the network at either terminal pair when the other terminal pair is terminated in Z_o.

2. The image propagation function γ of the network is a complex quantity whose real part is the attenuation loss of the network, and whose imaginary part is the phase, when the network is terminated in its image impedance. That is,

$$\gamma = \alpha + j\beta = \ln\left(\frac{E_i}{E_o}\right) = \ln\left(\frac{I_i}{I_o}\right),$$

where

γ = image propagation function

α = attenuation loss

β = phase

E_i, I_i = input voltage and current, respectively

E_o, I_o = output voltage and current, respectively,

when the network is terminated in its image impedance Z_o.

For the symmetrical lattice, the image parameters turn out

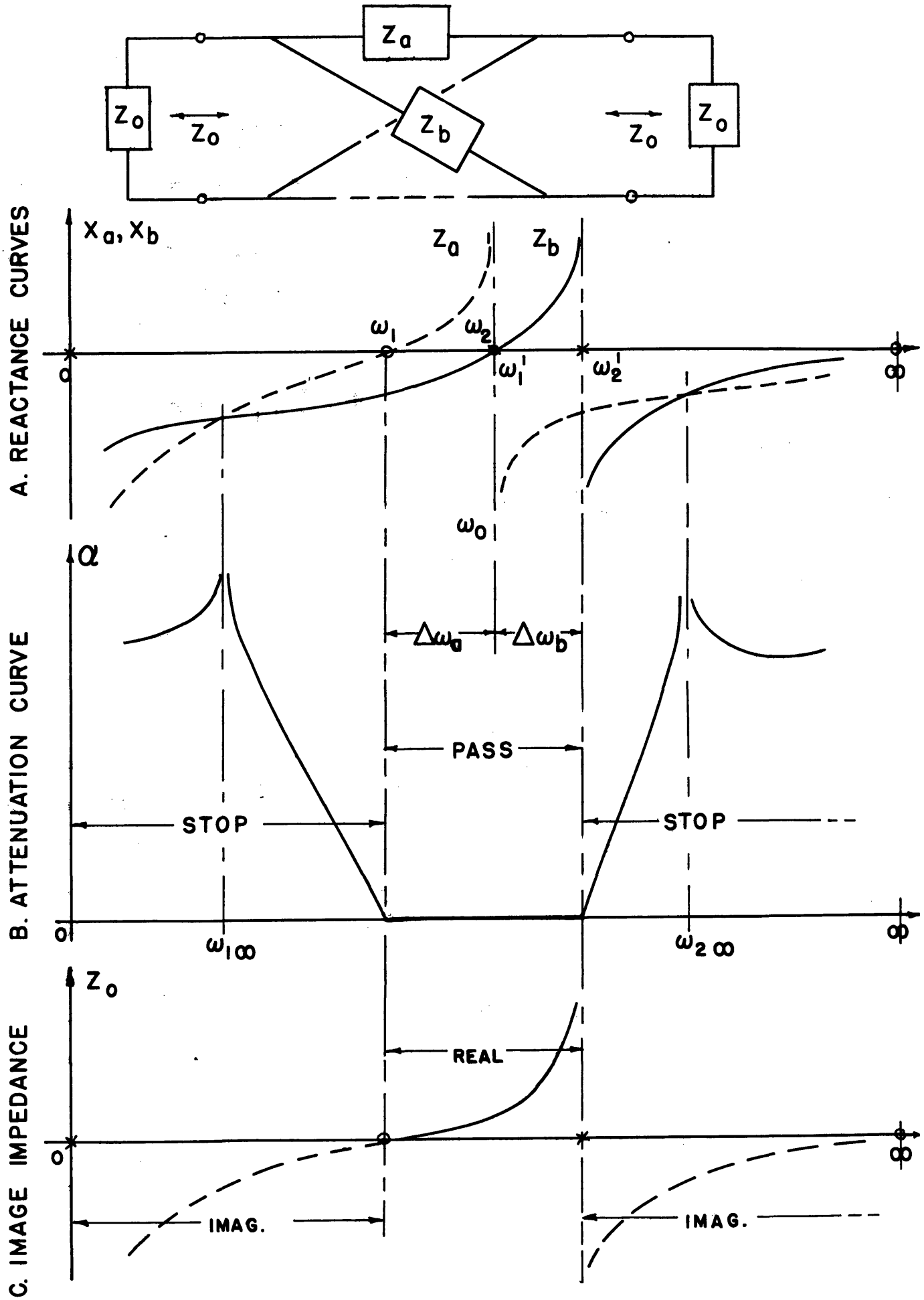

FIG. 28 THE CRYSTAL LATTICE FILTER

to be very simple functions of the series and shunt impedances Z_a and Z_b.[15] Thus,

$$Z_o = \sqrt{Z_a Z_b} \tag{19}$$

$$\gamma = \alpha + j\beta = \ln \frac{p + 1}{p - 1}$$

where

$$p = \sqrt{\frac{Z_b}{Z_a}}, \tag{20}$$

from which the attenuation loss is given by

$$\alpha = \ln \left| \frac{p + 1}{p - 1} \right| \tag{21}$$

The requirements for filtering action will now be discussed.

A region of zero attenuation will be a "flat" pass band, provided Z_o has such a value in that region that the filter can be properly terminated. Eq.(21) indicates that the attenuation will be zero whenever p is imaginary. When Z_a and Z_b are purely reactive networks (i.e., $Z_{a,b} = jX_{a,b}$ where X is real), then p as given by eq.(20) will be imaginary if X_a and X_b have opposite algebraic signs. Under these conditions, Z_o (eq. 19) will be a real function, and proper termination may be possible.

In a stop band, the attenuation must be greater than zero, which requires p to be real. X_a and X_b must therefore have the same algebraic signs. Where this is true, Z_o is imaginary and any real termination corresponds to a mismatch. The effect of this mismatch is to introduce a "reflection loss" which is very small compared to the attenuation loss in the stop band, and will be neglected.

Consideration of eq.(21) will show that where p =1, that is where $Z_a = Z_b$, the attenuation will be infinite.

Figure 28A shows how the conditions discussed above are satisfied by using crystal elements for the series and shunt arms

of the lattice. The corresponding curves of attenuation and image impedance are sketched in Fig. 28B and C.

Between zero frequency and w_1, the resonant radian frequency of Z_a, both reactances are capacitive or negative. This condition results in a region of real attenuation. Note the peak of attenuation at $w_{1\infty}$, where the series and shunt arm reactances are equal. Also observe that the image impedance is imaginary in this region.

If w_2, the antiresonant frequency of Z_a, is caused to coincide with w_1', the resonant frequency of Z_b (primes will be used to denote all parameters relating to Z_b), then a pass band will exist between the remaining two critical frequencies. The reactances will have opposite algebraic signs in this region and the image impedance will be real. Note that although the image impedance is real in the pass band, it takes on every value from zero to infinity in that region, so that a single resistance cannot provide a perfect match to the filter and a reflection loss will result from such a resistive termination. The reflection loss in the pass band may not be neglected as it was in the stop band. The problem of providing a suitable termination for the filter was handled largely by experimental procedure and will be more fully discussed in a later section.

Above w_2', the attenuation is again real and conditions are similar to those which exist below the lower cut-off frequency, w_1.

C. Problems of Filter Design

Design formulae are available in the literature[14] which, upon specification of the filter center frequency, band pass, impedance level and position of infinite attenuation peaks, yield the appropriate values of inductance and capacitance for the crystal equivalent circuit. There is one basic difficulty with such a design procedure. Once the desired values of the circuit parameters are calculated, there is no assurance that any crystals with such element values can be cut. Consultation with manufacturers of quartz crystals indicated that the situation was far more critical than expected. The following facts were gathered at that time:

1. For any specified crystal cut and desired value of resonant frequency, there exists a recommended set of dimensions for the crystal blank. An attempt to alter these dimensions might have an adverse effect on the crystal Q, assuming that the new dimensions could be obtained at all without introducing spurious modes of vibration.

2. Crystals with resonant frequencies very close to one another will have dimensions (hence equivalent circuit parameters) which differ very slightly.

3. Dimensions supplied for an 80 kc crystal lead to the following approximate values of circuit parameters:

$$L_1 = 120 \text{ henries}$$
$$C_1 = .04 \text{ micromicrofarads (mmf)} \qquad (22)$$
$$C_0 = 5.5 \text{ mmf (holder capacity will increase this value)}$$

It was felt that some design procedure was necessary which would take cognizance of the highly restricted properties of the filter crystals. The original method of analysis which was developed as part of this research will be presented in the section to follow.

D. Derivation of Design Procedure

It was pointed out in section B that the pass band of the crystal lattice filter extends from the zero of Z_a to the pole of Z_b, provided the other two critical frequencies coincide. However, because of the properties of the crystal cut, the spacing between critical frequencies of a single crystal (Δf), has a maximum value determined by the capacitance ratio r for the unmounted crystal, as explained in section A. For the -18.5° X-cut crystal, the value of r, taking into account the effect of crystal mount and holder capacity, will be about 250. Under these conditions, the value of Δf for an 80 kc crystal, given by eq.(18), would be about 160 cycles. The largest possible pass band for a crystal lattice filter with center frequency 80 kc would then be obtained from a symmetrical arrangement (i.e., $\Delta f_a = \Delta f_b$), and would be about 380 cps wide.

As was pointed out at the conclusion of section A, it is possible to reduce Δf by the use of external capacitors, keeping in mind the fact that a capacitor in series with a crystal raises f_1, while a capacitor in parallel lowers f_2. It is therefore possible to produce filter band widths smaller than 380 cps by many combinations of crystal critical frequencies and tuning capacitors. It will be shown however, that the proper combination of the aforementioned factors is highly restricted by the type of attenuation characteristic desired with any given band width.

The purpose of the design procedure to be developed is to express the image impedance Z_o and the shape of the attenuation characteristic in terms of Δf_a and Δf_b, which are the quantities altered through the use of external capacitors in Z_a and Z_b, respectively.

Although, as was pointed out in section B, the image impedance of the lattice filter varies monotonically from zero to infinity over the pass band, it is of interest to determine the numerical value of Z_o at the filter mid-frequency w_0 rad/sec.

From equation (11), and using the notation of Fig. 28, we obtain after satisfying the relation $w_0 = w_2 = w_1'$,

$$Z_a = -j\frac{w}{C_0}\frac{(w^2 - w_1^2)}{w^2(w^2 - w_0^2)} \tag{23}$$

$$Z_b = -j\frac{w}{C_0}\frac{(w^2 - w_0^2)}{w^2(w^2 - w_2'^2)} \tag{24}$$

Then by eq.(19), the image impedance becomes

$$Z_o = \frac{1}{w\sqrt{C_0C_0'}}\sqrt{\frac{w^2 - w_1^2}{-(w^2 - w_2'^2)}} \tag{25}$$

At mid-band frequency, $w = w_0$. Making this substitution and dividing the result by w_0^2 yields the image impedance at mid-band:

$$Z_{om} = \frac{1}{w_0\sqrt{C_0C_0'}}\sqrt{\frac{1 - (\frac{w_1}{w_0})^2}{(\frac{w_2'}{w_0})^2 - 1}} \tag{26}$$

From Fig. 28A,

$$w_1 = w_0 - \Delta w_a \tag{27}$$

$$w_2' = w_0 + \Delta w_b \tag{28}$$

where

$$w_0 \gg \Delta w_{a,b}$$

so that we may write

$$(\frac{w_1}{w_0})^2 = (1 - \frac{\Delta w_a}{w_0})^2 \doteq 1 - \frac{2\Delta w_a}{w_0} \tag{29}$$

$$(\frac{w_2'}{w_0})^2 = (1 + \frac{w_b}{w_0})^2 = 1 + \frac{2\Delta w_b}{w_0} \tag{30}$$

Substituting eqs.(29) and (30) into eq.(26), and writing the result in terms of real frequency, yields finally,

$$\boxed{Z_{om} = \frac{1}{2\pi f_0 \sqrt{C_0 C_0'}} \sqrt{\frac{\Delta f_a}{\Delta f_b}}} \tag{31}$$

It should be reiterated that eq.(31) gives the image impedance at the mid-band frequency f_0 only, and that the impedance at any other point must be calculated using eq.(25).

Of much greater moment in the design analysis undertaken here is the variation of attenuation with changes in Δw_a and Δw_b. Repeating equation (21),

$$\alpha = \ln \left| \frac{p + 1}{p - 1} \right| , \text{ where } p = \sqrt{\frac{Z_b}{Z_a}} .$$

Using the values of Z_a and Z_b from equations (23) and (24), we find

$$p = \sqrt{\frac{C_0}{C_0'} \frac{(w^2 - w_0^2)^2}{(w^2 - w_1^2)(w^2 - w_0'^2)}} \tag{32}$$

The attenuation at any point in the stop band may be determined from eq.(32). More specifically, consider the position of a peak of attenuation ($w_{1\infty}$ or $w_{2\infty}$ in Fig. 28B). Such a peak occurs when α is infinite or when p is equal to unity. Setting p = 1 in eq.(32) yields

$$(w^2 - w_1^2)(w^2 - w_2'^2) = k(w^2 - w_0^2)^2 \tag{33}$$

where

$$k \equiv \frac{C_0}{C_0'} \tag{34}$$

$$w = w_{1\infty} , w_{2\infty}$$

In order to obtain the parameters Δw_a and Δw_b explicitly in eq. (33), use is made of eqs.(27) and (28) to obtain

$$w_1^2 = (w_0 - \Delta w_a)^2 = w_0^2 - 2w_0 \Delta w_a \tag{35}$$

$$w_2'^2 = (w_0 + \Delta w_b)^2 = w_0^2 + 2w_0\Delta w_b \tag{36}$$

Substituting eqs.(35) and (36) into eq.(33) yields

$$(w^2 - w_0^2 + 2w_0\Delta w_a)(w^2 - w_0^2 - 2w_0\Delta w_b) = k(w^2 - w_0^2)^2$$

letting $x = w^2 - w_0^2$, multiplying out and rearranging terms,

$$(1 - k)x^2 + 2w_0(\Delta w_a - \Delta w_b)x - 4\Delta w_a\Delta w_b w_0^2 = 0 \tag{37}$$

let $$K \equiv \frac{\Delta w_b}{\Delta w_a}, \tag{38}$$

then equation (37) becomes

$$(1 - k)x^2 - 2w_0(K - 1)\Delta w_a x - 4K\Delta w_a^2 w_0^2 = 0 \tag{39}$$

Solving eq.(39) for x, and substituting $w^2 - w_0^2$ for x,

$$w^2 - w_0^2 = w_0 \frac{(K-1)\Delta w_a \pm \sqrt{[(K-1)^2 + 4K(1-k)]\Delta w_a^2}}{1-k} \tag{40}$$

Rearranging terms and writing eq.(40) in terms of real frequency, $f = \frac{w}{2\pi}$, yields finally

$$\boxed{f_{1\infty,2\infty}^2 = f_0\left[f_0 + \Delta f_a \frac{(K-1) \pm \sqrt{(K-1)^2 + 4K(1-k)}}{1-k}\right]} \tag{41}$$

where $$k \equiv \frac{C_0}{C_0'}, \quad \text{and} \quad K \equiv \frac{\Delta f_b}{\Delta f_a}$$

The following observations, based on physical reasoning and experiment will help to indicate the use of eq.(41) toward the further development of a design procedure.

1. Consider an attenuation peak on one side of the pass band, for example $f_{2\infty}$ in Fig. 28B. This peak can be made to fall anywhere between f_2' and infinity. It was found experimentally however, that an attempt to place the peak very close to the cut-off frequency will result in a filter with a very poor attenuation char-

acteristic beyond the peak, the attenuation loss dropping sharply past the peak to values as low as 20 db before rising again. In fact, not until the peak lies at least 500 cycles from the cut-off frequency, will the attenuation curve take on a satisfactory overall shape for the single filter stage. A glance at the 100 cycle filter characteristic shown in Fig. 35 will illustrate the desired characteristic.

2. Let us consider physically how an attenuation peak is obtained in the lattice filter structure. Reference to Fig. 28 will indicate that a peak occurs at the crossover points of Z_a and Z_b. Since the reactance-frequency curve always has a positive slope, it is necessary that the reactance of Z_b have a smaller absolute magnitude than that of Z_a at very low and very high frequencies if peaks are to occur on both sides of the pass band. However, it may be verified by considering the crystal equivalent circuits (Fig. 27B), and the approximate values of the parameters given by eq.(22), that near zero or infinite frequency the behavior of the reactance curve is determined almost exclusively by C_0. In order to obtain the required cross-over it is therefore necessary that C_0' be greater than C_0, so that the resultant reactances will have the relationship mentioned. This discussion seems to restrict the value of $k = \frac{C_0}{C_0'}$ in eq.(41) to values less than unity.

Returning to equation (41), an attempt to make k greater than unity will result in one of two conditions:

1. Considering the term under the square-root sign, note that if $k > 1$, then $(1-k)$ is negative. However, K is always positive, so that if k is so large that $|4K(1-k)| > (K-1)^2$, then no real f will satisfy eq.(41), and no attenuation peaks will occur.

2. If $|4K(1-k)| < (K-1)^2$, then the term under the square-root sign

will be positive. The resultant root however, will be smaller than the magnitude of (K-1). As a result, the two solutions of eq.(41) will either both be greater or less than f_0, depending on the magnitude of K. In other words, if k is greater than unity, but not too much greater, both attenuation peaks will lie on the same side of the pass band.

Assuming that a filter with high attenuation on both sides of the pass band is desired, we shall eliminate values of k greater than unity from further discussion and consider the quantitative effect of varying k within the range zero to unity.

Let us for the moment restrict the discussion to the symmetrical filter ($\Delta f_a = \Delta f_b$ or K = 1). Under this condition, eq. (41) becomes:

$$f^2 = f_0^2 \pm f_0 \Delta f_a \frac{2}{\sqrt{1-k}} \tag{42}$$

As k increases from zero to unity, eq.(42) shows that the attenuation peaks move from the cut-off frequencies out to zero and infinite frequency. It has been pointed out that for suitable attenuation characteristics, the position of the attenuation peaks should be not less than 500 cycles or so removed from the center frequency. If we require that a filter be built with peaks 1000 cycles from f_0, and further assume that f_0 is large compared to 1000 cps, as it will normally be (for this research f_0 is 80 kc), then eq.(42) may be written as

$$f = f_0 \pm \frac{\Delta f_a}{\sqrt{1-k}} \tag{43}$$

Note that wherever the spacing between f_0 and $f_{1\infty}$ or $f_{2\infty}$ is small compared to f_0, then eq.(43) will hold, and a symmetrical filter will have attenuation peaks which are symmetrically located about the center frequency of the filter.

Returning to the problem of producing attenuation peaks 1000 cycles from f_0, eq.(43) yields

$$\frac{\Delta f_a}{\sqrt{1-k}} = 1000 \text{ cps} \qquad (44)$$

For a 100 cycle filter, where $\Delta f_a = 50$ cps, eq.(44) yields

$$k = .9975 ,$$

while for a 10 cycle filter band pass, we obtain

$$k = .999975$$

In general, k must lie between about 0.95 and 1.00 to obtain a suitable symmetrical filter, with the required value of k drawing closer to unity as the band width decreases.

The effect of making the filter unsymmetrical (K different from unity) is to make the attenuation characteristic unsymmetrical. That is, the attenuation peaks will not be equally distant from f_0. The extent and character of this effect can best be illustrated by several examples.

The table below gives a comparison of the positions of $f_{1\infty}$ and $f_{2\infty}$ for K = 1 and K ≠ 1, given by eq.(41). The center frequency f_0 is 80 kc in all cases.

k	Δf_a	Δf_b	K	$f_{1\infty}$	$f_{2\infty}$
.9975	50 cps	50 cps	1	f_0 - 1000 cps	f_0 + 1000 cps
.9975	50	60	1.2	f_0 - 280	f_0 + 4290
.9975	50	40	0.8	f_0 - 4185	f_0 + 190
.999975	5 cps	5 cps	1	f_0 - 1000 cps	f_0 + 1000 cps
.999975	5	6	1.2	f_0 - 30	f_0 + 4030
.999975	5	4	0.8	f_0 - 4030	f_0 + 20

In general, if K ≠ 1, the attenuation peaks will be shifted up or down frequency, depending on whether K is greater or less

than unity. For the filters discussed above, changing K by 20% moved one of the peaks too close to f_0 in all cases, with the effect being worse for the narrower band width.

Summarizing the preceeding discussion, a filter with desirable attenuation characteristics should have the following properties:

$$\Delta f_a \cong \Delta f_b \tag{45}$$

$$.95 \leq \frac{C_0}{C_0'} < 1.0 \tag{46}$$

As the desired band width decreases, the tolerance on eq.(45) becomes smaller, and at the same time C_0 must be more nearly equal to C_0'. Since the capacitor C_0 across a crystal has a direct effect upon the separation between the critical frequencies (Δf) of the resultant network, then eqs.(45) and (46) are not independent. Recalling eq.(18), we obtain the equations,

$$\Delta f_a = \frac{f_1}{2r} = \frac{f_0 - \Delta f_a}{2r} \cong \frac{f_0}{2r} \tag{47}$$

$$\Delta f_b = \frac{f_1'}{2r'} = \frac{f_0}{2r'} \tag{48}$$

Then by equation (45) and using equation (10),

$$r = r' \quad \text{or} \quad \frac{C_0}{C_1} = \frac{C_0'}{C_1'} \tag{49}$$

Finally since $C_0 \cong C_0'$ by equation (46), eq.(49) yields

$$\underline{C_1 \cong C_1'} \tag{50}$$

This final result is highly significant since it leads directly to an extremely simple design procedure. It was mentioned in section C that two crystals with corresponding critical frequencies close to one another will have equivalent circuit para-

meters which differ very slightly. If the values of C_1 for the lattice crystals as originally ground could be made equal, then the use of series condensers to satisfy eq.(50) could be avoided, since only through the use of a series condenser can C_1 of a crystal be altered.

If no series condensers are employed however, then the resonant frequencies of Z_a and Z_b cannot be altered. Reference to Fig. 28A will show that the two resonant frequencies f_1 and f_1' (or f_0) are separated by half the band width or Δf. The remaining question then is: How can two crystal be ground with the same value of C_1, but with resonant frequencies Δf apart? Keeping in mind the fact that Δf is quite small compared to the filter center frequency f_0, the answer to this question is quite simple:

The resonant frequency of a crystal network is proportional to $\frac{1}{\sqrt{L_1 C_1}}$ by eq.(12). Therefore, by eqs.(1) and (2), the resonant frequency is proportional to $\frac{1}{W}$, where W is the crystal width times the cosine of 18.5°. Increasing the resonant frequency of a crystal by Δf will therefore require a small decrease in the crystal width. If at the same time, the crystal length is increased and/or its thickness decreased, then the $\frac{LW}{T}$ ratio (hence the value of C_1, by eq. 2) will remain the same.

Having thus satisfied the requirements that $C_1 = C_1'$, and that the crystals for Z_a and Z_b are ground with resonant frequencies $f_0 - \Delta f_a$ and f_0, respectively, it remains only to place capacitors in parallel with Z_a and Z_b so that the antiresonant frequencies of the resultant networks lie at f_0 and $f_0 + \Delta f_b$, respectively. Because of the tolerances involved, final adjustment of the attenuation characteristic must done experimentally.

E. Summary of Design Procedure

This section will present the design procedure for a crystal lattice filter based on the results of the analysis given in section D, while the sections to follow will illustrate the experimental equipment and techniques necessary to carry out the procedure. Finally, the filter used in this research will be described.

Design of filter with band width $B = 2\Delta f$, at frequency f_0:

1. Crystals 1 and 2 (for Z_a) should have resonant frequency of $f_0 - \Delta f$ cps.

2. Crystals 3 and 4 (for Z_b) should have resonant frequency of f_0 cps, and the $\frac{LW}{T}$ ratio at crystals 1 and 2.

3. Measure C_0 and C_1 of each crystal unit. The equipment necessary for this step is described in section F.

4. Using the relationship

$$r = \frac{C_{0T}}{C_1} = \frac{f_0}{2\Delta f} \quad , \tag{51}$$

calculate the total parallel capacitance (C_{0T}) necessary to place the antiresonant frequency of each crystal Δf cps above its resonant frequency. Obtain $C_{0X} = C_{0T} - C_0$ for each crystal.

5. Place variable capacitor of approximate value C_{0X} across each corresponding crystal. Using the equipment described in section F-1, tune capacitor until antiresonant frequency is Δf above resonant frequency. Place resultant units in lattice arrangement.

6. Using equipment described in section G, retune capacitors across crystals 3 and 4 only to obtain the desired attenuation characteristic. The band width will not be effected by this step.

7. Terminate filter in double-tuned transformers which present an impedance to the filter of approximately

$$Z_{om} = \frac{1}{2\pi f_0 C_{0T}} \quad . \quad \text{(from eq. 31)}$$

Using equipment described in section G, check filter pass band.

F. Measurement of Crystal Parameters

In order to carry out the design procedure outlined in section E, it is necessary to know the values of C_0 and C_1 for each filter crystal. While C_1 cannot be measured directly, it may be determined by the following procedure:

(a) Measure the crystal resonant and antiresonant frequencies, f_1 and f_2, respectively.

(b) Calculate $\Delta f = f_2 - f_1$

(c) By eq.(18), $$r = \frac{f_1}{2\Delta f}$$

(d) Measure C_0

(e) Then by eq.(10), $$C_1 = \frac{C_0}{r}$$

This section will describe the equipment and techniques used to accomplish the measurement of resonant frequency, antiresonant frequency, C_0 and series resistance. The latter measurement was made for the purpose of determining the effective crystal Q.

1. Measurement of resonant and antiresonant frequency. Fig. 29A shows the equipment used to measure f_1 and f_2 of the mounted crystal. At resonance, the crystal presents a minimum impedance and the VTVM will read maximum. The reverse is true at antiresonance. The 100 ohm resistors eliminate the effect of stray wiring capacity which would otherwise reduce the accuracy of the measurement. The General Radio 805C has a vernier dial which is calibrated to read 8 cycles per division at 80 kc (the filter center frequency used in this research). This dial can be read accurately to about 2 cycles.

The resonant frequency of the crystal has been precisely

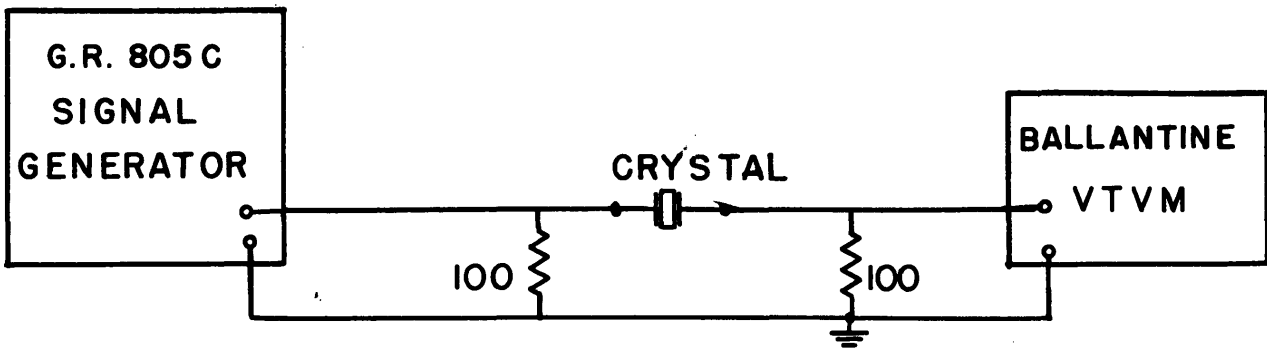

A. MEASUREMENT OF ω_1 AND ω_2

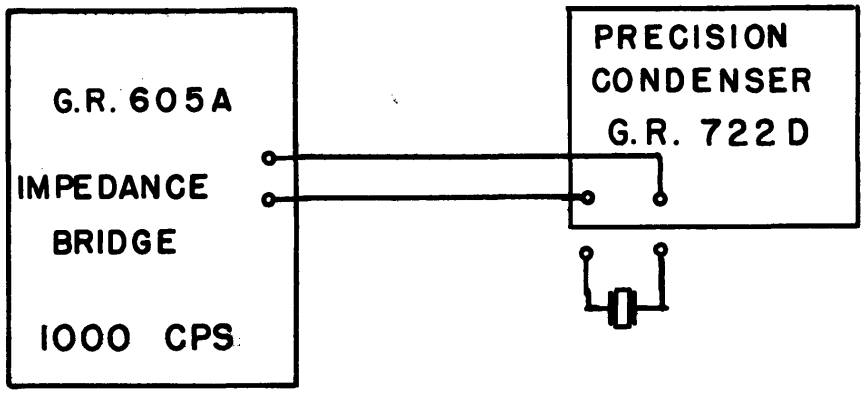

B. MEASUREMENT OF C_Q

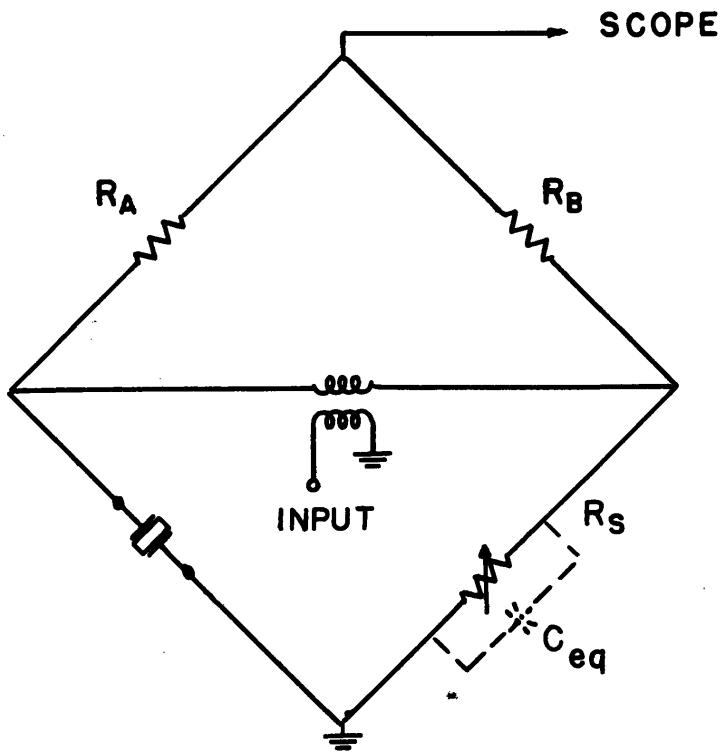

C. MEASUREMENT OF R

FIG. 29 QUARTZ CRYSTAL MEASUREMENT EQUIPMENT

ground into the crystal and is specified by the manufacturer, so that f_1 is not measured, but is used to calibrate the Signal Generator. Because of this fact, measurements of Δf, which is about 200 cycles before external capacitance is added, may be made accurately to about 2 cycles.

This equipment is also used for preliminary tuning of the lattice filter units as explained in step 5 of section E.

2. Measurement of C_0. It was pointed out in section D that at low frequencies the crystal impedance is essentially that of a capacitor of value C_0. Measurement of C_0 was therefore accomplished by a bridge measurement at 1 kc.

The apparatus used for making the measurement is shown in Fig. 29B. Because of the small values of capacitance which must be measured ($C_0 \approx 7$ micromicrofarads), the substitution method is used. The measurement procedure is as follows:

(a) Set Precision Condenser to some nominal value, say 100 $\mu\mu$f. Balance bridge at this point.

(b) Place crystal across Precision Condenser. It will now be necessary to decrease the capacitance of the Precision Condenser by an amount ΔC in order to restore balance.

(c) Then $C_0 = \Delta C$.

All measurements of crystal parameters were made with the crystal in a bakelite socket, similar to the one used in the final filter. The capacitance introduced by the socket, although very small, may not be neglected compared to C_0 of the crystal in its original holder.

3. Measurement of Effective Resistance. At its resonant frequency, a crystal appears as C_0 in parallel with the effective resistance R. L_1 and C_1, which normally are in series with R, are effectively

cancelled out by the resonance.

The value of R is measured by the simple bridge shown schematically in Fig. 29C. The input generator is a G.R. 805C Signal Generator which is tuned to the resonant frequency of the crystal. R_S is a 100,000 ohm decade resistance. R_A and R_B are precision resistors of 3,000 ohms each.

The equivalent shunt capacitance of the decade box (C_{eq}) partially balances out C_0, and the null indication on the oscilloscope is fairly sharp.

Fig. 30A shows the measured values of the equivalent circuit parameters for the four crystals used in the filter described in sections H and I.

Crystals 1 and 2 are identical crystals used in the series arms of the lattice. Small variations in the measured values of crystal parameters for these two crystals have been neglected, and the average values are presented here. The same is true for crystals 3 and 4, which are the shunt arm crystals.

To account for the capacitance of the bakelite crystal socket, 1.1 $\mu\mu$f should be added to all values of parallel capacitance (C_0) shown in Fig. 30A.

The value of inductance (L_1) was calculated from eq.(12), which combined with eqs.(10) and (18) yields,

$$L_1 = \frac{1}{8\pi^2 f_1 C_0 \Delta f} \qquad (52)$$

The values of $Q = \frac{2\pi f_1 L_1}{R}$ calculated from the circuit parameters are as follows:

For crystals 1 and 2, f_1 = 79,950 cps, $\underline{Q = 23,000}$

For crystals 3 and 4, f_1' = 80,002 cps, $\underline{Q = 14,500}$

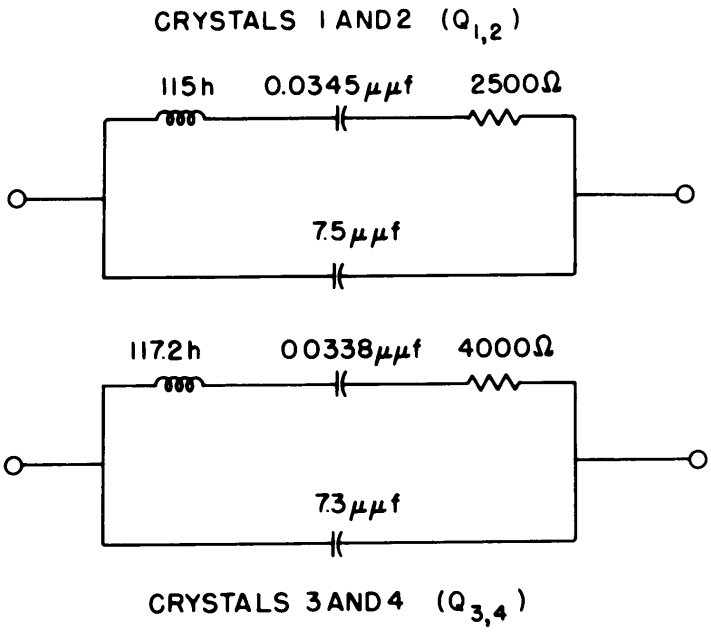

A. MEASURED CRYSTAL PARAMETERS

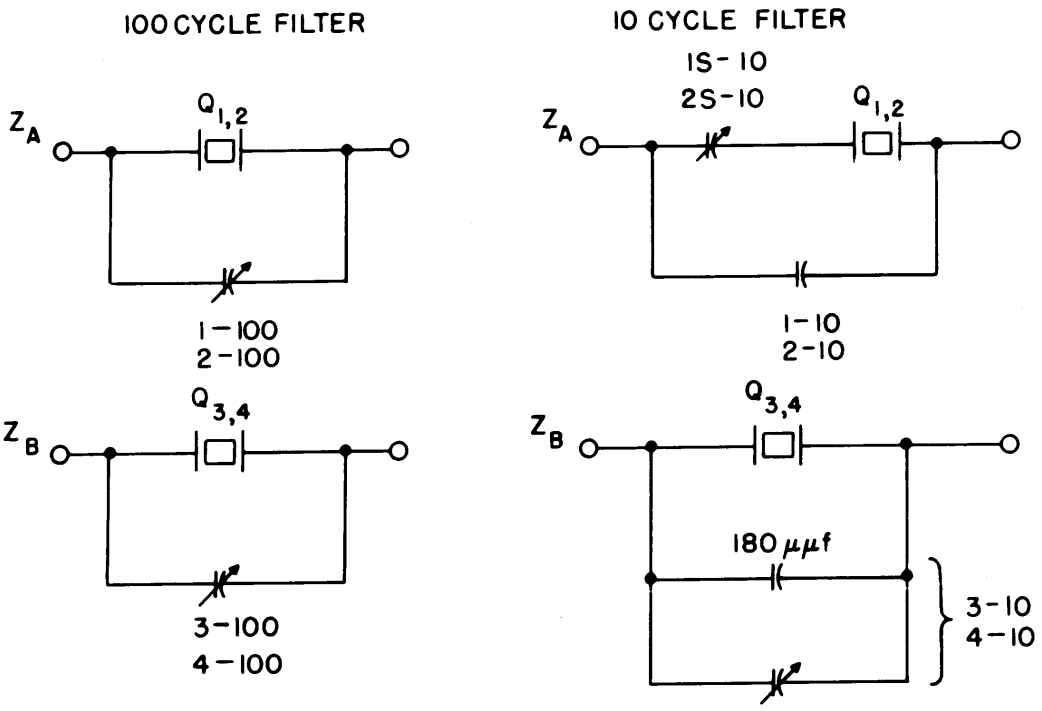

B. FILTER UNITS

FIG. 30 FILTER CRYSTAL PARAMETERS & TUNING CAPACITORS

G. Crystal Filter Characteristic Display Equipment

Once the filter crystals and their corresponding parallel tuning capacitors are adjusted to provide the positions of critical frequencies necessary to produce the desired band width (step 5, section E), only two additional adjustments are needed to complete the design of the lattice filter. First, the attenuation characteristic of the filter must be asjusted by varying the ratio of total parallel capacitance in Z_a (C_{OT}) to that in Z_b (C_{OT}'), as indicated by eq.(46). If the design prodedure has been carried out as outlined in section E, then C_{OT} and C_{OT}' will be very nearly equal, and an extremely small increase in C_{OT}' is all that is necessary to place the attenuation peaks in their proper position. Because of the tolerances involved, this step must be carried out experimentally. The final filter asjustment calls for terminating the filter so that a flat pass band is obtained over as large a range of the theoretical band width as possible. Because of the behavior of Z_o over the pass band (Fig. 28C), this step must be carried out experimentally, and some method of observing the filter band pass as the terminating circuits are adjusted is essential to the procedure.

Figure 31 is a block diagram of the equipment used in the final stages of filter design. The filter crystal and capacitor units are placed in a lattice structure terminated in 80 kilocycle double-tuned transformers. The G.R. 805C Signal Generator is capable of being read to accuracies of about 2 cps, after calibration with a filter crystal. For adjustment of the filter attenuation characteristic, the Signal Generator is tuned manually over the wide range of frequencies outside of the filter pass band, and a Ballantine (Model 300) Voltmeter (marked "VTVM" in

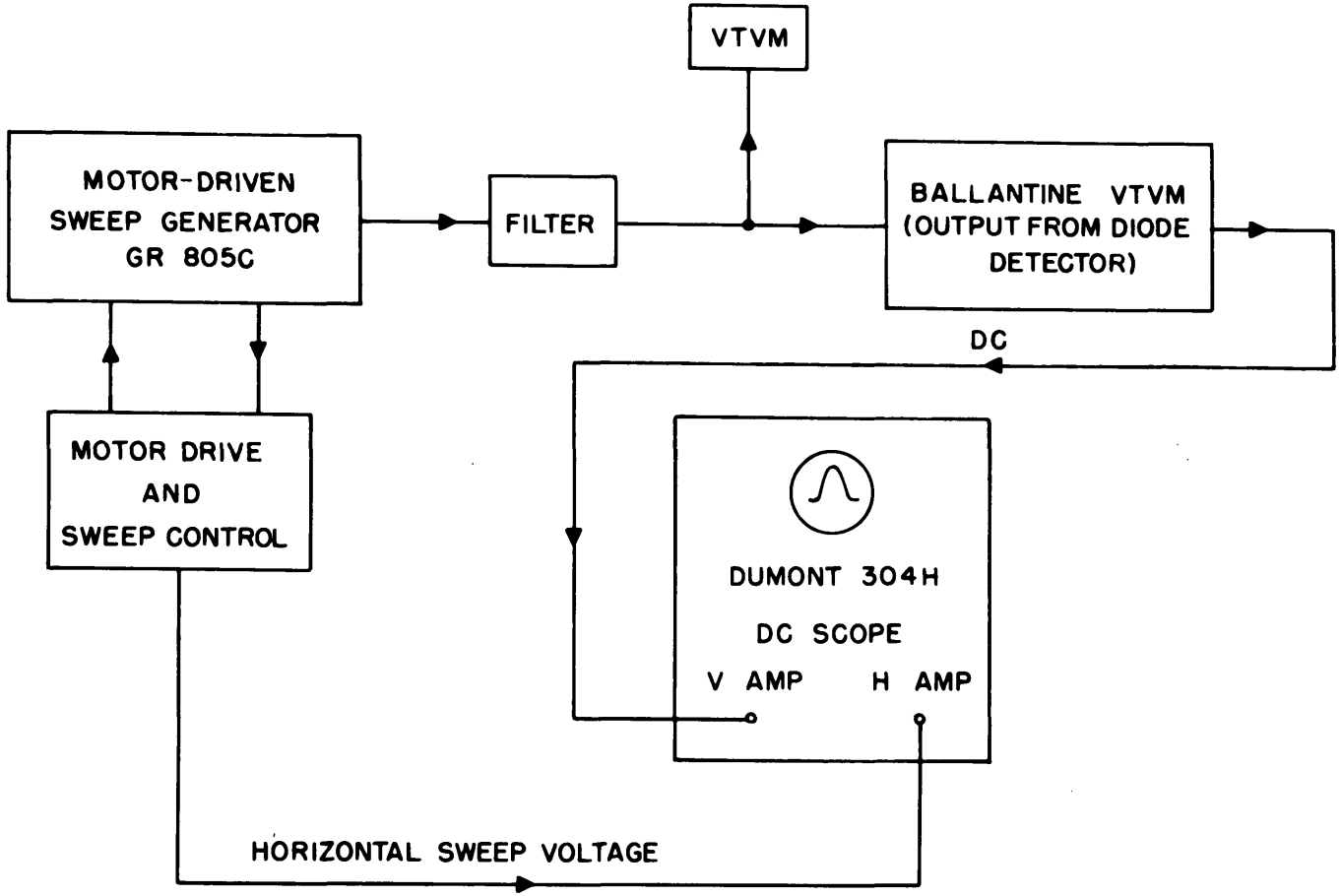

FIG. 31 BLOCK DIAGRAM OF FILTER CHARACTERISTIC DISPLAY EQUIPMENT

Fig. 31) is used to indicate relative response.

To avoid point-by-point measurement of the filter pass band characteristic, which would be difficult and inaccurate because of the narrow band widths involved, the G.R. 805C is converted to a motor-driven sweep generator. As the generator sweeps over the pass band it generates two signals. One signal is the normal generator output which goes directly to the filter. The output voltage of the filter is proportional to the filter response characteristic. This voltage is then fed to a Ballantine (Model 300) VTVM, which has an internal diode detector whose d-c output is proportional to the voltmeter input voltage. The detector output is amplified by a Brush (BL 932) D-C Amplifier (not shown in Fig. 31), and finally fed to a Dumont 304H D-C Oscilloscope. The second generator signal is a d-c voltage proportional to output frequency. This voltage becomes the horizontal sweep voltage of the oscilloscope. Thus, the frequency response curve of the filter pass band is plotted on the oscilloscope face.

The converted Signal Generator is shown pictorially in Fig. 32, while the motor driving circuit and the sweep control are shown in the schematic diagram, Fig. 33.

The horizontal sweep voltage is produced by a linear potentiometer which is ganged to the vernier dial of the generator. The potentiometer is excited by a 45 volt battery, so that as the vernier dial rotates to change frequency, the potentiometer output voltage changes proportionally.

The vernier dial (marked "Carrier Frequency Increment") is driven by a 10 rpm, single phase capacitor motor, via a spring-loaded dial cable. Two motor speeds are provided; a slow speed controlled by a Variac, to trace out the filter characteristic, and a faster speed for retrace, during which time the

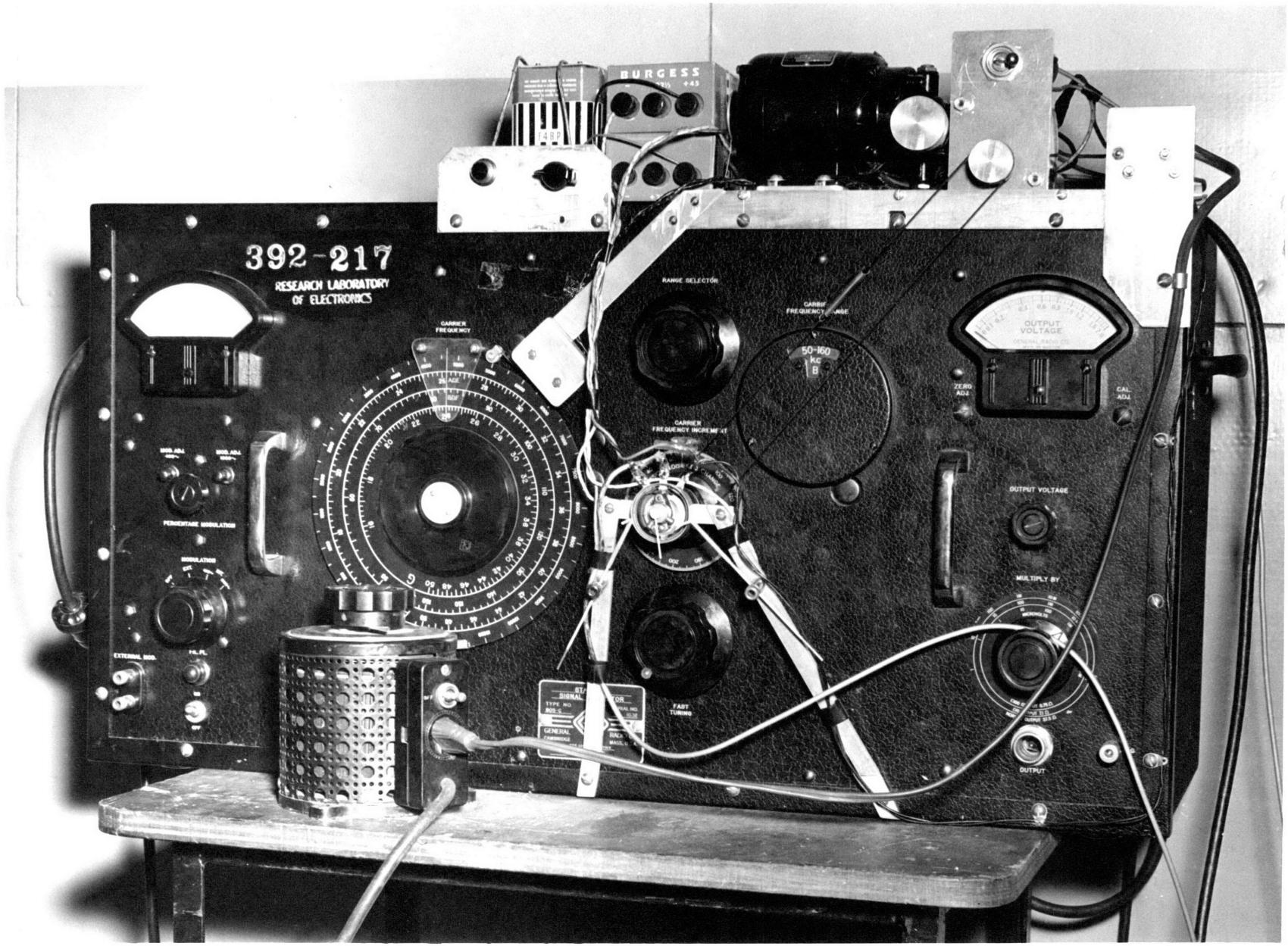

FIG. 32: MOTOR-DRIVEN SWEEP OSCILLATOR

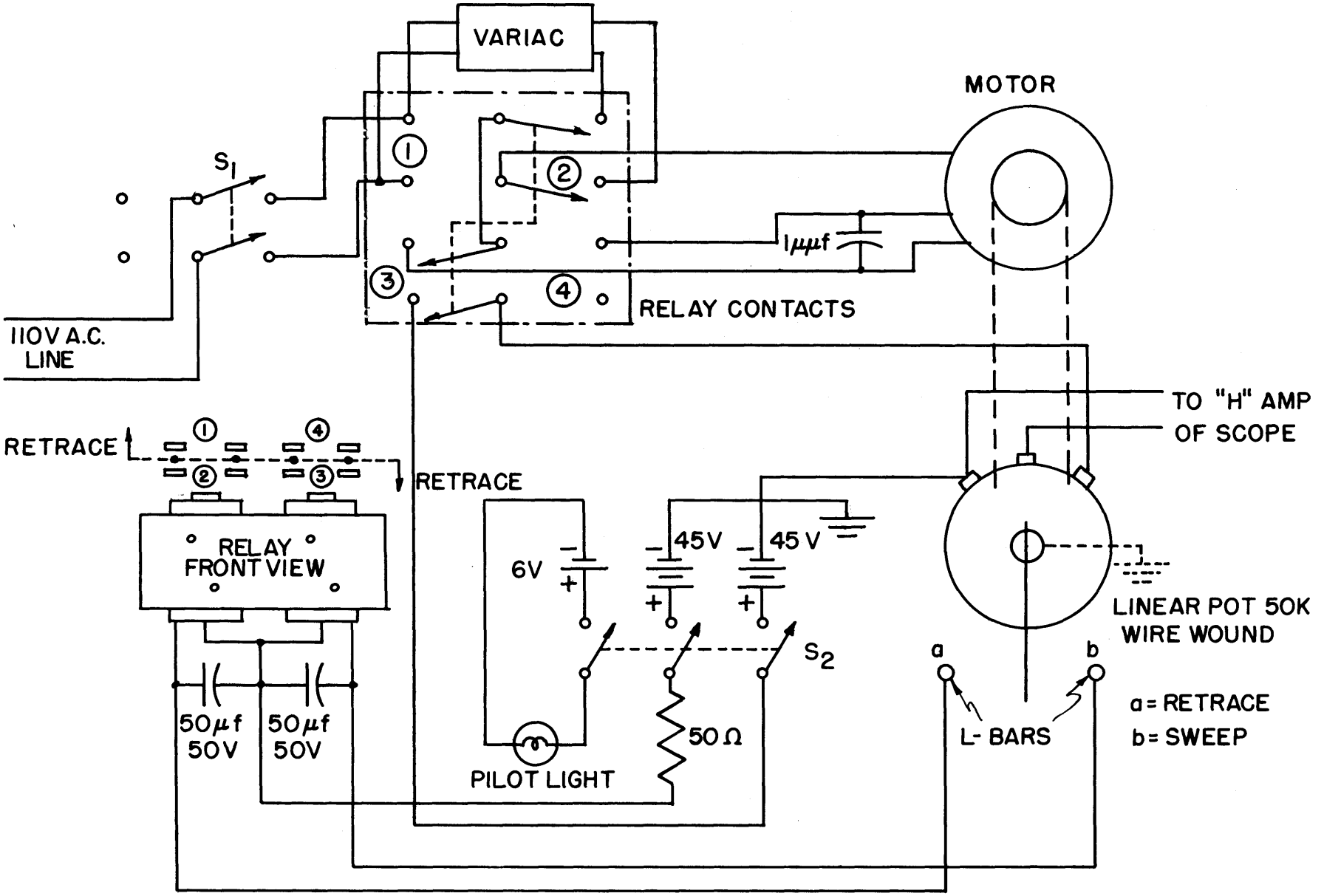

FIG. 33 SWEEP OSCILLATOR DRIVING CONTROL SCHEMATIC

oscilloscope trace is "blanked out".

The action of the sweep control is as follows:

Note in Fig. 32 that the center arm of the potentiometer has been extended and a metal rod soldered perpendicular to the arm. The rod points downward in the picture. Note also the two L-shaped bars at either side of the potentiometer. These bars are adjustable with relation to the potentiometer rod by means of the binding posts through which the bars pass. Let us assume that the vernier dial is being slowly rotated counter-clockwise by the Variac-controlled motor, and that the filter characteristic is being traced on the long-persistance oscilloscope screen. The potentiometer rod is approaching the L-bar to the right of the potentiometer. When the bar is struck by the rod, a relay circuit is closed (Fig. 33) which reverses the motor, places the motor directly across the line to increase the driving speed, and finally, disconnects the potentiometer exciting voltage, thereby "blanking out" the oscilloscope trace. The vernier dial now rotates in a clockwise direction until the L-bar on the left is struck, whereupon the relay returns all components to their "trace" conditions.

By adjusting the L-bars, any band up to 1,600 cps in width, centered at 80 kc, can be viewed. The Variac allows the speed to be lowered as the band width to be viewed is decreased, since a smaller band width requires a larger signal build-up time.

After initial adjustments of sweep width and sweep speed, the generator runs automatically, allowing the operator to make filter termination adjustments while continually observing the filter band-pass characteristic.

It should be pointed out that the sweep generator can be used at any frequency in the range of the G.R. 805C.

H. The 100 Cycle Filter

It was pointed out in Chapter II, section D, that for proper operation of the spectrum analyzer over its entire frequency range, two filter band widths, 100 cps and 10 cps, are necessary. The design of the 100 cps filter was carried out using the procedure outlined in section E. The 10 cps filter, which uses the same four filter crystals as the 100 cps filter, required a more complicated design procedure. Section I describes the 10 cps filter.

Design of filter with band width $B = 2\Delta f = 100$ cps, and center frequency $f_0 = 80$ kc.

1. Crystals 1 and 2 (for Z_a) were ground with resonant frequency $f_1 = f_0 - \Delta f =$ 79,950 cps.

2. Crystals 3 and 4 (for Z_b) were ground with resonant frequency $f_1' = f_0 =$ 80,002 cps. (This figure is within the .003% tolerance specified for the position of the resonant frequency. The two crystals, 3 and 4, are identical to a much smaller tolerance). Although the requirement of equal $\frac{LW}{T}$ ratio for all crystals was not specified at the time the crystals were ordered, the measured values of C_1 and C_1' (step 3) are sufficiently close to one another to permit the construction of a symmetrical filter.

3. Using the equipment described in section F, the values of C_0 and C_1 for each crystal were measured (see Fig. 30).

Crystals 1 and 2: $C_1 = .0345$ μμf
$C_0 = 8.6$ μμf

Crystals 3 and 4: $C_1 = .0338$ μμf
$C_0 = 8.3$ μμf

The values of C_0 and C_0' include the capacitance of the bakelite crystal socket which houses the crystal unit.

4. Using eq.(51),

$$r = \frac{80,000}{2 \times 52} = 769 \quad (\Delta f \text{ is } 52 \text{ cps because } f_0 \text{ is } 80,002)$$

whence,

$$C_{OT} = 769 \quad .0345 = 26.5 \ \mu\mu f$$

$$C_{OT}' = 769 \quad .0338 = 26.0 \ \mu\mu f$$

and

$$C_{OX} = 26.5 - 8.6 = 17.9 \ \mu\mu f$$

$$C_{OX}' = 26.0 - 8.3 = 17.7 \ \mu\mu f$$

5. Having thus calculated the approximate values of external capacitance (C_{OX}) which must be added to each crystal to place its antiresonant frequency Δf above its resonant frequency, the remainder of the design procedure was carried out experimentally. A variable ceramic capacitor (4-30 $\mu\mu f$) was placed across each crystal. Using the equipment shown in Fig. 29A, the capacitors were adjusted to yield the proper arrangement of critical frequencies.

6. The resulting crystal units were placed in a lattice structure, similar to the filter schematic shown in Fig. 34. The test lattice contained only the 100 cycle filter components which may be identified in Fig. 34 by consulting Fig. 30B. By slightly increasing the tuning capacitance across crystals 3 and 4, a symmetrical attenuation characteristic with peaks at about 800 cycles above and below the center frequency and maximum attenuation of 70 db was obtained. The characteristic display apparatus described in section G was used to determine the attenuation curve.

The filter characteristic plotted in Fig. 35 was obtained after the entire filter (Fig. 34) was constructed. The presence of only one attenuation peak, and the loss of 10 db of attenuation

from the characteristic obtained in the test lattice is most likely due to the stray capacitance introduced by the selector switch and 10 cycle filter components (Fig. 34). Because the filter tuning capacitance is of the order of 20 $\mu\mu$f, the stray capacitance effects cannot be neglected. It was found that removing some of the 10 cycle components from the filter circuit resulted in a decided improvement in the attenuation characteristic. These components, even when not connected directly into their proper circuit positions by the selector switch, will place stray capacitance between each crystal and ground, and will therefore prevent the balanced lattice structure from providing a sharp null (peak of attenuation). Redesign of the switching circuit to avoid components from contacting the crystal terminals unnecessarily, and the use of low-capacitance switch elements would result in a better attenuation characteristic. For the purposes of this research, the characteristic shown in Fig. 35 is quite adequate.

7. The final step in the design procedure calls for terminating the filter so as to obtain a flat pass band characteristic over as wide a range of the theoretical 104 cycle band width as possible. The image impedance at the center frequency is given by eq.(31), which for a symmetrical filter as designed here yields,

$$Z_{om} = \frac{1}{2\pi f_0 C_{0T}} .$$

For the 100 cycle filter, Z_{om} = 75,000 ohms. By terminating the filter in 80 kc tuned circuits with various impedances at antiresonance, it was found that values of termination different from Z_{om} did not alter the extent of the flat region (about 60 cps), but merely shifted this region away from a symmetrical location about f_0. The terminating circuits shown in Fig. 34 present an impedance of 73,000 ohms to the filter.

I. The 10 Cycle Filter

If the 10 cps filter were to be designed using the procedure outlined in section E, two additional crystals (for Z_a) would have to be obtained. Crystals 3 and 4, used in the 100 cycle filter, could be used again, but crystals 1 and 2 do not have the proper resonant frequency. It was possible however to build a suitable filter for this research with a 10 cps pass band, using the same crystals manufactured for the 100 cps filter.

It was mentioned above that crystals 1 and 2 do not have the correct resonant frequency for the 10 cps filter application. However, it was pointed out in section A that a capacitance placed in series with a crystal will raise its resonant frequency. Consider the possibility of placing capacitance in series with crystals 1 and 2 so as to place f_1 within 5 cycles of f_0. Reference to the equivalent circuits shown in Fig. 27B indicates that a capacitance in series with a crystal has the effect of decreasing C_A. Hence, by eq.(5), C_1 is likewise decreased. If we now recall that the primary requirement for building a filter with attenuation peaks sufficiently far removed from f_0 to yield a suitable attenuation curve is that all parallel capacitances used in the filter elements be nearly equal (eq. 46), then it becomes apparent that a symmetrical filter cannot be built. That is, if $C_{OT} \cong C_{OT}'$, but C_1 is less than C_1' (as a result of the use of series capacitance in Z_a), then $r > r'$, and $\Delta f_b > \Delta f_a$ (eqs. 47 and 48). It will be shown later in this section that to design a filter with a pass band of 10 cycles, and $C_{OT} = C_{OT}'$, it was necessary to make $\Delta f_a \cong 3$ cps and $\Delta f_b \cong 7$ cycles, whereby $K \cong 2.3$ (eq. 41).

Concidering eq.(41) and the discussion of section D pertaining to this equation, we observe that the effect of making

K greater than unity is to shift the attenuation peaks to the right of where they would occur for a symmetrical filter. For example, the table below equation (44) in section D shows that for k of such value that the attenuation peaks occur 1,000 cps removed from f_0 in a symmetrical filter, an asymmetrical filter with K = 1.2 will have its attenuation peaks located 30 cps below f_0 and 4030 cps above f_0 (for the 10 cycle filter). For the filter at hand, where $K \cong 2.3$, consideration of eq.(41) shows that the best possible attenuation characteristic which can be obtained will have a peak below f_0, but can have no peak above f_0 (except at very high frequencies where the peak can have no effect on the skirts of the attenuation curve). This is exactly the type of characteristic obtained experimentally (Fig. 35).

In order to illustrate the design of a filter using series as well as parallel capacitances, the procedure for calculating the required values of capacitances used in the 10 cycle filter will be presented here. It should be pointed out that the calculations presented here will be the final group in a series of similar trial-and-error calculations which are necessary to determine the values of capacitance which will produce a filter with a total band width of 10 cps and with equal parallel capacitances in Z_a and Z_b. This procedure converges very rapidly to the correct solution because it is known that Δf_b is greater than Δf_a, and that Δf_a must therefore be less than 5 cps. At any rate, the values calculated need only be approximate, since all critical adjustments are performed experimentally.

1. For crystals 1 and 2 (Z_a), with no added capacitance (except the bakelite socket), the following values were measured:

$f_1 = 79{,}950$ cps, $C_1 = .0345$ $\mu\mu f$

$f_2 = 80{,}105$ cps, $C_0 = 8.6$ $\mu\mu$f.

2. Using eqs.(8) and (9), the values of the parameters of the Foster impedance form of crystal equivalent circuit (Fig. 27B), were found as follows:

$$C_A = C_1 + C_0 = 8.6 + .0338 = 8.6338 \ \mu\mu f \tag{53}$$

$$C_B = \frac{C_0}{C_1} C_A = 2150 \ \mu\mu f \tag{54}$$

3. Assume $f_a = 3$ cps. It is then required to move f_1 from 79,950 cps to 79,999 (since $f_0 = 80{,}002$). Under these conditions, the separation between resonant and antiresonant frequencies will be

$$\Delta f_a'' = f_2 - 79{,}999 = 106 \text{ cps}$$

4. By eqs.(10) and (18),

$$r'' = \frac{f_1}{2\,\Delta f_a''} = \frac{C_{BT}}{C_{AT}} = 379 \tag{55}$$

where C_{BT} and C_{AT} are respectively the total values of C_B and C_A which are necessary to yield a crystal unit with resonant frequency 79,999 and antiresonant frequency 80,105. However, only the resonant frequency is being altered at this point, so that a capacitance will be placed in series with the crystal, and only C_A will be effected. Therefore $C_{BT} = C_B = 2150$ $\mu\mu$f (eq. 54) From eq. (55),

$$C_{AT} = \frac{C_{BT}}{r''} = \frac{2150}{379} = 5.68 \ \mu\mu f \tag{56}$$

5. The value of C_A before series capacitance is added is 8.6338 $\mu\mu$f. To satisfy equation (56), an external capacitance (C_{AX}) must be placed in series with the crystal. The value of C_{AX}, which will produce $C_{AT} = 5.68$ $\mu\mu$f, is easily calculated to be

$$C_{AX} = 16.6 \ \mu\mu f. \tag{57}$$

6. The remaining calculation involving Z_a is the one which yields the value of parallel capacitance which must now be placed across the crystal and the series capacitance C_{AX} to move the antiresonant frequency of the unit from 80,105 cps to 80,002 cps (f_0). In order to accomplish this calculation, we must revert to the equivalent circuit involving C_1 and C_0. Using eqs.(5) and (6) we obtain for the crystal and series capacitance combination:

$$C_1'' = \frac{(C_{AT})^2}{C_{AT} + C_{BT}} = \frac{(5.68)^2}{2150 + 5.68} = .015 \ \mu\mu f \tag{58}$$

$$C_0'' = \frac{C_{AT}C_{BT}}{C_{AT} + C_{BT}} = 5.48 \ \mu\mu f \tag{59}$$

Note that placing capacitance in series with the crystal has lowered C_1, C_0, and C_A, but has not affected C_B.

7. To bring f_2 to 80,002 cps, or equivalently, to produce Δf_a= 3 cps, requires that the total parallel capacitance (C_{0T}) across Z_a be of such value that

$$r = \frac{C_{0T}}{C_1''} = \frac{f_1}{2\,\Delta f_a} = \frac{79,999}{2 \cdot 3} = 13,300 \tag{60}$$

From eqs. (58) and (60), we obtain

$$C_{0T} = rC_1'' = 200 \ \mu\mu f. \tag{61}$$

Finally, from eqs.(61) and (59), we obtain for the value of parallel capacitance which must be placed across Z_a,

$$C_{0X} = C_{0T} - C_0'' = 194.52 \ \mu\mu f. \tag{62}$$

8. For crystals 3 and 4 (Z_b), requiring that $C_{0T}' = 200 \ \mu\mu f$ (eq. 61), will yield (since $C_1' = .0338 \ \mu\mu f$)

$$r' = \frac{C_{0T}'}{C_1'} = \frac{200}{.0338} = 5900 , \tag{63}$$

whereby,

$$\Delta f_b = \frac{f_1'}{2r'} = 6.78 \text{ cps} \tag{63}$$

The total band width is therefore 3 + 6.78 = 9.78 cps.

9. Using the values of capacitances calculated in the previous discussion as a guide, the actual construction of the 10 cps filter proceeded as follows:

A ceramic variable capacitor (5-20 $\mu\mu$f) was placed in series with crystal 1 (C_{AX} = 16.6 $\mu\mu$f). A 200 $\mu\mu$f mica capacitor was then placed across this combination (C_{OT} = 195 $\mu\mu$f). Using the equipment shown in Fig. 29A, the variable capacitor was adjusted to produce an antiresonant frequency of 80,002 cps for the unit. This process was repeated for crystal 2 (see Fig. 30B)

The units for the shunt arms (Z_b) were produced by parallel capacitance in the form of a 180 $\mu\mu$f mica capacitor and a variable ceramic capacitor (4-30 $\mu\mu$f) placed across crystals 3 and 4. These units were pre-tuned to antiresonance at 80,009 cps.

The filter units were then placed in a test lattice structure, and the attenuation characteristic adjusted by tuning the capacitors across crystals 3 and 4.

The value of image impedance at f_0, calculated from eq.(31) is 6,850 ohms. However, no attempt was made to change the filter termination from the value used in the 100 cps filter (73,000 ohms), because the narrow band width involved (compared to the 100 cps case) makes the effect of varying the termination (step 7, section H) inconsequential.

The crystal filter stage is shown schematically in Fig. 34. The 10 cycle and 100 cycle filter tuning capacitors may be identified by referring to Fig. 30B. A single rotary switch (two-gang) accomplishes the changeover from the 10 cps to the 100 cps band width. It was found that the 10 cps filter had a smaller voltage output at f_0 than the 100 cps filter. To equalize the

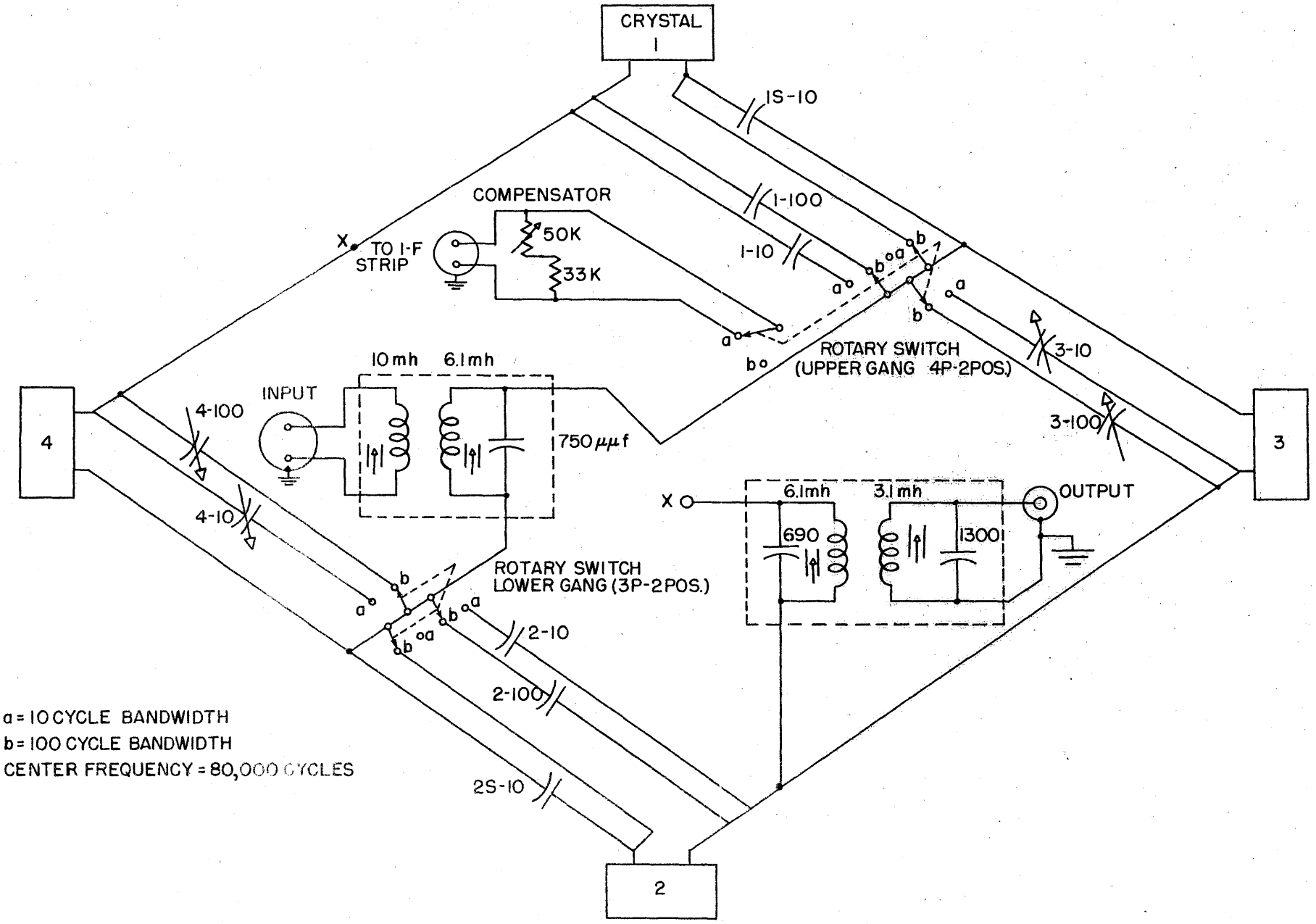

FIG. 34 CRYSTAL FILTER SCHEMATIC

outputs of the two filters, the "compensator" places attenuation in the path of the signal in the i-f strip (see Fig. 10) when the filter is in the 100 cycle band width position. The compensator is adjusted, when the analyzer is initially calibrated (Chapter III, section A), to provide equal voltage outputs at both filter band widths for a fixed sinusoidal input signal.

A photograph of the crystal filter unit is presented in Fig. 9 (Chapter II).

The attenuation characteristics of the 10 and 100 cycle filters are shown in Fig. 35, along with the response curve of a simple tuned circuit. As explained in section D of Chapter II, the tuned circuit, which has a band width of 100 cps (to 3 db points) does not have the flat pass band or the sharply rising skirts which are characteristic of the crystal lattice filter.

The 100 cps filter is symmetrical (the lack of an attenuation peak to the right of the center frequency is explained in section H). The pass band is flat (within 0.5 db) for 60 cps, and has a width (to 3 db points) of about 90 cps. The theoretical flat band width of this filter is 104 cps, but the variation of image impedance over the pass band makes proper termination of the filter impossible with a single resistance, so that the pass band is flat for only about 60% of the theoretical value.

The band width (to 3 db points) of the 10 cps filter is 10 cycles, within 1 cps (measurements of greater accuracy than this were not possible with the equipment available, nor were they necessary). The attenuation curve for this filter has a peak below f_0, but not above f_0, as predicted by the design analysis.

FIG. 35: CRYSTAL FILTER ATTENUATION CHARACTERISTICS

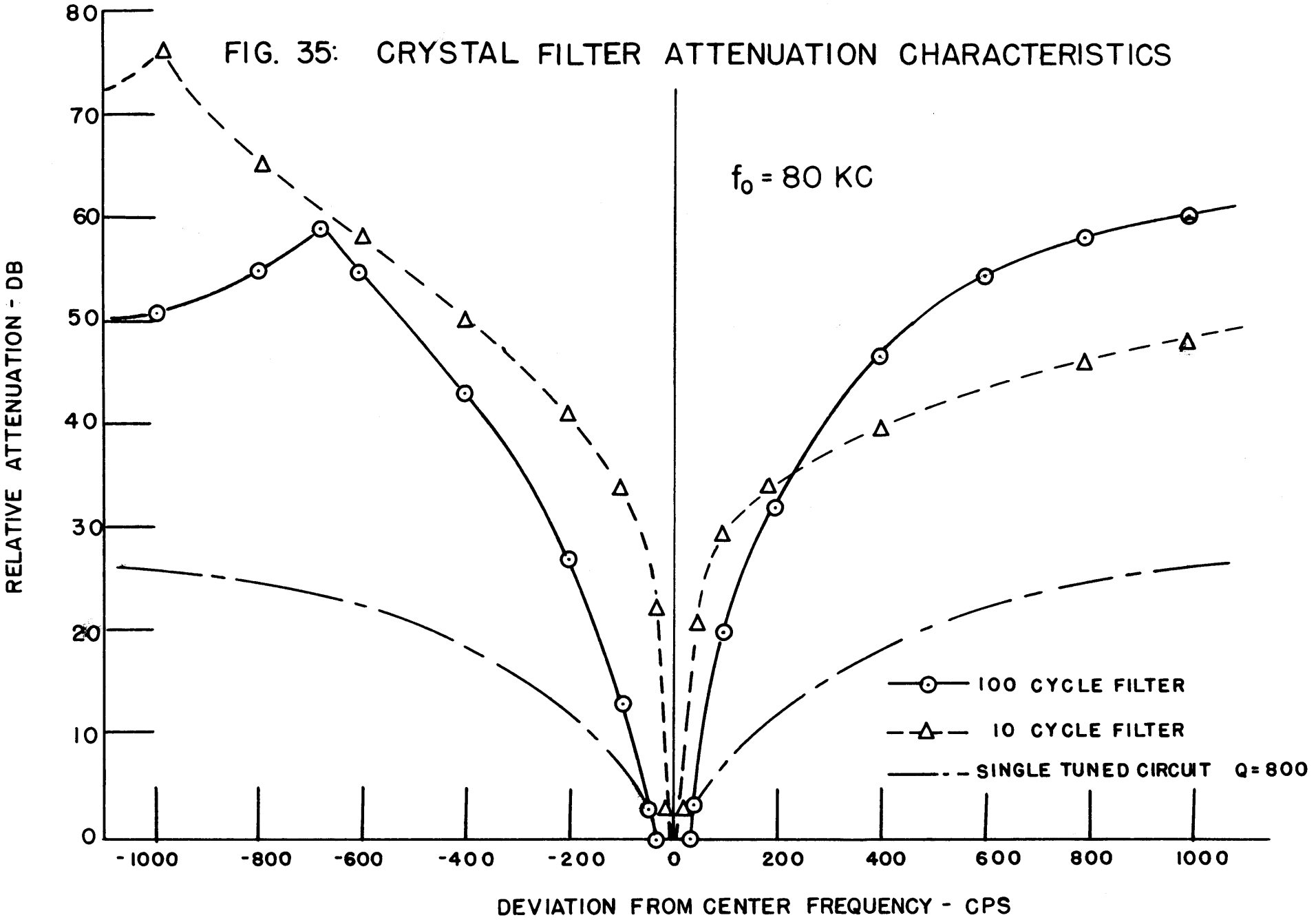

APPENDIX II

THE IDEAL SQUARE-LAW DETECTOR

Consider the peak-reading detector circuit shown in Fig. 36. It will be assumed that the reactance of the detector load capacitance is very small compared to R at the carrier frequency, but is very large compared to R at all modulation frequencies.

The rectifying element has the characteristic

$$i = ke^2 \tag{1}$$

The input voltage will be assumed to be a sinusoidally modulated carrier. That is,

$$E_{in} = E_c (1 + m \cos w_m t) \cos w_o t \tag{2}$$

$$= E' \cos w_o t \tag{3}$$

where

$$E' = E_c (1 + m \cos w_m t) \tag{4}$$

$$m = \frac{\text{r-m-s modulation voltage}}{\text{r-m-s carrier voltage}}$$

and

$$w_o >> w_m$$

Under equilibrium conditions, the capacitor will charge to a voltage

$$E_a = I_b R \tag{5}$$

where I_b is the average rectifier current.

The voltage across the rectifier is then

$$e = E' \cos w_o t - E_a \tag{6}$$

and

$$E_a = E' \cos \theta \tag{7}$$

where θ is half the angle of conduction per cycle of carrier frequency as indicated in Fig. 36.

Combining equations (1) and (6) yields

$$i = k (E' \cos w_o t - E_a)^2, \quad \text{for } e > 0 \tag{8}$$

$$= 0 \quad , \quad \text{for } e < 0$$

Letting $w_o t = \theta'$, then the average current becomes

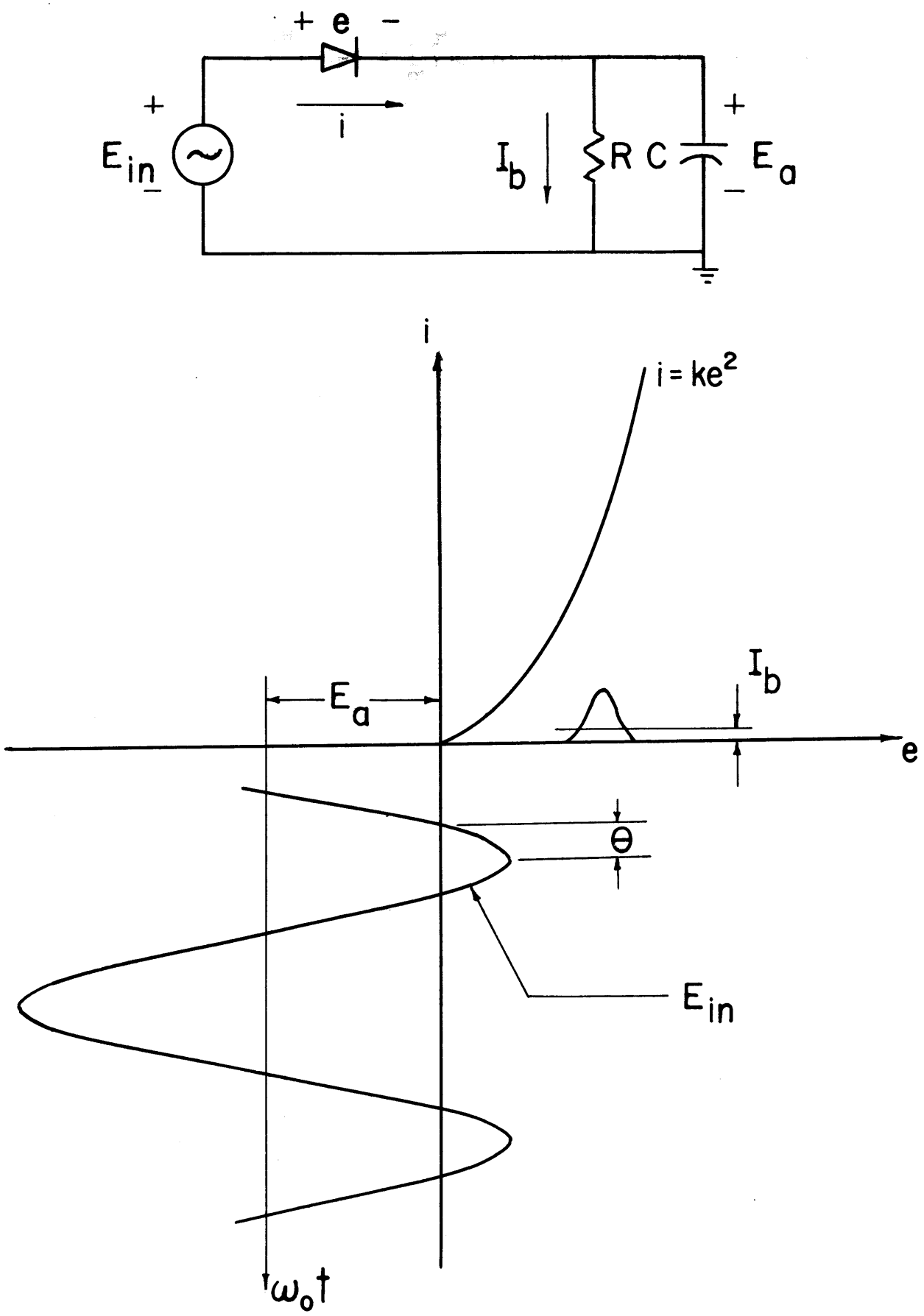

FIG. 36 THE IDEAL SQUARE-LAW DETECTOR

$$I_b = \frac{1}{\pi}\int_0^{\theta} i\, d\theta' = \frac{1}{\pi}\int_0^{\theta} k\,(E' \cos\theta' - E_a)^2\, d\theta'$$

Expanding the integrand and carrying out the integration,

$$I_b = \frac{k}{\pi}\left[\left(\frac{E'^2}{2} + E_a^2\right)\theta + \frac{E'^2 \sin 2\theta}{4} - 2E_aE' \sin\theta\right] \quad (9)$$

Using $\sin 2\theta = 2 \sin\theta \cos\theta$, eq.(9) becomes

$$I_b = \frac{k}{\pi}\left[\left(\frac{E'^2}{2} + E_a^2\right)\theta + \sin\theta\left(\frac{E'^2}{2}\cos\theta - 2E_aE'\right)\right] \quad (10)$$

Substituting eq.(7) into eq.(10) and regrouping yields

$$I_b = \frac{k}{\pi}\left(\frac{\theta}{2} + \theta\cos^2\theta - \frac{3}{2}\sin\theta\cos\theta\right) E'^2$$

$$I_b = K\,E'^2 \quad (11)$$

Returning to eq.(4), another relationship is obtained for E'^2,

$$E'^2 = E_c^2\,(1 + m\cos w_m t)^2$$

$$= E_c^2\,(1 + 2m\cos w_m t + m^2\cos w_m^2 t)$$

or approximately,

$$E'^2 = E_c^2\,(1 + 2m\cos w_m t), \quad \text{for } 1 \gg m \quad (12)$$

Combining the results of eq.(11) and eq.(12),

$$I_b = K\,(E_c^2 + 2mE_c^2\cos w_m t) \quad (13)$$

The detector output voltage is then (by eq. 5),

$$E_a = KR\,(E_c^2 + 2mE_c^2\cos w_m t) \quad (14)$$

If an apparent modulation index (m_a) is now defined as

$$m_a = \frac{\text{r-m-s detector output voltage at modulation frequency}}{\text{rectified d-c output voltage}}$$

then by inspection of eq.(14),

$$m_a = \frac{KR\,\frac{2m}{\sqrt{2}}\,E_c^2}{KR\,E_c^2} = \sqrt{2}\,m$$

That is, the apparent modulation index for a square-law detector is $\sqrt{2}$ times the actual input r-m-s modulation index.

APPENDIX III

CONVERSION OF F.M. TO A.M. IN A RESONANT CAVITY

When a microwave carrier is tuned to the slope of a resonant cavity, any small deviation of the carrier frequency will be converted to an equivalent amplitude modulation of the carrier envelope. The purpose of this appendix is to derive an expression for a given frequency deviation in terms of the amplitude-modulation index which results from a cavity conversion. Amplitude modulation present on the carrier envelope prior to the introduction of the cavity will be neglected.

The resonant cavity, shown in Fig. 37, has the same type of relative response curve as does a simple tuned circuit. For very large values of Q, which are always characteristic of X-Band cavities, the relative response curve can easily be shown to have the equation

$$V = \frac{V_{max}}{1 + jQ\left(\frac{w}{w_o} - \frac{w_o}{w}\right)} \tag{1}$$

where

w_o = resonant frequency of cavity, rad/sec.

$$Q = \frac{\text{resonant frequency}}{\text{bandwidth of response curve to half-power points}}$$

Substituting the value $a = \frac{w}{w_o}$ into equation (1) yields

$$\frac{V}{V_{max}} = \frac{1}{1 + jQ\left(a - \frac{1}{a}\right)} \tag{2}$$

If the magnitude of the relative response is denoted by W,

$$W = \left| \frac{V}{V_{max}} \right|$$

then by taking the magnitude of eq.(2),

$$W = \sqrt{\frac{1}{1 + Q^2\left(a - \frac{1}{a}\right)^2}} \tag{3}$$

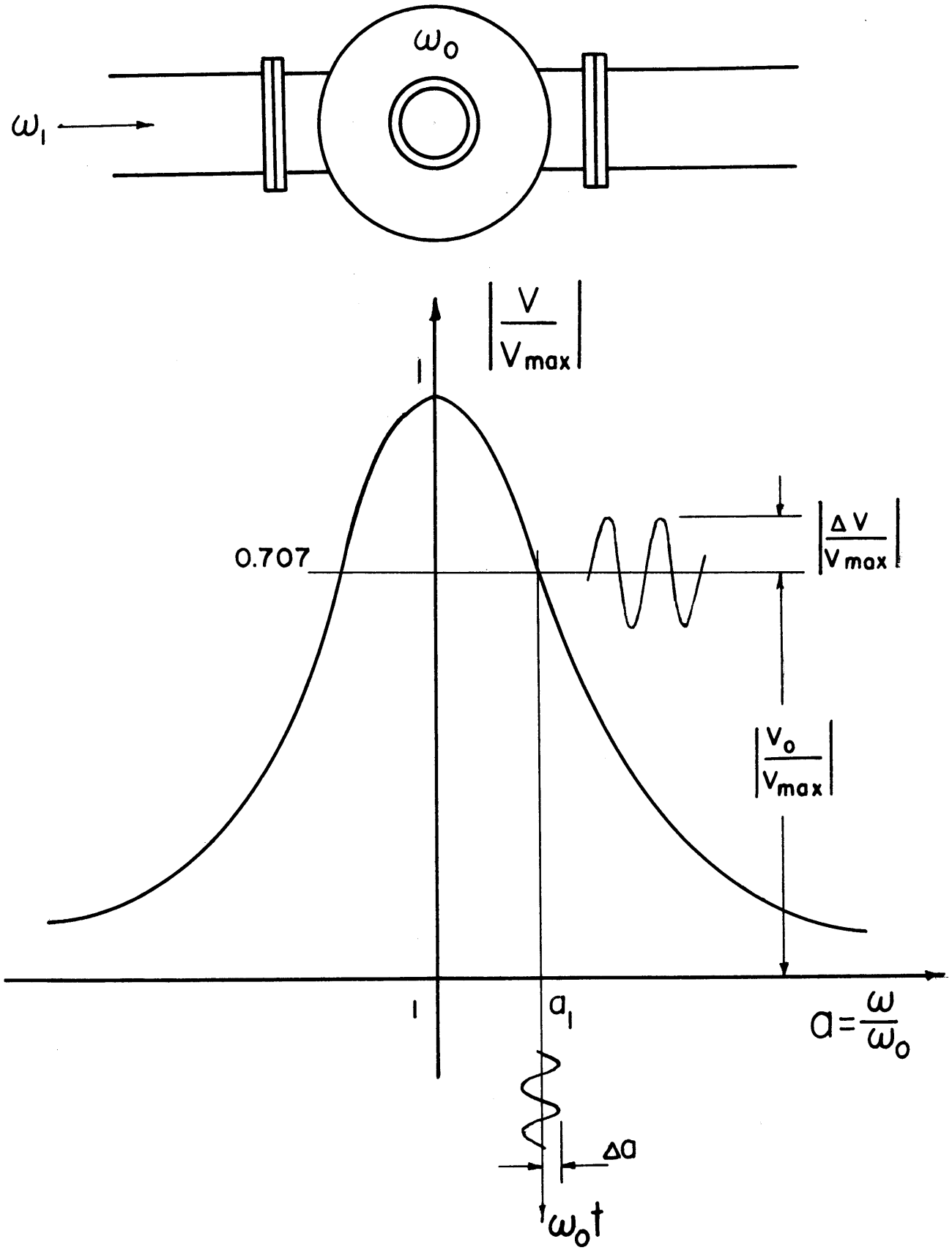

FIG. 37 RELATIVE RESPONSE CURVE OF A RESONANT CAVITY

Consider now a carrier of such frequency f_i, that the carrier falls at a_i, where the response is down 3 db, as shown in Fig. 37.

From eq.(3), the response falls 3 db when

$$Q\left(a - \frac{1}{a}\right) = 1$$

so that

$$a_i = 1 + \frac{1}{2Q}, \quad \text{for} \quad Q > 100 \tag{4}$$

Assume that the carrier deviates in frequency sinusoidally by a small amount Δf. Then since $f_o = \frac{w_o}{2\pi} \gg \Delta f$, and $Q > 100$,

$$a = \frac{\Delta f}{f_i} = \frac{\Delta f}{f_o} \tag{5}$$

By inspection of Fig. 37, it can be seen that W, the relative voltage deviation, which is produced by a, the relative frequency deviation, is given by

$$W = \left|\frac{\Delta V}{V_{max}}\right| = \left|\left(\frac{dW}{da}\right)_{a_i}\right| \Delta a \tag{6}$$

where $\left(\frac{dW}{da}\right)_{a_i}$ is the slope of the relative response curve at the half-power point.

To calculate the slope of the response curve at the half-power point, and thereby get ΔW in terms of Δa, we proceed as follows;

$$W^2 = \frac{1}{1 + Q^2\left(a - \frac{1}{a}\right)^2} \quad \text{from eq.(3)} \tag{7}$$

or

$$\frac{1}{W^2} = 1 + Q^2\left(a - \frac{1}{a}\right)^2 \tag{8}$$

Differentiating equation (8) yields

$$-2W^{-3}\frac{dW}{da} = Q^2\, 2\left(a - \frac{1}{a}\right)\left(1 + a^{-2}\right) \tag{9}$$

At the half-power point a_i, the response W is equal to $\frac{1}{\sqrt{2}}$.

Substituting this value of W, and the value of a_i from equation (4) into equation (9), and reducing yields

$$\left(\frac{dW}{da}\right)_{a_i} = -\frac{1}{2} \cdot \frac{2Q + 1}{2\left(1 + \frac{1}{Q}\right)} \quad , \text{ which for } Q \text{ 100 yields}$$

$$\left|\left(\frac{dW}{da}\right)_{a_i}\right| = \frac{Q}{\sqrt{2}} \tag{10}$$

Equation (10) is the expression for the magnitude of the slope of the relative response curve at the half-power point. Substituting this expression into eq.(6), and making use of eq.(5),

$$\Delta f = \frac{2 f_o}{Q} \left|\frac{\Delta V}{V_{max}}\right| \text{ cps.} \tag{11}$$

The above relation gives the value of a frequency deviation in terms of the voltage deviation it produces. The spectrum analyzer however, measures amplitude-modulation index. For a relation between f and m (amplitude-modulation index), we note from Fig. 37 that the voltage output at the carrier frequency from the resonant cavity is $\frac{1}{\sqrt{2}}$ times the maximum output voltage. This fact leads to the result that

$$m = \left|\frac{\Delta V}{V_o}\right| = \frac{1}{\sqrt{2}}\left|\frac{\Delta V}{V_{max}}\right| \tag{12}$$

and eq.(11) becomes

$$\Delta f = \frac{f_o}{Q} m \text{ cps.} \tag{13}$$

For X-Band: f_o = 10,000 mc.

Q = 5,000 (this value is somewhat conservative, most X-Band cavities having larger Q values)

Assuming a modulation index (m) of 105 db below one volt (5.62 microvolts), eq.(13) gives Δf = 11.24 cps. In this research the relationship $\underline{\Delta f = 10 \text{ cps}}$ for $\underline{m = -105 \text{ db}}$ will be used.

BIBLIOGRAPHY

1. Ridenour, Radar System Engineering, Vol. 1, Radiation Laboratory Series, (McGraw-Hill Book Co., New York), 1948

2. Doppler Radar Systems, Measurements Laboratory, Sperry Gyroscope Co., Oct. 15, 1943, Report #5220-131

3. Goldman, S., Frequency Analysis, Modulation and Noise, (McGraw-Hill Book Co., New York), 1948

4. Johnson, J.B., "The Schottky Effect in Low-Frequency Circuits", Physics Review, 26, July, 1925, 71-85.

5. Collins, G.B., Microwave Magnetrons, Vol. 6, Radiation Lab. Series, (McGraw-Hill Book Co., New York), 1948

6. Hamilton, D.R., J.K. Knipp and J.B.H. Kuper, Klystrons and Microwave Triodes, Vol. 7, Rad. Lab. Series, (McGraw-Hill Book Co., New York), 1948

7. Torrey, H.C. and C.A. Whitner, Crystal Rectifiers, Vol. 15, Rad. Lab. Series, (McGraw Hill Book Co., New York), 1948

8. Very-High-Frequency Techniques, Vol. II, Radio Research Laboratory, Harvard University, (McGraw-Hill Bk. Co., N.Y.) 1947

9. Kelleher, R.L., "The Measurement of the Noise Power Spectrum of an Ultra-High-Frequency Transmitter", M.I.T. Electrical Engineering Dept. M.S. Thesis, (1949)

10. Herold, E.W., "The Operation of Frequency Convertors and Mixers for Superheterodyne Reception", Proc. IRE, Feb. 1942

11. Terman, F.E., Radio Engineers' Handbook, (McGraw-Hill Book

Co., New York), 1943

12. Millman, J. and H. Taub, "Notes on Electronic Circuitry", Course R235, E.E. Dept, City College of New York, (1950)

13. Peterson, H. and G.R. Keith, "Balanced Modulators", Bell System Technical Journal, 7-131, (1928)

14. Mason, W.P., Electromechanical Transducers and Wave Filters, (D. Van Nostrand Co.,Inc, New York) 1942

15. Guillemin, E.A., Communications Networks, Vol. II, (John Wiley and Sons, Inc., New York), 1935

16. Mason, W.P.,"Electric Wave Filters Employing Quartz Crystals as Elements", Bell System Technical Journal, V13, pp.405-452, (1934)

17. Burns, G.K., "Manufacture of Quartz Crystal Filters", Bell System Technical Journal,V19, pp. 221-248 (1940)

18. Arquimbau, L.B., Vacuum Tube Circuits, (John Wiley & Sons Inc., New York), 1948